ROYAUME DU MAROC
Université Mohammed V - RABAT -
جامعة محمد الخامس – الرباط –
Faculté des sciences
كلية العلوم
DOCTORAL STUDY CENTER - SCIENCE & TECHNOLOGY

Sr. No. 3158

Thesis

In order to obtain the title of: ***Doctor of Philosophy***

Research Center: Center of Materials Science
Research Group: Laboratory of Composite Materials, Polymers and Environment
Discipline: Chemistry
Specialty: Physical and Theoretical Chemistry of Materials

Thesis defended in: December 13, 2018 by:

Muhammad Azeem ARSHAD

Kinetics of thermal degradation mechanisms in polymer/metal composites and new mechanistic approaches to solar cell degradation and crystallization in amorphous materials

Thesis Examination Committee

Mohammed HALIM	Professor, Mohammed V University, Faculty of Sciences, Rabat	Chairman
Gabriel PINTO	Professor, Polytechnic University of Madrid, Technical School of Industrial Engineering (ETSI), Madrid	Examiner
Rosario BENAVENTE	Professor, The Spanish National Research Council (CSIC) Institute of Polymer Science and Technology, Madrid	Examiner
Abderrahman ELIDRISSI	Professor, Mohammed I University, Faculty of Sciences, Oujda	Examiner
Abdelfettah BARHDADI	Professor, Mohammed V University, École Normale Supérieure (ENS), Rabat	Rapporteur/ Examiner
Nisar Naeem SHEIKH	Professor, Al Akhawayn University, School of Science and Engineering, Ifrane	Rapporteur/ Examiner
AbdelKrim MAÂROUFI	Professor, Mohammed V University, Faculty of Sciences, Rabat	Supervisor

Academic Year: 2017-18

✉ Faculty of Sciences, Ibn Batouta Avenue, P.O. Box 1014, Rabat, Morocco
☎ 00212 537 77 18 76 🖷 00212 537 77 42 61; http://www.fsr.um5.ac.ma

Dedicated

to

Ammi, Abbu and Baji

(May their souls rest in peace, Aameen!)

Acknowledgements

In the name of ALLAH, the Beneficent, the Merciful.
All praise is due to ALLAH, the Lord of the universe.

I express my deepest gratitude to **P**rof. **A**bdelKrim **M**aâroufi from the University of Mohammed V, Faculty of Sciences, Materials Science Center, Laboratory of Composites Materials, Polymers and Environment (LCMPE), Rabat, for supervising me during all these years of research. Though, I lack in words thanking him, simply, I am really very grateful to him for his kindness, keen and relevant advice, and constructive criticism. Without his guidance and persistent assistance, this thesis would not have been possible.

I would like to also express my gratitude to **P**rof. **M**ourad **E**l **B**elkacemi, Dean of the Faculty of Sciences, Rabat, for his encouragement and aid.

A bundle of thanks goes also to **P**rof. **M**ohammed **H**alim from the University of Mohammed V, Faculty of Sciences and Director of the Materials Science Center, Rabat, who honored me by accepting to chair the examination committee of this thesis and for his enthusiastic interest in my work.

Many thanks go to **P**rof. **G**abriel **P**into from the Universidad Politécnica de Madrid, Departamento de Ingeniería Química Industrial y del Medio Ambiente, Escuela Técnica Superior de Ingenieros Industriales (ETSI), Madrid, Spain, for honoring me by kindly accepting to be among the members of the thesis examination committee, and for traveling a long distance in order to take part into it. I offer him my profound gratitude for being there whenever I needed support.

I would like also to express my gratefulness and appreciation to **P**rof. **R**osario **B**enavente from the Instituto de Ciencia y Tecnología de Polímeros (CSIC), Madrid, Spain, for the assessment of my thesis and for traveling a long distance in order to join the thesis examination committee. I am grateful to her for her collaboration, time and assistance.

I am grateful as well to the thesis examiner, **P**rof. **A**bderrahman **E**lIdrissi from the **Mohammed I** University, Faculty of Sciences, Oujda, Morocco, for being a member of the thesis examination committee and for his kind collaboration.

A special gratitude is deserved by the thesis rapporteur, **P**rof. **A**bdel**F**ettah **B**arhdadi from the University of Mohammed V, École Normale Supérieure (ENS), Rabat, Morocco, for his interest and significant efforts to analyze this work.

My sincere gratitude goes also to the thesis rapporteur, **P**rof. **N**isar **N**aeem **S**heikh from the Al Akhawayn University, School of Science and Engineering, Ifrane, Morocco, for sparing time out of his busy schedule in order to evaluate this thesis.

I am also very thankful to **M**oroccan **A**gency for **I**nternational **C**ooperation (AMCI) for facilitating my doctoral studies in Morocco by granting me a bursary. Particular thanks to **M**r. **K**amal **O**uld **T**afquirt, Director, International University Hostel (CUI), Rabat, Morocco, for providing me a comfortable accommodation during all my studies in Morocco.

I would like also to mention and acknowledge the support received from the family and friends, especially from the laboratory fellows.

In the end, all my gratitude to whoever contributed to the success of this thesis, explicitly/ implicitly and openly/in secret.

بسم الله الرحمن الرحيم

En: In the name of ALLAH, the Beneficent, the Merciful.

Fr: Au nom de Dieu, le tout Miséricordieux, le très Miséricordieux.

سَبِّحِ اسْمَ رَبِّكَ الْأَعْلَى. الَّذِي خَلَقَ فَسَوَّىٰ. وَالَّذِي قَدَّرَ فَهَدَىٰ.

الأعلى: 1-3

En: Glorify the name of your Lord, the Most High. Who creates (everything), then perfectionates (it). And Who makes (everything) according to a measure, then guides (to its understanding).

Fr: Glorifie le nom de ton Seigneur, le Très Haut. Celui Qui a crée et agencé harmonieusement. Qui a décrété et guidé.

Abstract

Polymer composites filled with metal particles establish an interesting class of materials with wide-reaching applications from macro to nano scale. Our research group demonstrated in the previous researches that such polymer/metal composites possess fascinating electrical/dielectric properties. The present thesis continues developing these earlier researches by reporting a thorough study on structural, morphological and thermal properties of polymer/metal composites. For this purpose, insulating and conducting polymer composites comprising epoxy and urea-formaldehyde cellulose (UFC) resins filled with metal (aluminum, zinc and tin) particles are prepared and structurally characterized by SEM-EDX, XRD and FTIR analyses. Structural and morphological analyses reveal that the composites are homogenous and the polymer-metal interfaces are physical in nature. Thermogravimetric analysis (TGA) profiles of polymer/metal composites suggest that the thermal degradation of epoxy/metal composites follows quasi single-step process; however thermal degradation of UFC/metal composites goes to completion in several complex steps. Thus, an innovative reaction model determination methodology is put forward to address the encountered kinetic problem of determining the reaction model under variable activation energy conditions. Kinetic analysis of the thermal degradation of epoxy/metal composites predicts autocatalytic reaction mechanism for epoxy/metal composites; while, UFC/metal composites pursue highly complicated multi-step nucleation/growth mechanisms. The suggested methodology is exploited also to develop novel approaches for predicting accurate lifetimes of polymer solar cells and kinetically modeling the crystallization processes in amorphous materials.

Keywords: Polymer composites, metals, TGA/DTG, thermal degradation, kinetics, mechanism, organic photovoltaics, crystallization.

Résumé

Les composites polymères chargés par des particules du métal constituent une classe intéressante de matériaux avec des applications étendues de l'échelle macro à l'échelle nanométrique. Les recherches de notre équipe ont montré que les matériaux composites polymère/métal ont des propriétés électriques/diélectriques fascinantes. La présente thèse est une continuation du développement de ces recherches antérieures en rapportant une étude approfondie des propriétés structurales, morphologiques et thermiques des composites polymère/métal. A cet effet, des composites polymères isolants et conducteurs comprenant des résines époxy et urée-formaldéhyde cellulose (UFC) chargées par des particules métalliques (aluminium, zinc et étain) ont été préparés et structurellement caractérisés par des analyses SEM-EDX, XRD et FTIR. Les analyses structurales et morphologiques révèlent que les composites sont homogènes et que les interfaces polymère-métal sont de nature physique. Les profils d'analyses thermogravimétriques (ATG) des composites polymère/métal suggèrent que la dégradation thermique des composites époxy/métal suit un processus quasi-mono-étape, tandis que la dégradation thermique des composites UFC/métal est achevée en plusieurs étapes complexes. Pour cela, une méthodologie innovante de détermination du modèle de réaction a été proposée pour résoudre cet important problème cinétique de détermination du modèle de réaction dans des conditions d'énergie d'activation variable. L'analyse cinétique de la dégradation thermique des composites époxy/métal prédit un mécanisme de réaction auto-catalytique pour les composites époxy/métal. Tandis que, les composites UFC/métal obéissent à des mécanismes de nucléation/croissance très complexes en plusieurs étapes. La méthodologie suggérée a été exploitée aussi pour développer de nouvelles approches pour prédire les durées de vie précises des cellules solaires polymères et modéliser cinétiquement les processus de cristallisation dans les matériaux amorphes.

Mots-clés: Composite polymère, métaux, ATG/DTG, dégradation thermique, cinétique, mécanisme, photovoltaïque organique, cristallisation.

ملخص

البوليمير عبارة عن مركب مليء بجزيئات معدنية، تتكون من اصناف مثيرة من المواد، تدخل في تطبيقات كثيرة وتشمل مجالات واسعة تنبري من الماكرو الى غاية النانو .وتبين أبحاثنا السابقة خصائص كهربائية بديعة لمادة البوليمير في مقابل المركب المعدني، سواء كان موصلا او عازلا .والأطروحة الحالية هي استمرار في تطوير الأبحاث التي قمنا بها سابقا من خلال التركيز على الدراسة المعمقة والشاملة للخصائص البنيوية والمورفولوجية وكذا الحرارية لمادة البوليمير مقابل المركب المعدني .فقد تم تهيئ مركب لهذا الغرض، من البوليمير العازل او الموصل والذي يتألف من الراتنج المليء بالمعادن) الألمنيوم والزنك والقصدير، (كراتنج الايبوكسي و راتنج سليلوز اليوريا الفورماليهايد، (UFC)ثم تم توصيفها بنيويا بواسطة أجهزة التحليل SEM-EDX ، XRD و . FTIRوتكشف التحاليل المورفولوجية ان التركيبة متجانسة وتتواجد البي- مراحل البوليميرات والمعادن في الطبيعة الفيزيائية .كما تم إجراء قياسات الاستقرار الحراري المتأصل، وانماط التفاعل الظاهر، وحركيه التفكك الحراري للمركب البوليمير المعدني على المعطيات التحليلية الحرارية للمواد التي تحت الدراسة .بالإضافة الى ان النتائج المحصل عليها تظهر على أن اقحام جسيمات معدنية قادرة على تحسين الاستقرار الحراري لمركب البوليمير المعدني، وعلاوة على ذلك، فان المركب الموصل يظهر استقرارا أكثر .وكذلك تشير ملامح التفاعل لمركب البوليمير المعدني حيث ان التفكك الحراري لمركب الايبوكسي المعدني يحتاج الى خطوه واحدة، في حين ان التفكك الحراري لمركب UFC المعدني يخلص في عده خطوات معقدة .كما تجدر الاشارة الى ان التحليل الحركي للتفكك الحراري من مركب الايبوكسي المعدني بإمكانه تقدير آلية التفاعل ذاتية التحفيز .إضافة إلى ذلك، فان آليه تفاعل الايبوكسي لا تتغير مع طبيعة أو محتويات الجزيئات المعدنية .من ناحية أخرى، يتبع مركب ال UFC المعدني آليات تنوي ونمو معقدة للغاية ومتعددة المراحل والخطوات .على عكس مركب الايبوكسي المعدني فآليه التفكك الحراري من راتنج UFC يظهر الارتباط الوثيق للطبيعة بمحتويات الجزيئات المعدنية .وفي كلتا الحالتين، فان ارتباط درجه الحرارة بالقدرات الحرارية والانشطة المحفزة للمعادن يلعب أدوارا حاسمه في تأويل سلوكيات التفكك الحراري لمركب البوليمير المعدني .وفي المرحلة التالية، نقترح منهجيه جديدة ومبتكرة لبحث مشكلة هامه تخص الحركة في تحديد نموذج التفاعل في ظروف طاقة التفعيل المتغيرة .وتستغل المنهجية المقترحة لوضع سبيل جديد لاستقراء العمر الدقيق للخلايا الشمسية البوليميرية ونمذجة الحركة لعمليات التبلور في المواد غير المتبلورة.

Publications

1. M.A. Arshad, A. Maaroufi, Kinetics of photodegradation mechanisms in organic photovoltaics, Physica B: Condensed Matter, 545 (2018) 465–474.
2. M.A. Arshad, A. Maaroufi, Kinetic approach to degradation mechanisms in polymer solar cells and their accurate lifetime predictions, Journal of Power Sources, 391 (2018) 134–147.
3. M.A. Arshad, A. Maaroufi, Unfolding complex thermal degradation mechanisms in polymer composites, Society of Plastics Engineers, 2018.
   DOI: 10.2417/spepro.006991
4. M.A. Arshad, A. Maaroufi, Recent advances in kinetics and mechanisms of condensed phase processes: A mini-review, Reviews on Advanced Materials Science, 51 (2017) 177–187.
5. M.A. Arshad, A. Maaroufi, Recent progress in kinetics of thermal degradation mechanisms in polymer composites, MOJ Polymer Science, 1 (2017) 120–125.
6. M.A. Arshad, A. Maaroufi, R. Benavente and G. Pinto, Thermal degradation of urea-formaldehyde cellulose composites filled with aluminum particles: kinetic approach to mechanisms, Journal of Applied Polymer Science, 134 (2017) 44826–44838.
7. M.A. Arshad, A. Maaroufi, R. Benavente and G. Pinto, Predicting thermal degradation mechanisms in urea-formaldehyde cellulose composites filled with tin particles, Polymer Composites, 39 (2018) 4341–4354.
8. M.A. Arshad, A. Maaroufi, R. Benavente and G. Pinto, Kinetics of the thermal degradation mechanisms in urea-formaldehyde cellulose composites filled with zinc particles, Journal of Materials Science: Materials in Electronics, 28 (2017) 11832–11845.
9. M.A. Arshad, A. Maaroufi, G. Pinto, S. El-Barkany, A. Elidrissi, Morphology, thermal stability and thermal degradation kinetics of cellulose-modified urea–formaldehyde resin, Bulletin of Materials Science, 39 (2016) 1609–1618.
10. M.A. Arshad, A. Maaroufi, Thermal degradation mechanism of composites of polymers filled with metal particles, Society of Plastics Engineers, 2015.
    DOI: 10.2417/spepro.006183
11. M.A. Arshad, A. Maaroufi, R. Benavente and G. Pinto, Thermal degradation mechanisms of epoxy composites filled with tin particles, Polymer Composites, 36 (2015) 9–20.

12. M.A. Arshad, A. Maaroufi, Relationship between Johnson-Mehl-Avrami and Šesták-Berggren Models in the kinetics of crystallization in amorphous materials, Journal of Non-Crystalline Solids, 413 (2015) 53–58.
13. M.A. Arshad, A. Maaroufi, A new kinetic approach to analyze the thermally stimulated photodegradation of solar devices, IEEE proceedings, 2014.
    DOI: 10.1109/irsec.2014.7059837
14. M.A. Arshad, A. Maaroufi, An innovative reaction model determination methodology in solid state kinetics based on variable activation energy, Thermochimica Acta, 585 (2014) 25–35.
15. M.A. Arshad, A. Maaroufi, R. Benavente and G. Pinto, Kinetics of the thermal decomposition mechanisms of conducting and non-conducting epoxy/Al composites, Journal of Materials and Environmental Science, 5 (2014) 1342–1354.
16. M.A. Arshad, A. Maaroufi, R. Benavente, J.M. Pereña, G. Pinto, Thermal degradation kinetics of insulating/conducting epoxy/Zn composites under nonisothermal conditions, Polymer Composites, 34 (2013) 2049–2060.
17. M.A. Arshad, A. Maaroufi, Kinetics of dynamic percolation mechanisms in carbon-filled polymer composites, Polymer, (2018) to be submitted.
18. M.S. Ahmad, M.A. Arshad, A. Maaroufi, et al. Pyrolysis Kinetics and thermodynamic behavior of Para grass, Applied Energy, (2018) to be submitted.

Oral and Poster Presentations

1. M.A. Arshad, A. Maaroufi, An innovative reaction model determination methodology in solid state kinetics based on variable activation energy, Doctoriales, February 19-21, 2015, Faculty of Sciences Rabat, Morocco.
2. M.A. Arshad, A. Maaroufi, A new kinetic approach to analyze the thermally stimulated photodegradation of solar devices, 2nd International Renewable and Sustainable Energy Conference, October 17-19, 2014, Ouarzazate, Morocco.
3. M.A. Arshad, A. Maaroufi, An Explicit Relationship between Avrami and Šesták Models holds in the Kinetics of Crystallization Processes in Amorphous Materials, The 12th International Conference on Condensed Matter and Statistical Physics (ICCMSP), October 30-November 01, 2013, Errachidia, Morocco.
4. M.A. Arshad, A. Maaroufi, R. Benavente and G. Pinto, Non-Isothermal Degradation Kinetics of epoxy/Al Composites As Building Blocks of Polymer Solar Panels, Asian CORE workshop "Fundamentals and Applications of Nanophotonics, Photovoltaics and Bio-photonics", March 6-8, 2013, Rabat, Morocco.
5. M.A. Arshad, A. Maaroufi, R. Benavente and G. Pinto, Thermal degradation kinetics of insulating/conducting polymer/metal composites, Doctoriales, January 14-15, 2013, Rabat, Morocco.
6. M.A. Arshad, A. Maaroufi, R. Benavente, J.M. Pereña, G. Pinto, Mechanistic predictions of metal-polymer interactions by thermal degradation data treatment under non-isothermal conditions, ITMC, October 27-29, 2011, Casablanca, Morocco.
7. M.A. Arshad, A. Maaroufi, Theoretical thermal analysis; yesterday, today and tomorrow: an elaborated review of history, current challenges and future research trends, Second Moroccan days on nano-science and nanotechnology, June 16-17, 2011, Fez, Morocco.
8. M.A. Arshad, A. Maaroufi, R. Benavente, J.M. Pereña, G. Pinto, Study and comparison of thermal degradation kinetics of thermosetting polymers loaded with metallic fillers, 27^{th} World Congress of the Polymer Processing Society (PPSC), May 9-14, 2011, Marrakesh, Morocco.
9. M.A. Arshad, A. Maaroufi, R. Benavente, J.M. Pereña, G. Pinto, Influence of percolation threshold on the thermal degradation kinetics of polymer/metal composites, 7^{th} colloquium on organic polymers and their applications, May 5-7, 2011, Tangier, Morocco.

Table of Contents

List of Figures

List of Tables

General Introduction

Polymers constitute an important class of materials. For centuries, they have been applied as materials for food, leather, sizing, fibers, structures, waterproofing, and coatings. During the last decades, their use has been expanded to include more advanced applications, such as membranes, foams, fibers, films, medicines, electronic appliances, packaging and applications demanding high modulus at elevated temperatures. Polymer applications are multiplied by making their composites due to the low density, ease of processing, ability to absorb mechanical shock, flexibility, corrosion resistance and electrical properties control of the finished product. An interesting class of polymer composites is established by integrating metallic particles into polymers. Polymer/metal composites can be categorized into electrically/thermally insulating and conductive types. Insulating composites are useful as thermal grease, thermal interface materials, and electric cable insulation. Conductive composites, on the other hand, can be used for thermoelectrical and thermomechanical applications, and in organic photovoltaics. Nevertheless, the efficiencies and commercialization potential of the mentioned materials are defined by their structures/properties. Particularly, the thermally stimulated processes taking place in those materials over long temperature ranges need to be understood. What more challenging is the quantitative description of the mechanisms of those thermally stimulated solid state processes.

For many years, our group has been carrying out researches on the development of economical, environmentally friendly, and multipurpose polymer/metal composites with intriguing properties for a number of wide-reaching applications. Among the studied composites, composites of epoxy and bio-composites of urea-formaldehyde cellulose (UFC) filled with metals (Al, Zn and Sn) have been found worth considering due to their quite interesting electrical/dielectric properties. Though, as described earlier, the mechanisms of thermally stimulated epoxy/metal and UFC/metal composites demand understanding for their eventual exploitation. Kinetic analysis in this regard indeed plays a vital role. It should however be pointed out that the thermally stimulated condensed phase processes are especially known for their complexities; even apparently simple reactions can consist of multiple steps. In addition, the pre-exiting approaches (based on single-step approximation) remain unable to kinetically interpret the intricate mechanisms of multi-step processes.

In the frame of reference above, the present thesis composed of seven chapters as following:

The first chapter of this thesis reports the state of the art survey of literature concerning polymers and their composites. It gives an introduction to polymer and polymer composites with a particular emphasis on polymer composites filled with metal particles. Various techniques of structural characterization and thermal analysis are also reviewed and discussed.

The second chapter is associated with the pre-existing kinetic approaches to model the solid state processes. Certain matters on complexity of condensed phase processes and ICTAC kinetic committee recommendations on coping with them are pointed out. Afterwards, an account of the most recent advances in the domain of condensed phase kinetics and solutions to certain important kinetic problems, by putting forward innovative and advanced kinetic approaches, is reported.

Chapters 3 furnishes a detailed account of the preparation and structural characterization of insulating/conducting polymer composites of epoxy and UFC filled with aluminum, zinc and tin particles. The obtained results are also discussed.

Chapter 4 deals with the thermal stabilities and temperature dependent processes taking place in epoxy/metal and UFC/metal composites by TG/DTG analyses. In this context, the assessment of the thermal degradation profiles of epoxy/metal and UFC/metal composites is presented, interpreted and discussed.

Chapter 5 is related to model the experimentally obtained thermal degradation profiles of epoxy/metal and UFC/metal composites (Chapter 4) by employing solid state kinetics approaches. Kinetic parameters of neat epoxy and UFC resins and their respective composites are evaluated. The probable thermal degradation mechanisms of resins and their composites are predicted on the basis of kinetic analysis, and an account of the influence of nature and contents of metals on the thermal degradation mechanism of resins is given and discussed.

Chapter 6 is associated with the contribution in renewable and sustainable energy research with special regard to organic photovoltaics. In this chapter, certain crucial flaws in the well-known temperature accelerated lifetime testing of polymer solar cells are pointed out. Alternatively, an advanced method to predict lifetimes of polymer solar cells has been proposed which takes into account systematic kinetic modeling of various possible degradation processes in polymer solar cells under natural weathering conditions. This method has effectively been tested on various solar energy materials and solar cells.

In chapter 7, a new kinetic approach to model the crystallization processes in amorphous materials is suggested. On the basis of this approach, an explicit relationship between two important condensed phase reaction models i.e. Johnson-Mehl-Avrami and Šesták-Berggren models have been developed that holds in the crystallization kinetics of amorphous materials. The validity conditions of the proposed relationship along with its phenomenological limits are also discussed.

Introduction Générale

Les polymères constituent une classe importante de matériaux. Ils ont été utilisés pendant des siècles comme matériaux pour l'alimentation, le cuir, le collage, les fibres, les médicaments, l'imperméabilisation et les revêtements. Au cours de ces dernières décennies, leur utilisation a été étendue pour couvrir des applications un peu plus avancées, telles que les membranes, le cuir, les fibres, les films, les médicaments, les appareils électroniques, les emballages et les applications exigeant des modules élevés aux hautes températures. Les applications des polymères sont multipliées par la fabrication de leurs composites en raison de la faible densité, de la facilité de traitement, de la capacité à absorber les chocs mécaniques, de la flexibilité, de la résistance à la corrosion et du contrôle des propriétés électriques du produit fini. Une classe intéressante de composites polymères est établie en introduisant des particules métalliques dans des polymères. Le composite polymère/métal peut être aussi bien de type isolant électrique/thermique que de type conducteur. Les composites isolants sont utiles comme pate thermique, matériaux d'interface thermique et ils peuvent être utilisés aussi dans l'isolation des câbles électriques. Les composites conducteurs, quant à eux, peuvent être utilisés pour des applications thermoélectriques et thermomécaniques, ainsi que dans le photovoltaïque organique. Néanmoins, l'efficacité et le potentiel de commercialisation des matériaux mentionnés sont définis par leurs structures/propriétés. En particulier, les processus thermiquement stimulés se déroulant dans ces matériaux sur de longues plages de température doivent être compris. En outre, ce qui est encore plus difficile c'est la description quantitative des mécanismes des processus stimulés thermiquement à l'état solide.

Depuis de nombreuses années, notre groupe mène des recherches sur le développement de composites polymères/métal en terme économique, écologique et polyvalent avec des propriétés fascinantes pour un certain nombre d'applications de grande envergure. Parmi les composites étudiés, les composites d'époxyde et les bio-composites d'urée-formaldéhyde-cellulose (UFC) chargés de métaux (Al, Zn et Sn) se veulent bien faire l'objet de notre étude en raison de leurs propriétés électriques/diélectriques très intéressantes. Bien que, comme décrit précédemment, les mécanismes des composites époxyde/métal et UFC/métal stimulés thermiquement exigent une compréhension pour une éventuelle exploitation. L'analyse cinétique à cet égard joue en effet un rôle essentiel. Il convient toutefois de souligner que les processus en phase condensée stimulée thermiquement sont particulièrement connus pour leurs complexités; même des réactions apparemment simples peuvent comporter plusieurs étapes. De plus, les approches préexistantes (basées sur une approximation en une seule étape) restent incapables d'interpréter, de point de vu cinétique, les mécanismes complexes de processus multi-étape.

Dans le cadre de référence ci-dessus, la présente thèse est composée des sept Chapitres suivants:

Le premier chapitre de cette thèse est consacré à l'état de la l'art sur les polymères et leurs composites. Il présente les polymères et les composites à matrices polymères, notamment les

composites à base de polymères chargés de particules métalliques. Diverses techniques de caractérisation structurelle et d'analyse thermique sont examinées et discutées.

Le deuxième chapitre porte sur les approches cinétiques préexistantes pour modéliser les processus à l'état solide. Certaines défaillances relatives à la complexité des processus en phase condensée et aux recommandations du comité cinétique d'ICTAC visant à les gérer sont signalées. Ensuite, nous présenterons les progrès les plus récents dans le domaine de la cinétique de phase condensée et la résolution de certains problèmes cinétiques importants en proposant des approches cinétiques innovantes et avancées.

Le Chapitre 3 consiste à présenter une description détaillée de la préparation et de la caractérisation structurelle des composites isolants/conducteurs à matrice polymère de l'époxyde et UFC chargés de particules d'aluminium, de zinc et d'étain. Les résultats obtenus sont également discutés.

Le Chapitre 4 traite des stabilités thermiques et des processus dépendant de la température se produisant dans le composite époxyde/métal et UFC/métal par analyses TG/DTG. Dans ce contexte, l'évaluation des profils de dégradation thermique des composites époxyde/métal et UFC/métal est présentée, interprétée et discutée.

Le Chapitre 5 est lié à la modélisation des profils de dégradation thermique obtenus expérimentalement pour le composite époxyde/métal et UFC/métal (Chapitre 4) en utilisant des approches cinétiques à l'état solide. Les paramètres cinétiques des résines époxyde et UFC pures et de leurs composites sont évalués. Les mécanismes probables de dégradation thermique des résines et de leurs composites sont prédits sur la base d'une analyse cinétique. Un compte rendu de l'influence de la nature et du contenu des métaux sur le mécanisme de dégradation thermique des résines est présenté et discuté.

Chapitre 6 se veut une contribution à la recherche sur les énergies renouvelables et durables en accordant une attention particulière au photovoltaïque organique. Dans ce Chapitre, on a pu signaler certains défauts cruciaux dans des tests bien connus sur la durée de vie accélérée des cellules solaires polymères. Alternativement, On a proposé une méthode avancée pour prédire la durée de vie des cellules solaires polymères, qui prend en compte la modélisation cinétique systématique de divers processus de dégradation possibles dans les cellules solaires polymères à des conditions climatiques naturelles. Cette méthode a été testée avec succès sur divers matériaux d'énergie solaire et cellules solaires.

Le Chapitre 7 fait l'objet d'une nouvelle approche cinétique pour modéliser les processus de cristallisation dans les matériaux amorphes. Sur la base de cette approche, on a développé une relation explicite entre deux modèles importants de réaction en phase condensée, à savoir les modèles de Johnson-Mehl-Avrami et de Šesták-Berggren, cette relation englobe la cinétique de cristallisation des matériaux amorphes. La relation proposée ainsi que ses limites phénoménologiques sont également discutées.

Chapter 1

A brief review on structures and characterizations of Polymers and Composites of Polymers

1.1. Introduction

This chapter reports a brief review on structures and certain properties of polymers and polymer composites. Initially, a general description of polymeric materials along with their classification is given. Special emphasis is then put on the composites of polymers (particularly epoxy and urea-formaldehyde cellulose or UFC resins) filled with metal particles, and some of the important researches on the mentioned composites reported in the literature are pointed out. Finally, the familiar techniques to characterize polymer composites morphologically and thermally are reviewed. This chapter will serve in interpreting and discussing the results of structural/thermal analyses of epoxy/metal and UFC/metal composites in the upcoming chapters.

1.2. Polymers

Polymers are long chain organic/inorganic or organic-inorganic hybrid molecules which are assembled from many smaller molecules called monomers. In fact, the word polymer is a combination of 'poly' means several and 'mer' means unit i.e. a polymer is a giant molecule constituting upon many units of the same kind which arrange themselves inside that giant molecule by following repetition. Another common name for many synthetic polymers is plastic which comes from the Greek word plastikos i.e; suitable for molding or shaping. Majority of the objects and articles in everyday use, for instance, packing, wrapping, and building materials are synthesized polymers.

1.3. Classification of polymers

Polymers can be classified generally as well as in accordance with the mode of polymerization as detailed in the following sections [1]:

1.3.1. Natural polymers

Polymers are widely found in nature. The human body contains many natural polymers such as proteins and nucleic acids, DNA. Cellulose, another natural polymer, is the principle structure building block of plants. Most natural polymers are condensation polymers, and in their formation from monomers, water is a by-product. One such example is the starch which is made up of hundreds of glucose monomers and that splits out water molecules as they chemically combine [2]. Broadly, natural polymers include, cellulose, starch, proteins, etc. (vegetable origin), rubber, cotton, wool, leather, silk, etc (animal origin), and silicates (minerals). It should

be mentioned that the chemical transformation of the functional groups of natural polymers is capable of establishing a derivative class of natural polymers called 'regenerated polymers'. For instance, cellulose derivatives: cellulose acetate, cellulose nitrate, viscose rayon, etc.

1.3.2. Synthetic polymers

These polymers do not exit in nature and are synthetically prepared. However, they often possess structures close to those of natural polymers. For example, thermoplastics, elastomers, thermosets, etc. Synthetic polymers constitute an invaluable class of polymers in regard particularly to their wide reaching applications. They can further be classified into the following sub-groups:

1.3.2.1. Thermosets

Thermosets or thermosetting polymers are synthetic materials that strengthen during thermal treatment, but cannot be successfully remolded or reheated after their initial heat-forming. Thermosetting plastics will burn when heated after the initial molding contrary to the thermoplastics those can be heated, shaped and cooled as often as necessary without causing a chemical change. Thermosetting plastics, however, have a number of advantages. Unlike thermoplastics, they retain their strength and shape even when heated. This makes thermosetting plastics well-suited to the production of permanent components and large, solid shapes. Additionally, these components have excellent strength attributes (although they are brittle), and will not become weaker when the temperature increases.

Thermoset plastic products are typically produced by heating liquid or powder within a mold, allowing the material to cure into its hardened form. These products can be removed from the mold even without allowing it to cool. The reaction used to produce thermosetting plastic products is not always the result of heating, and is sometimes performed by chemical interaction between specialized materials. Typical examples of thermosetting plastics include epoxies, polyesters, silicones, phenolics, etc. Vulcanized rubber is also an excellent example of a thermosetting plastic as seen in case of a superheated automobile tire which burns but can not be molded into a new shape.

Each type of thermosetting plastic has a unique set of properties. Epoxies, for example, exhibit elasticity, exceptional chemical resistance and are relatively easy to cure. Phenolics however are fairly simple to mold, brittle, strong and hard. Because of their wide range of

characteristics, thermosetting plastics find uses in an extensive variety of applications including, electrical insulation, casting and encapsulation, adhesives, bonding of other materials, surface coatings and domestic appliances [3].

1.3.2.2. Thermoplastics

A thermoplastic, also called a thermo-softening plastic is a plastic which becomes pliable or moldable around their glass transition temperatures (Tg) to a solid state upon cooling. In fact, they become soft when heat is applied and have a smooth, hard finish when cooled. There are a wide range of available thermoplastic formulas that have been created for many different applications. A thermoplastic polymer is made up of long, unlinked polymer molecules, generally with a high molecular weight. Because the molecular chains are unlinked, they rely on other interactions, such as dipole-dipole interactions, aromatic ring stacking, or Van der Waals forces. The molecular chains of thermoplastics generally demonstrate partial alignment (ordering) when cooled below their glass transition temperatures (Tg), resulting in a smooth surface finish and significant structural strength; above that temperature, thermoplastics are elastic. As the temperature increases, thermoplastics gradually soften, eventually melting. Unlike the thermosetting polymers, the thermoplastics can be melted and reused without any change in material properties; moreover, these polymers are worth recycling. Beverage bottles and household containers with resin identification codes are generally thermoplastic polymers. Some of the most commonly found thermoplastic polymers include polyethylenes and polypropylenes. The major difference between thermosets and thermoplastics is based upon their behavior towards the application of heat. Thermosetting polymers undergo an irreversible molecular change when sufficient heat is applied, whereas thermoplastic polymers can be heated and cooled over and over again. Thermoset polymers are used to create permanent structures and are used extensively in composite materials [4].

1.3.2.3. Elastomers

Elastomers often called ‘rubbers’ are the complex materials that exhibit unique combinations of useful properties, the most important being elasticity and resilience. All elastomers have the ability to deform substantially by stretching, compression or torsion and then return almost to their original shape after removal of the force causing the deformation. Their resilience enables them to return quickly to their original shape, enabling for example dynamic seals to follow

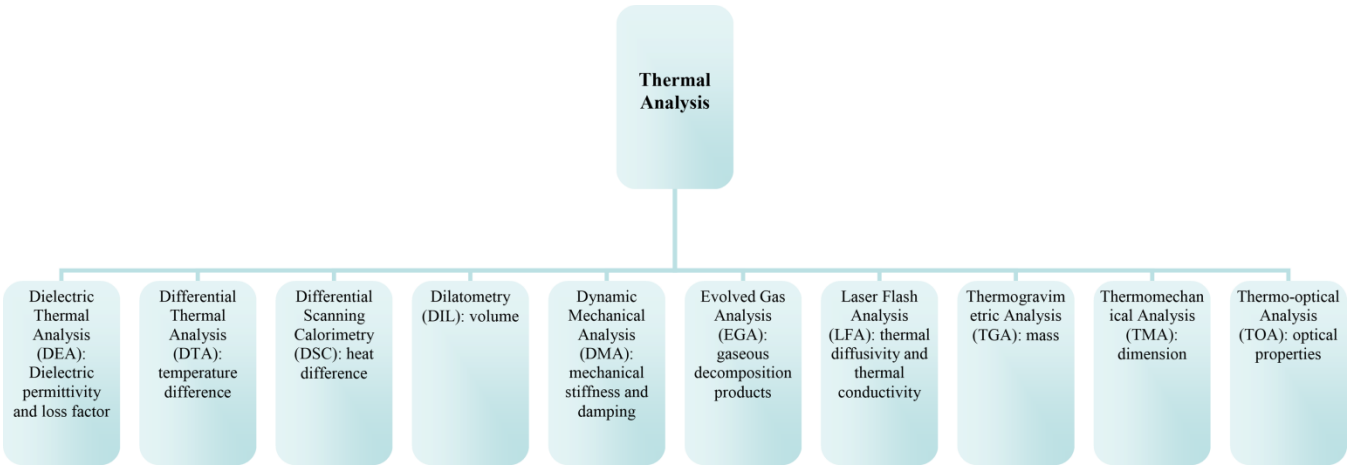

Figure 1.16: Classification of thermal analysis.

The techniques which are related to the scope of the current study will be elaborated in the upcoming sections.

1.11.1. Thermogravimetric analysis (TGA)

Thermogravimetric analysis commonly abbreviated as TGA is a kind of thermal analysis in which the mass loss of a material is measured as a function of increasing temperature (Non-isothermal TGA), or as a function of time at constant temperature (Isothermal TGA) or sometimes under constant mass loss [85]. TGA can provide information about how a material degrades under thermal effect. Degradation under the influence of temperature gives important information regarding the chemical structure of the studied material. It may also provide information about the occurrence of physical phenomena, such as second-order phase transitions including, vaporization, sublimation, absorption, adsorption, and desorption. Likewise, TGA can provide information about chemical phenomena including chemisorptions, desolvation (especially dehydration), decomposition/degradation and solid-gas reactions (e.g., oxidation, reduction, etc.) [85]. TGA is commonly used to determine selected characteristics of materials that exhibit either mass loss or gain due to decomposition, oxidation, or loss of volatiles (such as moisture). Common applications of TGA are:

- Materials characterization through the analysis of characteristic decomposition patterns
- Determination of organic contents in a sample
- Determination of inorganic (e.g. ash) contents in a sample, which may be useful for corroborating predicted material structures or simply used in chemical analysis

- Studies on reaction kinetics and mechanisms [86, 87]

It is an especially useful technique for the study of polymeric materials, including thermoplastics, thermosets, elastomers, plastic films, fibers, coatings, paints and composites [86]. It relies on a high degree of precision. For that reason, the basic instrumental requirements for TGA are a precision balance with a pan loaded with the sample and a programmable furnace. The furnace can be programmed either in isothermal or in non-isothermal mode. Although a non-isothermal analysis is more common, an isothermal analysis can illuminate specific reaction kinetics. Regardless of the furnace programming, the sample is placed in a small, electrically heated furnace equipped with a thermocouple to monitor accurate measurements of the temperature by comparing its voltage output with that of the voltage-versus-temperature table stored in the computer's memory. A reference sample may be placed on another balance in a separate chamber. The atmosphere in the sample chamber may be purged with an inert gas (often nitrogen or helium) to prevent oxidation or other undesired reactions. Figure 1.17 shows the TGA apparatus used to carry out the current research.

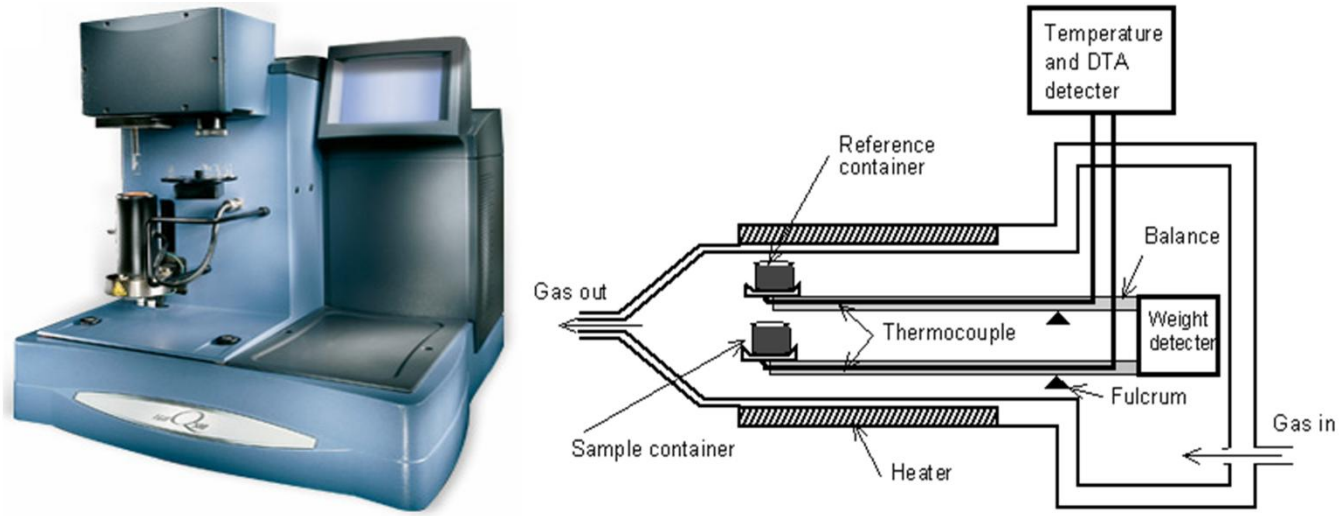

Figure 1.17: A Q500 V20.0 TGA analyzer along with its cross-sectional view [88].

The TGA instrument continuously weighs a sample as it is heated to higher temperatures and can be coupled with FTIR and Mass spectrometric analysis. As the temperature increases, various components of the sample are decomposed and the weight percentage of each resulting mass change can be measured. Results are plotted with temperature on the abscissa and mass loss on the ordinate (details can be found in **Chapter 3)**. The data are adjusted using curve smoothing

and first derivatives are often also plotted to determine points of inflection for more in-depth interpretations [87].

TGA can be used to evaluate the thermal stability of a material. In a desired temperature range, if a species is thermally stable, there will be no observed mass change. Negligible mass loss corresponds to little or no slope in the TGA trace. TGA also gives the upper use temperature of a material. Beyond this temperature the material will begin to degrade.

TGA has a wide variety of applications, including analysis of ceramics and thermally stable polymers. Ceramics usually melt before they decompose as they are thermally stable over a large temperature range, thus TGA is mainly used to investigate the thermal stability of polymers. Most polymers melt or degrade before 200°C. However, there is a class of thermally stable polymers that are able to withstand temperatures of at least 300°C in air and 500°C in inert gases without structural changes or strength loss, which can be analyzed by TGA [89].

Any material can lose mass during heating by three different ways which are through chemical reactions, the release of adsorbed species and decomposition. However, it is important to associate the thermal stability of a material to the nature of gas and its pressure under which the TGA is performed [90]. Polyoxazole, which completely decomposes when heated in air, retains ~60 % mass when heated in N_2. Thus, polyoxazole is thermally stable in nitrogen up to 630 °C, whereas in air, it is almost completely decomposed at that temperature [91].

1.11.2. Differential scanning calorimetry (DSC)

Differential scanning calorimetry or DSC is a thermoanalytical technique in which the difference in the amount of heat required to increase the temperature of a sample and reference is measured as a function of temperature. Both the sample and reference are maintained at nearly the same temperature throughout the experiment. Generally, the temperature program for a DSC analysis is designed such that the sample holder temperature increases linearly as a function of time. The reference sample should have a well-defined heat capacity over the range of temperatures to be scanned. The term DSC was coined to describe this instrument which measures energy directly and allows precise measurements of heat capacity [92].

The basic principle underlying this technique is that when a sample undergoes a transformation such as phase transition (physical), heat will be required to flow through it and the reference in order to maintain the both at the same temperature. The amount of heat required

depends on whether the process is exothermic or endothermic. By observing the difference in heat flow between the sample and reference, differential scanning calorimeters are able to measure the amount of heat absorbed or released during such transformation. DSC may also be used to observe more subtle physical changes, such as glass transitions, crystallization, etc. It is widely used in industrial settings as a quality control instrument due to its applicability in evaluating sample purity and for studying polymer curing [93-95].

Differential scanning calorimetry can be used to measure a number of characteristic properties of a sample. Using this technique it is possible to observe fusion and crystallization events as well as glass transition temperatures T_g. DSC can also be used to study oxidation, as well as other chemical reactions [93, 94, 96]. Glass transitions may occur as the temperature of an amorphous solid is increased. These transitions appear as a step in the baseline of the recorded DSC signal. This is due to the sample undergoing a change in heat capacity; no formal phase change occurs [93, 95]. As the temperature increases, an amorphous solid will become less viscous. At some point the molecules may obtain enough freedom of motion to spontaneously arrange themselves into a crystalline form. This is known as the crystallization temperature (T_c). This transition from amorphous to crystalline solid is an exothermic process and results in a peak in the DSC signal. As the temperature increases, the sample eventually reaches its melting temperature (T_m). The melting process results in an endothermic peak in the DSC curve. The ability to determine transition temperatures and enthalpies makes DSC a valuable tool in producing phase diagrams for various chemical systems [93]. A simple differential scanning calorimeter with its mode of functionality has been shown in Figure 1.18.

DSC is widely used for examining polymeric materials to determine their thermal transformations. The observed thermal transformations can be utilized to compare materials; although, the transitions do not uniquely identify composition. Composition of unknown materials may be complementarily evaluated by using techniques such as IR, XRD, etc. Melting points and glass transition temperatures for most polymers are available from standard compilations and the method can show polymer degradation by the lowering of expected melting point, T_m. T_m depends on the molecular weight of the polymer and thermal history, so lower grades may have lower melting points than expected. The percent crystalline contents of a polymer can be estimated from the crystallization/melting peaks of the DSC graph as reference heats of fusion can be found in the literature [98].

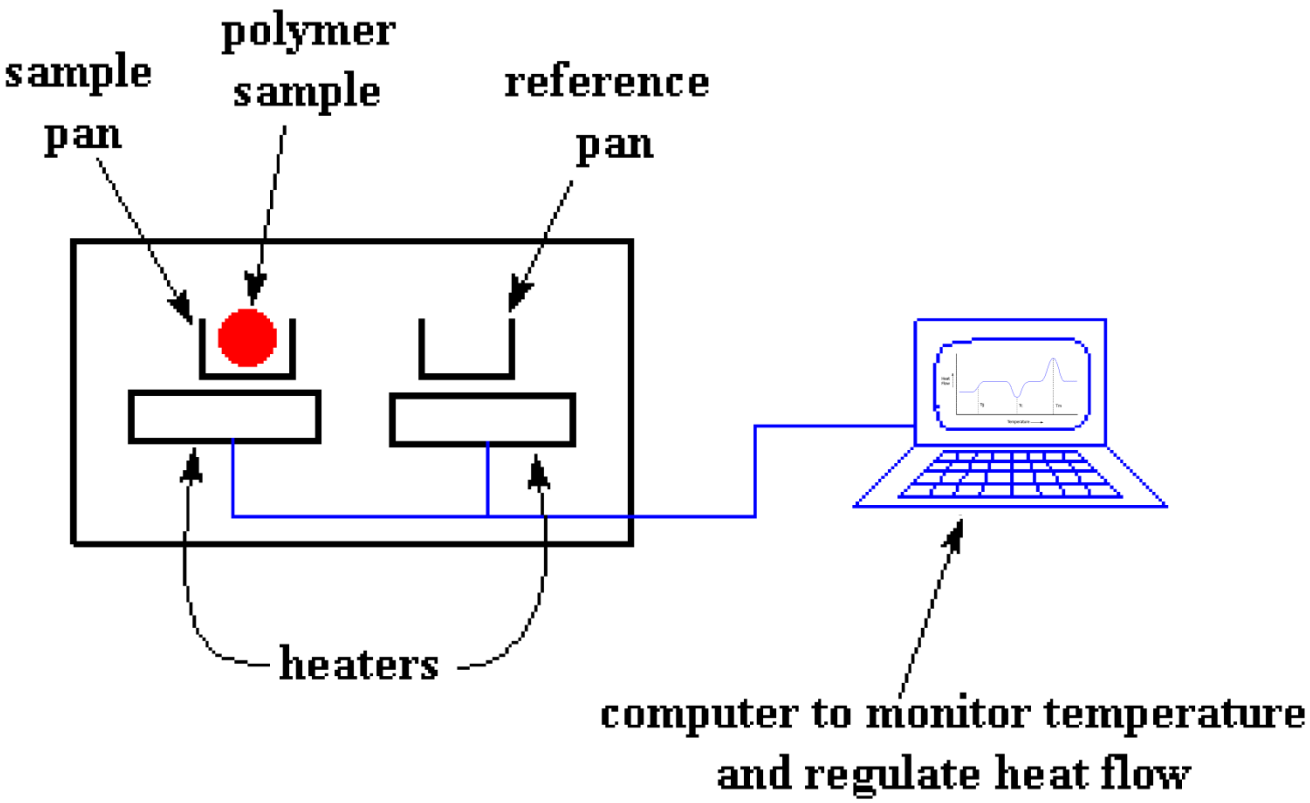

Figure 1.18: A simple differential scanning calorimeter [97].

DSC can also be used to study thermal degradation of polymers using an approach such as Oxidative Onset Temperature/Time (OOT); however, the user risks contamination of the DSC cell, which can be problematic. Thermogravimetric Analysis (TGA) may be more useful for decomposition behavior determination as been utilized in our study. Impurities in polymers can be determined by examining thermo-grams for anomalous peaks and plasticizers can be detected at their characteristic boiling points. In addition, examination of minor events in first heat thermal analysis data can be useful as these apparently "anomalous peaks" can in fact also be representative of process or storage thermal history of the material or polymer physical aging. Comparison of first and second heat data collected at consistent heating rates can allow the analysts to have acquaintance about both the polymer processing history and material properties.
In certain cases, simultaneous Thermal Analysis (STA) is employed to study the thermal behaviors of materials. Simultaneous Thermal Analysis (STA) refers to the simultaneous application of Thermogravimetry (TGA) and differential scanning calorimetry (DSC) to the same sample in a single instrument. The internal/external testing conditions should be perfectly

identical for the TGA/DSC signals; for instance, same atmosphere, gas flow rate, vapor pressure of the sample, heating rate, thermal contact to the sample crucible and sensor, radiation effect, etc. The information gathered can even be enhanced by coupling the STA instrument to an Evolved Gas Analyzer (EGA) like Fourier transform infrared spectroscopy (FTIR) or mass spectrometry (MS).

1.11.3. Differential thermal analysis (DTA)

An alternative technique, which shares much in common with DSC, is differential thermal analysis (DTA). In this technique it is the heat flow to the sample and reference that remains the same rather than the temperature. When the sample and reference are heated identically, phase changes and other thermal processes cause a difference in temperature between the sample and reference. Both DSC and DTA are capable of providing similar information. DSC measures the energy required to keep both the reference and the sample at the same temperature whereas DTA measures the difference in temperature between the sample and the reference when they are both kept under the same heat [99]. Nevertheless, DSC furnishes relatively precise information and therefore generally preferable over DTA in the case of analyzing thermally activated phase transformations in materials.

1.12. Conclusion

In the present chapter, a brief introduction to the polymers and composites of polymers is given, and an account of the techniques of their structural characterization and thermal analysis is reported. Emphasis is put on the metal-filled polymer composites with special regard to composites of epoxy and urea-formaldehyde (UFC) resins filled with metal particles. The information presented in this chapter will be useful in the interpretation of results and discussion on the morpholgies and thermal degradtion bevahiors of epoxy/metal and UFC/metal composites in the upcoming chapters.

Chapter 2

Kinetic Analysis of Thermally Stimulated Solid State Processes

2.1. Introduction

A thermally stimulated solid state process belongs to that class solid state processes in which the system needs to cross a potential energy barrier in order to shift it from reactants to products. The energy distribution along the relevant coordinates in such a system is known to be governed by Boltzmann statistics. If the processes occurring in solid state are taken into consideration, several prominent physical phenomena and chemical reactions fall in this category. Physical phenomena include; vaporization and sublimation, glass transition and glass aging, nucleation, melting and crystallization of polymers, solid-solid phase transitions (for instance, allotropic, ferromagnetic to paramagnetic transitions, etc.), etc. On the other hand, chemical reactions comprise; thermal decomposition of organic/inorganic materials, polymerization/depolymerization and cross linking reactions in polymers and thermal/thermo-oxidative degradation of polymeric materials. Thermally stimulated solid state processes can be theoretically modeled by employing solid state kinetics. Indeed, kinetic modeling of such processes simulates their reaction rates by parameterizing generally the two variables i.e; degree of conversion 'α' and temperature 'T', using activation parameters and reaction model(s) in order to probe those process [100, 101].

Kinetic analysis of solid state processes is carried out by thermal analysis methods (TGA and DSC principally) which are not species specific. By measuring the evolution of overall physical properties (mass loss or heat variations of the system) of a system, these methods provide information on macroscopic kinetics. The macroscopic kinetics is inherently complex because it includes information about multiple steps that can occur simultaneously. Unscrambling complex kinetics presents a serious challenge that can only be met by kinetic methods that provide means of detecting and treating multi-step processes (parallel and/or consecutive). In accordance with the results of the ICTAC Kinetics Project [102-106] and ICTAC kinetic committee recommendations [107], only the methods that use multiple thermal histories (isothermal/non-isothermal) can meet this challenge. Indeed, isoconversional or model-free methods are the most popular of the methods based on the use of multiple thermal histories. The present chapter provides an introduction to the kinetics of solid state processes, emphasizing on the most common kinetic methods, model-free as well as model-fitting. Certain important problems faced by various kinetic methods and the appropriate ways to resolve those problems will also be suggested.

2.2. Theoretical basis of solid state kinetics

The progress of a thermally stimulated condensed phase process, determined by thermogravimetric analysis (TGA), is denoted by a term degree of conversion 'α' which is defined as following:

$$\alpha = \frac{m_0 - m_t}{m_0 - m_\infty} \tag{2.1}$$

Where, 'm_0' is the initial mass of reactant, 'm_t' is its mass at certain temperature (non-isothermal analysis) or time (isothermal analysis) during the reaction and 'm_∞' is its mass at the end of reaction. If differential scanning calorimetry (DSC) is employed to carry out the kinetic analysis, the degree of conversion can be determined by the following expressions:

In non-isothermal DSC,

$$\alpha_T = \frac{\Delta H_T}{\Delta H_{Total}} = \frac{\int_{T_0}^{T} \left(\frac{dH}{dT}\right) dT}{\int_{T}^{T_\infty} \left(\frac{dH}{dT}\right) dT} \tag{2.2}$$

In isothermal DSC,

$$\alpha_t = \frac{\Delta H_t}{\Delta H_{Total}} = \frac{\int_{t_0}^{t} \left(\frac{dH}{dt}\right) dt}{\int_{t}^{t_\infty} \left(\frac{dH}{dt}\right) dt} \tag{2.3}$$

Where, T_0, T & T_∞ and t_0, t & t_∞ are the onset, arbitrary and end process temperatures/times respectively; dH is the heat released in an infinitesimally small temperature or time interval dT or dt respectively.

In condensed phase processes, the reaction rate dα/dt being a function of 'α' can be represented as:

$$\frac{d\alpha}{dt} = kf(\alpha) \tag{2.4}$$

Table 2.1: Well known reaction models of solid state processes.

Reaction Model	Notation	*f(α)*
Reaction order [111]	RO (n)	$(1-\alpha)^n$
Contracting area [111]	R2	$2(1-\alpha)^{1/2}$
Contracting volume [111]	R3	$3(1-\alpha)^{2/3}$
Mampel (1^{st} order reaction model) [107]	F1	$(1-\alpha)$
Johnson-Mehl-Avrami equation [112]	JMA (p>1)	$p(1-\alpha)\{-\ln(1-\alpha)\}^{1-1/p}$
JMA (p = 2) [107]	A2	$2(1-\alpha)\{-\ln(1-\alpha)\}^{1/2}$
JMA (p = 3) [107]	A3	$3(1-\alpha)\{-\ln(1-\alpha)\}^{2/3}$
JMA (p = 2) [107]	A4	$4(1-\alpha)\{-\ln(1-\alpha)\}^{3/4}$
1D-diffusion [113]	D_1	$1/2\alpha$
2D-diffusion [114]	D_2	$-1/\ln(1-\alpha)$
3D-diffusion (Ginstling equation) [115]	D_3	$\frac{3(1-\alpha)^{2/3}}{2\{1-(1-\alpha)^{1/3}\}}$
3D-diffusion (Jander's equation) [116]	D_4	$\frac{3}{2\{(1-\alpha)^{-1/3}-1\}}$
Šesták-Berggren model [117]	SB (m, n)	$(\alpha)^m(1-\alpha)^n$
Prout-Tompkin equation [111] (Autocatalysis)	P-T	$\alpha(1-\alpha)$
Power Law [118] (Nucleation)	Pr	$r(\alpha)^{(1-1/r)}$

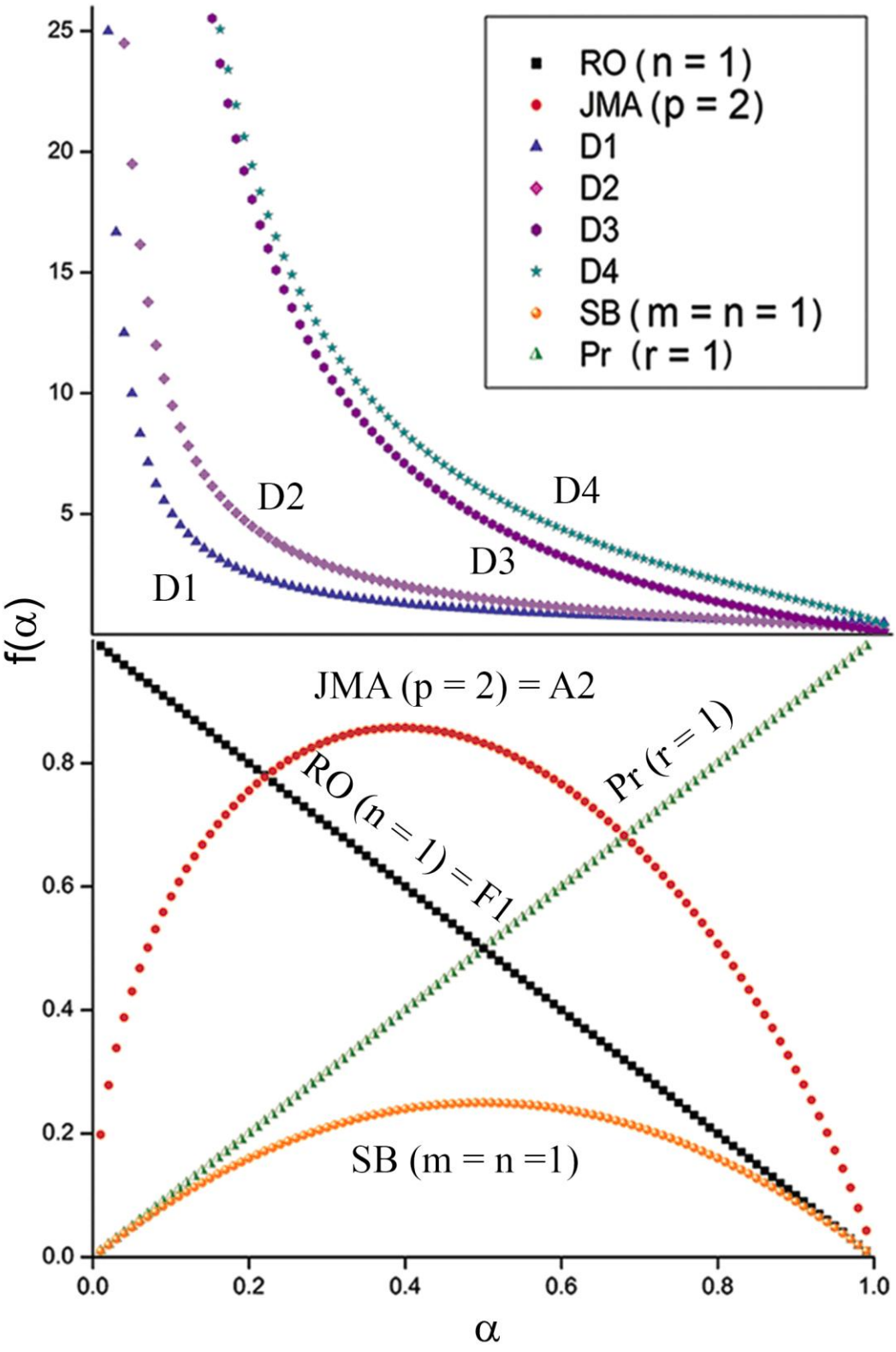

Figure 2.1: Graphical representation of different cases of well known solid state reaction models (Table 2.1).

Eq. (2.4) is the basic kinetic equation of condensed phase processes. In the case of thermally stimulated processes, the value of rate constant 'k' is often substituted in Eq. (2.4) by Arrhenius equation which then takes the following form;

$$\frac{d\alpha}{dt} = A\exp(-E_\alpha / RT) f(\alpha) \tag{2.5}$$

Where, 'A' is the pre-exponential factor, E_α is the energy of activation, f(α) is the function of degree of conversion, called reaction model, and R is gas constant. Physically, 'A' describes the collision frequency of the particles involved in the formation of activated complex, Eα is the activation energy barrier(s) of reaction, and f(α) is an expression for the mechanism(s) of reaction [100]. A union of {*A, E_α, f(α)*} is known as kinetic triplet. Unlike rate laws in homogenous kinetics which usually depend on reaction order, a rate law for an elementary solid-state reaction may depend on factors such as rate of nuclei formation, interface advancement, diffusion, and/or geometrical shape of solid particles. These factors lead to several decomposition models [108-110] that do not exist in homogenous kinetics. Some well known solid state reaction models are given in Table 2.1 and Figure 2.1. In order to evaluate the kinetic triplet, usually activation energy is determined initially, followed by the reaction model and eventually the pre-exponential factor. The same methodology has been adopted in this work.

2.3. Determination of activation energy

Isoconversional methods are employed to examine the variation in activation energy with the degree of conversion, and therefore the nature and complexity of process. Isoconversional methods are based on the isoconversional principle which states that; "*At certain degree of conversion, the rate of a solid state reaction depends only upon the temperature*". A solid state process is fairly approximated as single step if the variation in its activation energy with the degree of conversion, determined by isoconversional methods, is insubstantial; otherwise, the reaction is deemed as following a complex reaction pathway. Isoconversional methods can be isothermal/non-isothermal, differential/integral and linear/nonlinear [100].

2.3.1. Differential isoconversional method

Taking logarithm of Eq. (2.5) gives the following linear differential isoconversional method, known as the Friedman's method [119].

If reaction model is known over the whole domain of α, then the following equation is helpful in determining the pre-exponential factor over that domain:

$$A_\alpha = \frac{\exp(C_\alpha)}{f(\alpha)} \tag{2.37}$$

2.7. Computing reaction models in the case of multi-step processes

Although the *h(α)* functions as shown in Table 2.4 and graphically in Figure 2.4 can may guide to the most probable reaction models in the case of single-step processes, yet such processes are not very common in solid state kinetics in accordance with the variable activation energy concept [137, 139, 158, 159]. An accurate picture of reaction model over the whole range of degree of conversion for complicated multi-step reactions can however be visualized by the proposed approach. By definition, *h(α)* function is expressed as following:

$$\frac{f'(\alpha)}{f(\alpha)} = h(\alpha) \tag{2.38}$$

Integration of Eq. (2.38) yields the following relation:

$$f(\alpha) = \exp\left(\int_{\alpha_0}^{1} h(\alpha) d\alpha \right) \tag{2.39}$$

Where, α_0 is a value greater than zero, obtained by adding an infinitesimally small positive digit to zero. Reaction models of complex condensed phase processes can be determined by performing numerical integration of the curve obtained from Eqs. (2.26)-(2.29) in non-isothermal kinetics and/or Eq. (2.33) in isothermal kinetics over (0, 1] and taking natural exponent of the resulting definite integral. A relatively more efficient numerical integration algorithm which is also recommended in the present work is the Guassian Quadrature or its modified form [160, 161]. This alternate approach could be quite helpful for determining the reaction models for complicated processes.

A serious issue in the case of multi-step processes is associated with identifying the mechanisms of the individual reactions within them. This trouble originates from the fact that only nucleation/growth models show peak functions, and the rest of reaction models (if available in the reaction model curve) might not be visible in the plots of *f(α)*. In order to solve this matter,

an advanced kinetic function $F(\alpha, T)$, taking into account the variation of reaction mechanism with temperature, is introduced in non-isothermal kinetics which is defined as [153, 154]:

$$F(\alpha, T) = \frac{df(\alpha)}{dT} = f'(\alpha)\frac{d\alpha}{dT} = \frac{1}{\beta} f'(\alpha)\frac{d\alpha}{dt} \tag{2.40}$$

The obtained characteristic shapes of $F(\alpha, T)$ functions by applying Eq. (2.40) on the well known reaction models shown in Table 2.1, using an arbitrary single-step reaction simulated by Runge-Kutta (RK4) method at 10 °C.min^{-1}, are represented in Figure 2.5.

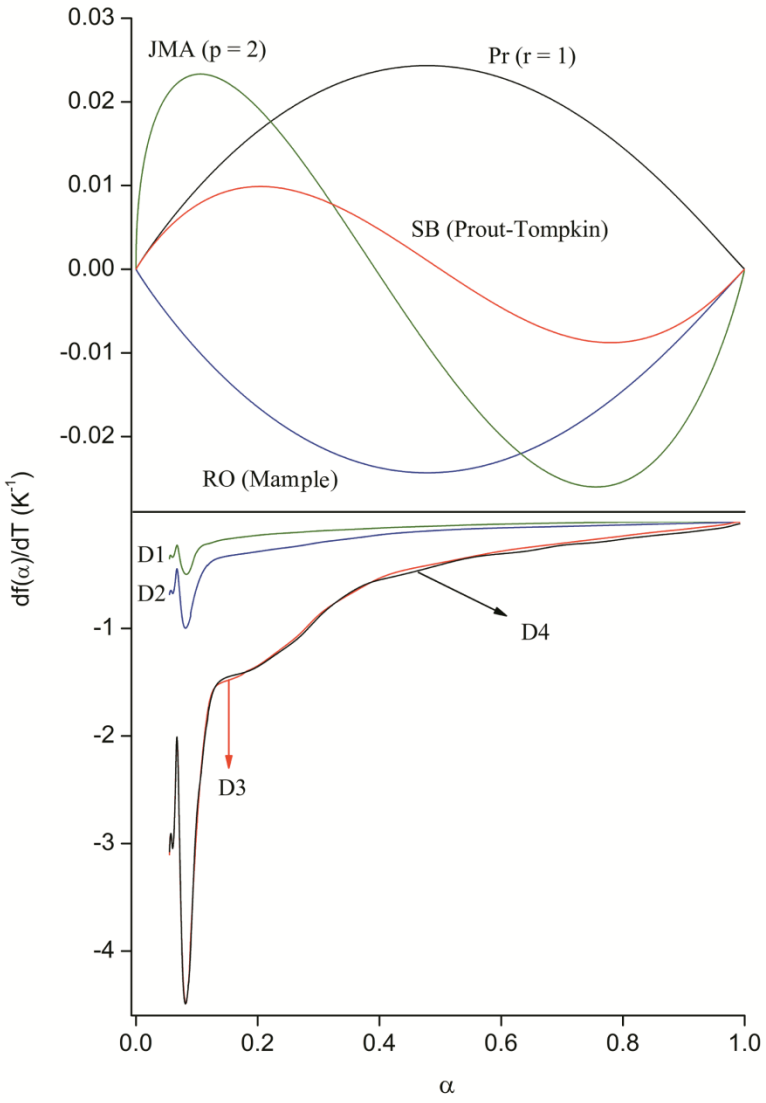

Figure 2.5: Graphical representation of the application of new kinetic function F(α, T) = df(α)/dT on reaction models descried in Figure 2.1 at 10 °C.min^{-1}.

The activation energy and pre-exponential factor related to the simulated single-step reaction are: E = 80 kJ.mol^{-1} and A = 2×10^{8} s^{-1}, respectively. It is suggested that $F(\alpha, T)$ function could be highly useful in identifying and distinguishing between various individual reaction mechanisms in a multi-step process.

The efficacy of the advanced kinetic approach over the pre-existing reaction model determination methodologies in order to kinetically interpret solid state reaction mechanisms has already been elaborated in the literature [126]. Certain important applications of the advanced kinetic approach on various emerging research domains include, polymers/polymers composites [162] (will be discussed in **Chapters 4-5**), fuel [163], materials science and engineering [164-166], management and valorization of waste [167], and crystallization in amorphous materials (will be elaborated in **Chapter 7).** In addition, the suggested approach is not limited to the mentioned domains but it has also been extended to organic photovoltaics (OPV's) in order to manipulate the stability and degradation issues in OPV devices (details will be given in chapter 6).

2.8. Conclusion

In this chapter, a brief account of the kinetics of thermally stimulated solid state processes is given and discussed. Various kinetic approaches to model the thermally activated processes in solid state along with their merits and demerits are reported. Certain important issues concerning the mechanisms of complicated multi-step condensed phase processes are also pointed out and addressed. The information presented in this chapter will serve in one hand, predicting the thermal degradation mechanisms of epoxy and urea-formaldehyde composites filled with metal particles. On the other hand, it will be exploited in putting forward plausible solutions to some of the important problems regarding the stability and degradation of organic photovoltaic devices and kinetics of crystallization in amorphous materials.

Chapter 3

Formation and Structural Characterization of Polymer (Epoxy, UFC)/Metal (Al, Zn, Sn) Composites

3.1. Introduction

Polymer composites establish a fascinating class of materials in particular regard to their valuable worldwide applications [168]. Indeed, the low density of these composites got various advantages over other materials, including facility of processing, ability to absorb mechanical shock, flexibility, corrosion resistance and electrical properties control [169]. These composites are used in different technological applications in a variety of areas such as chemical sensors, conductive adhesives, photothermal optical recording, self regulating heaters, electromagnetic/radio frequency interference (EMI/RFI) shielding for electronic devices (computer and cellular housings for example), cold seals, electromagnetic shielding effectiveness (EMSE) on the plane-wave, over-current protection devices, direction finding antennas, intermediate layers for high voltage cables, static charges dissipating materials, energy storage, flame retardancy, organic electronic components: photovoltaic solar cells (OPVs), shape memory devices, organic light emitting diodes (OLEDs), and many more [170].

As discussed in the 1st chapter, composites of polyepoxy or simply epoxy (term attributed to cured epoxy resin) and urea-formaldehyde cellulose (UFC) belong to the mentioned class of polymer composites. An important subclass of epoxy and UFC polymer composites is formed by filling them with metal particles [32, 52, 63, 66-68, 171, 172]. The polymer/metal composites thus generated may either be electrically/thermally insulating or conducting; although both of them are equally useful due to their wide-reaching applications [32, 62, 63, 170, 173-175]. Nevertheless, there are still several crucial issues with these materials that remain to be addressed. One necessary task is developing process control for their eventual efficiency optimization. This task indeed requires profound insights into the said materials; necessarily, their molecular structures and nature and type of phases/bonding exist in them need consideration.

In the above mentioned frame of reference, the present chapter deals with the preparation, and structural characterization of epoxy and UFC composites filled with aluminum (Al), zinc (Zn) and tin (Sn) particles. The general criteria for the metals' selection in the present research work for the formation of composites have been their non-poisonous, abundance and cheapness, light weight, good conductance, ability of exhibiting self passivity, and more prominently ease of the formation of composites [31, 171, 172, 176]. Specifically, the linkage between polymer (particularly in the case of epoxy) and aluminum is industrially important in view of improving

the polymer adhesion by the addition of aluminum [59]. Polymer/zinc composites might be capable of depicting improved thermal and mechanical stability, electrical bi-stability (demonstrated by a system with two stable equilibrium states), electromagnetic interference shielding, and antimicrobial activity [177-180]. While, particular interest in tin lies due to its malleability and ductility, ease of alloy formation by having low melting point, and relatively higher chemical inertness [181]. Therefore in this chapter, the formation of epoxy and UFC composites filled with Al, Zn and Sn particles and their structural characterizations by scanning electron microscopy (SEM), x-ray diffraction (XRD) and Fourier transform infrared (FTIR) spectroscopy will be reported. The obtained results will then be interpreted, compared and discussed.

3.2. Experimental details

3.2.1. Formation of epoxy and UFC composites filled with metals

The epoxy matrix used was diglycidyl ether of bisphenol-A (DGEBA/Epoxy F) associated with a hardener (HY956) of triethylene tetramine of Ciba-Geigy society. The chemical formulae of epoxy and hardener are given in Figure 3.1.

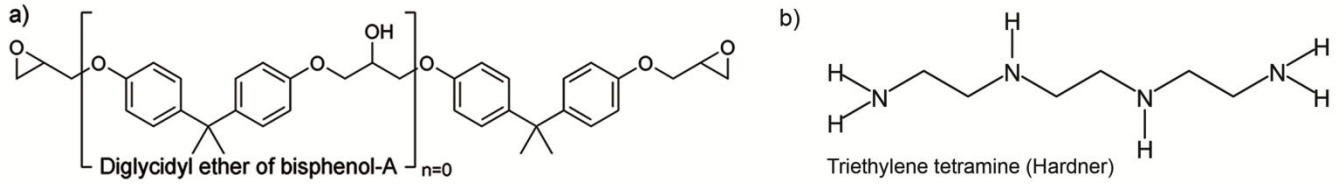

Figure 3.1: Chemical formulae of (a) diglycidyl ether of bisphenol-A (DGEBA). (b) Triethylene tetramine (TETA)

Some of the characteristics of cured epoxy resin are shown in Table 3.1 [170].

Table 3.1: Physical characteristics of epoxy used in the study at room temperature [170].

Sample	d (g/cm^3)	ρ (μΩ.cm)	η (mPa.s)
Epoxy F	1.14	1.34×10^{14}	9×10^{3}-10×10^{3}

The fillers were commercial powders of aluminum, zinc and tin delivered by Panreac (Castellar del Vallès, Spain) with some of the characteristics which have been listed in Table 3.2. All the composites were prepared by introducing calculated quantities of metallic powder into the fluid resin and dispersed manually to obtain the homogeneity. The formed viscous suspensions were made to flow in Teflon mould casts and placed during one hour on the rotating rollers in oven maintained at 100 °C. The mixtures were rotated during polymerization process, in order to prevent the sedimentation of the particles whose densities were larger than those of polymeric ones [170].

Table 3.2: Physical characteristics of the metals employed in the study at room temperature [170].

Sample	Purity (%)	φ (μm)	d (g/cm^3)	ρ (μΩ.cm)
Aluminium	98	30-70	2.70	2.653
Zinc	96	15±10	7.14	6.024
Tin (β)	97	15±10	7.29	11.5

A probable curing reaction scheme of the formation of epoxy resin (during the formation of composites) is given in Figure 3.2, in the general form [14].

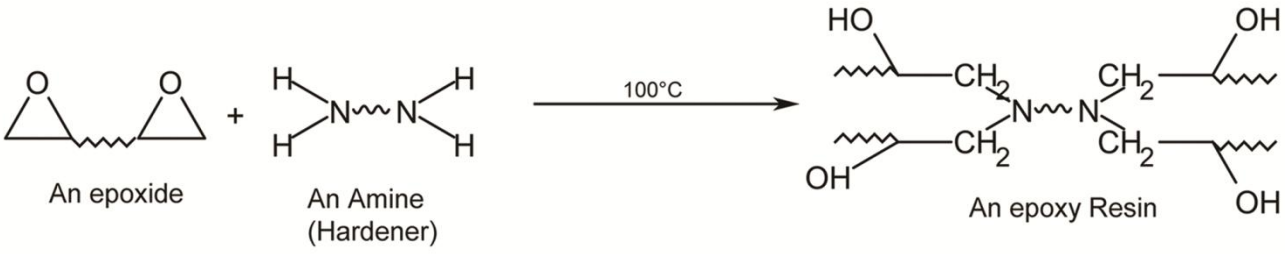

Figure 3.2: Curing reaction between DGEBA (Diglycidyl ether of bisphenol-A) and amine.

In order to form UFC/metal composites, commercial grade urea-formaldehyde resin filled with α-cellulose having density 1.38 g.cm^{-3} was obtained from Aicar S.A (Cerdanyola del Vallès, Spain). The total contents of α-cellulose contained by UFC resin were 30% by weight.

The fillers were commercial powders of aluminum, zinc and tin delivered by Panreac (Castellar del Vallès, Spain) with some of the characteristics already given in Table 3.2. Both the resin and the metal powders were thoroughly dried at 60 °C for 48 h prior to use.

Composites of metal-filled UFC were fabricated (by Professor Gabriel Pinto from Departamento de Ingeniería Química Industrial y del Medio Ambiente, ETSI, Industriales, Universidad Politécnica de Madrid, 28006 Madrid, Spain)* via blending and hot pressing route, by mixing the polymer matrix and the powders of metallic fillers for 2 h in an especially designed internal mixer which operates with a rotation frequency of 60 revolutions per minute (rpm). The mixings were followed by compression molding in a specifically designed mold with three cavities of 30.0 mm diameter and 3.0 mm thickness each one. The molding parameters were 20 MPa and 150 °C for 30 min. The freshly prepared samples were cooled at room temperature for 30 min. In order to improve the sample finishing and better structural characterization results, the surfaces were polished with sandpaper [52, 66, 68].

3.2.2. Morphological analysis of neat epoxy/UFC and metal-filled epoxy and UFC composites by scanning electron microscopy (SEM), x-ray diffraction (XRD) and Fourier transform infrared (FTIR) analyses

In order to carry out the morphological analysis of neat epoxy and UFC resins and metals-filled composites of epoxy and UFC, in each case, an insulator/conductor pair of composites was chosen above and below the electrical conducting percolation threshold as shown in Table 3.3, in accordance with the discussion carried out in **Chapter 1**. Each composite in insulator/conductor pairs was symbolized as shown in Table 3.3.

The homogeneity of pure epoxy and epoxy/metal composites, their morphologies, and the dispersion of metallic particles inside the composite materials along with the polymer-metal interphases were analyzed by the scanning electron microscope Philips XL30 with an accelerating voltage of 20 kV of UATRS (Unités d'Appui Techniques à la Recherche Scientifique du CNRST: Centre National pour la Recherche Scientifique et Technique, Maroc)*. In the case pure UFC and UFC/metal composites, ultra high resolution cold field emission scanning electron microscope UHR Cold-Emission FE-SEM SU8000 (HITACHI, Tokyo, Japan) of Instituto de Ciencia y Tecnología de Polímeros (ICTP), CSIC, Madrid, Spain (under the direction of Professor Rosario Benavente)*, with accelerating voltages 2-3 kV was employed.

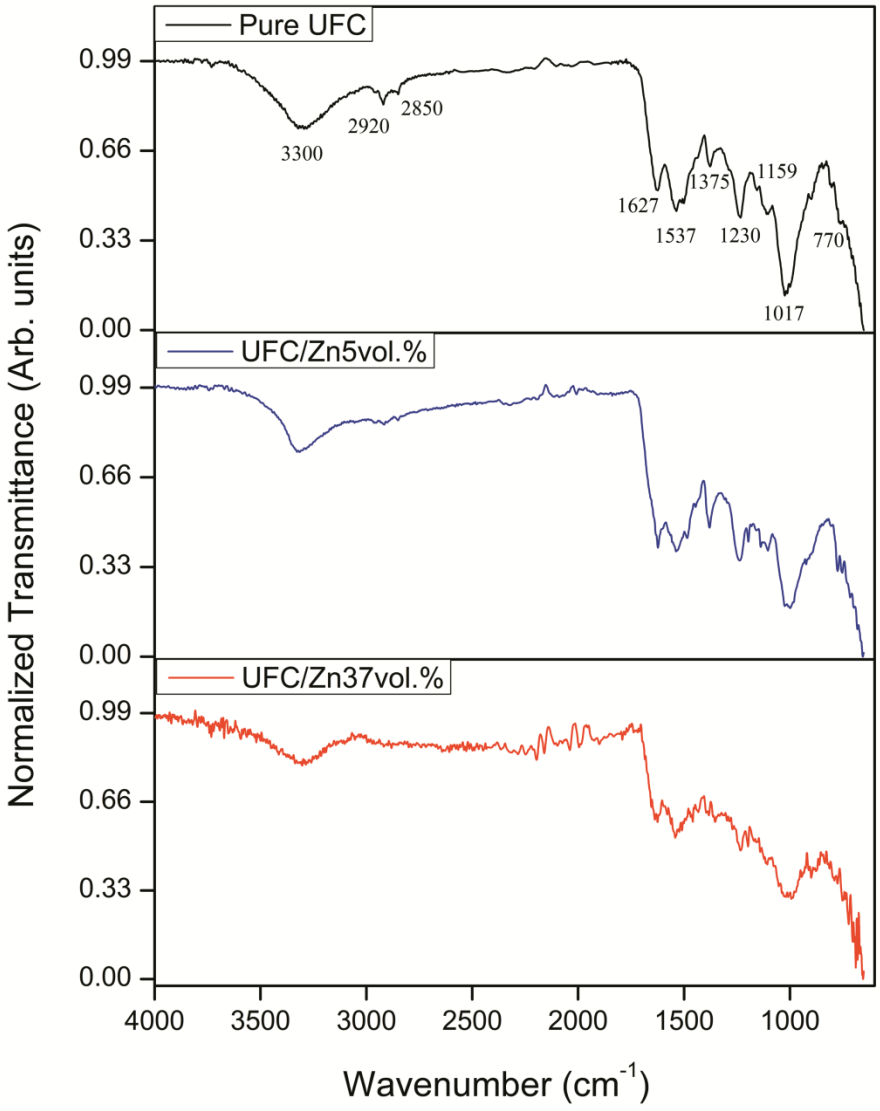

Figure 3.28: Fourier transform infrared spectra of pure UFC, UFC/Zn5vol.% and UFC/Zn37vol.%.

Figure 3.28 points out that the FTIR spectra of UFC/Zn composites are analogous to each other and to the FTIR spectrum of pure UFC resin. It therefore reveals that the UFC resin is not chemically modified by the nature and contents of zinc during the formation of composites. The reduction in the band/peak intensities in the case of UFC/Zn37vol.% is more probably due to decrease in relative proportion of UFC in the conducting composite, as pointed out in XRD of UFC/Zn37vol.% composite.

The FTIR analysis results of UFC/Sn composites along with the FTIR spectrum of pure UFC resin are shown in Figure 3.29.

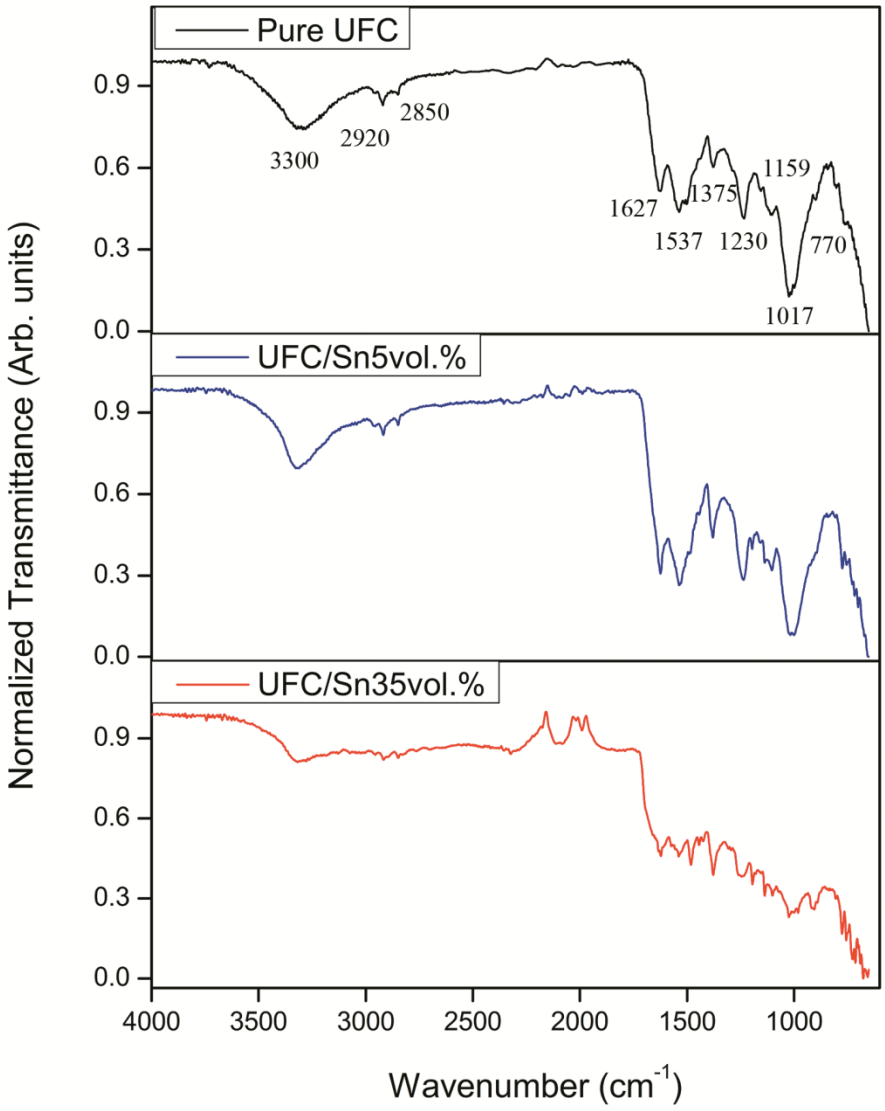

Figure 3.29: FTIR spectra of pure UFC, UFC/Sn5vol.% and UFC/Sn35vol.%.

Similar to UFC/Al and UFC/Zn composites, the FTIR spectra of UFC/Sn composites seem resembling with each other and to that of pure UFC which verifies that the introduction of tin into UFC resin during the formation of UFC/Sn composites does not result into chemical reaction(s). Accordingly (and neglecting the noise), remarkable reduction in the peak intensities of UFC/Sn35vol.% composite FTIR spectrum is due to decrease in the relative proportion of UFC in conducting composite, as pointed out in XRD of UFC/Sn35vol.% composite.

The congruent information thus obtained by SEM, XRD and FTIR analyses of pure UFC and UFC/metal composites suggests that these materials are fairly homogeneous, and that the interactions between UFC and metals in composites might not be chemical in nature [192, 194, 195].

3.4. Conclusion

In the present chapter, a detailed account of the preparation and structural characterization of insulating and conducting polymer composites of epoxy and UFC filled with aluminum, zinc and tin have been given. The epoxy/metal composites were successfully prepared by a conventional polymer composite formation technique, while UFC/metal composites were prepared by an especially designed experimental protocol. Epoxy/metal and UFC/metal composites thus formed were structurally characterized by SEM, XRD and FTIR analyses. Structural characterization results of epoxy/metal composites reveal that the composites are fairly homogeneous, and the polymer-metal interactions do not probably result in any kind of chemical interphase formation. Similar results are given by UFC/metal composites. On the whole, the obtained inferences suggest that the influence of metals on the morphologies of studied polymers depend on the nature/contents of metals and polymers. For instance, tin induces similar mechanical effects on the morphologies of epoxy and UFC. Aluminum, on the other hand is capable of introducing cracks in the structure of epoxy (at higher filler loadings) which may probably affect negatively on its mechanical properties. Nevertheless, aluminum diminishes the porosity in UFC/Al composites which may lead to improve the mechanical properties of UFC/Al composites. Zinc, although, has an inverse effect on the morphologies of epoxy and UFC in comparison with aluminum. We find that epoxy/Zn composites demonstrate insignificant porosity with expectedly good mechanical performance. However, zinc introduces cracks in UFC structure and enhances its porosity which might adversely affect the mechanical properties of UFC/Zn composites. The obtained results elucidate that the composites are worthy to be subjected to further assessments. The information obtained in this chapter will assist in explaining and interpreting the results of thermal behaviors of the polymer/metal composites in the upcoming chapter.

Chapter 4

Thermal Analysis of Polymer (Epoxy, UFC)/Metal (Al, Zn, Sn) Composites

4.1. Introduction

In the previous chapter, a detailed account of the structural characterization of epoxy and UFC composites filled with particles of metals (Al, Zn and Sn) was given and discussed. It was eventually inferred that the polymer/metal composites were of adequate quality to carry out further characterizations/analyses in order to address the process control issues for their eventual efficiency optimization. Responding to the said issues further demands consideration of the temperature dependent processes taking place in the composites and their underlying mechanisms. In this frame of reference, the present chapter deals with the assessment of the thermal behavior of epoxy and UFC composites filled with Al, Zn and Sn particles over long temperature ranges. The obtained results will be compared, interpreted and discussed.

4.2. Thermogravimetric (TG) and differential thermogravimetric (DTG) analyses of polymer/metal composites

The thermoanalytical data of epoxy, UFC and their composites were collected by Q500 V20.0 TGA analyzer (TA Instruments-Waters, Massachusetts, Unites Sates) from the Instituto de Ciencia y Tecnología de Polímeros (ICTP), CSIC, Madrid, Spain (under the direction of Professor Rosario Benavente)*, under non-isothermal experiment mode, employing samples of nearly similar geometries having masses 8-12 mg, in the range of heating rates, β = 2–25 °C.min^{-1} to carry out the kinetic study of resin and composites from 30 to 600 °C under 90 ml.min^{-1} nitrogen flow (Figure 1.16). The ICTAC kinetic committee recommendations for collecting reliable thermoanalytical data and for performing kinetic analysis [107, 206] were respected while undertaking this study.

4.3. Thermal degradation behaviors of neat epoxy and epoxy/metal composites

The thermogravimetric (TG) and derivative of thermogravimetric (DTG) curves of pure epoxy as functions of temperature at different heating rates, under the experimental conditions described in the previous section, are shown in Figure 4.1. The basic purpose of drawing TG/DTG curves versus temperature over different heating rates is to verify replicability (and therefore reliability) of experiments and to speculate about the nature (single-step/multi-step) of degradation pathway [107, 206] and its variation with heating rate [207, 208].

* The concerned is gratefully acknowledged.

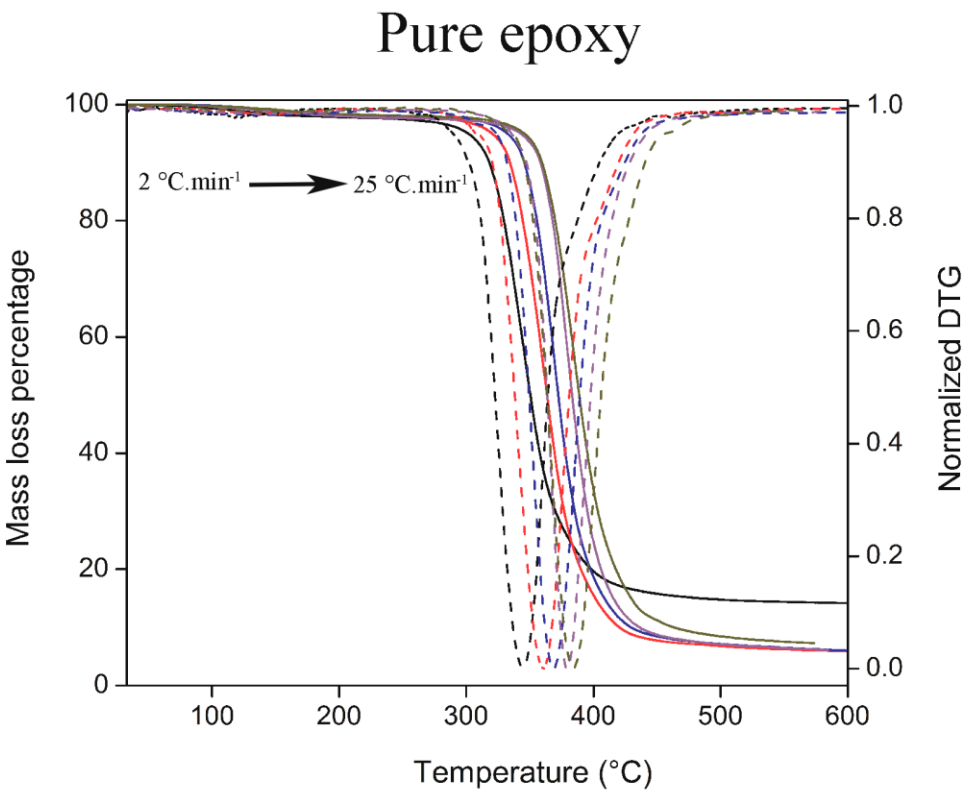

Figure 4.1: TG/DTG curves of neat epoxy resin at different heating rates.

It can be seen in Figure 4.1 that not only the inset (initial) and offset (final) temperatures but also T_m (temperature at maximum reaction rate) shift towards higher temperatures by increasing the heating rate. The shift of a TG/DTG curve to higher temperatures generally occurs when the heating rate is increased, and it is typical for all non-isothermal experiments (see the upcoming sections). This is because, at lower heating rate, the temperature profile along the cross-section can be assumed linear, as both the outer surface and the inner core of the material attain same temperature at certain time (as sufficient heating time is available to the material). On the other hand, at a higher heating rate, a significant difference in temperature profile exists along the cross-section of the material. Therefore, the higher temperature is required to progress the heat transfer [209].

Kinetically considering, heating rate is the major variable that determines the position of nonisothermal TG curves. In accordance with Eq. (2.7) (see **Chapter 2**), for any given degree of conversion, an increase in the value of heating rate is necessarily related to an increase in the upper limit of the integral. Consequently, an increase in the heating rate shifts the whole

TG/DTG curve toward higher temperature. Practically, doubling of heating rate causes the TG/DTG curve to shift by 15 °C [87].

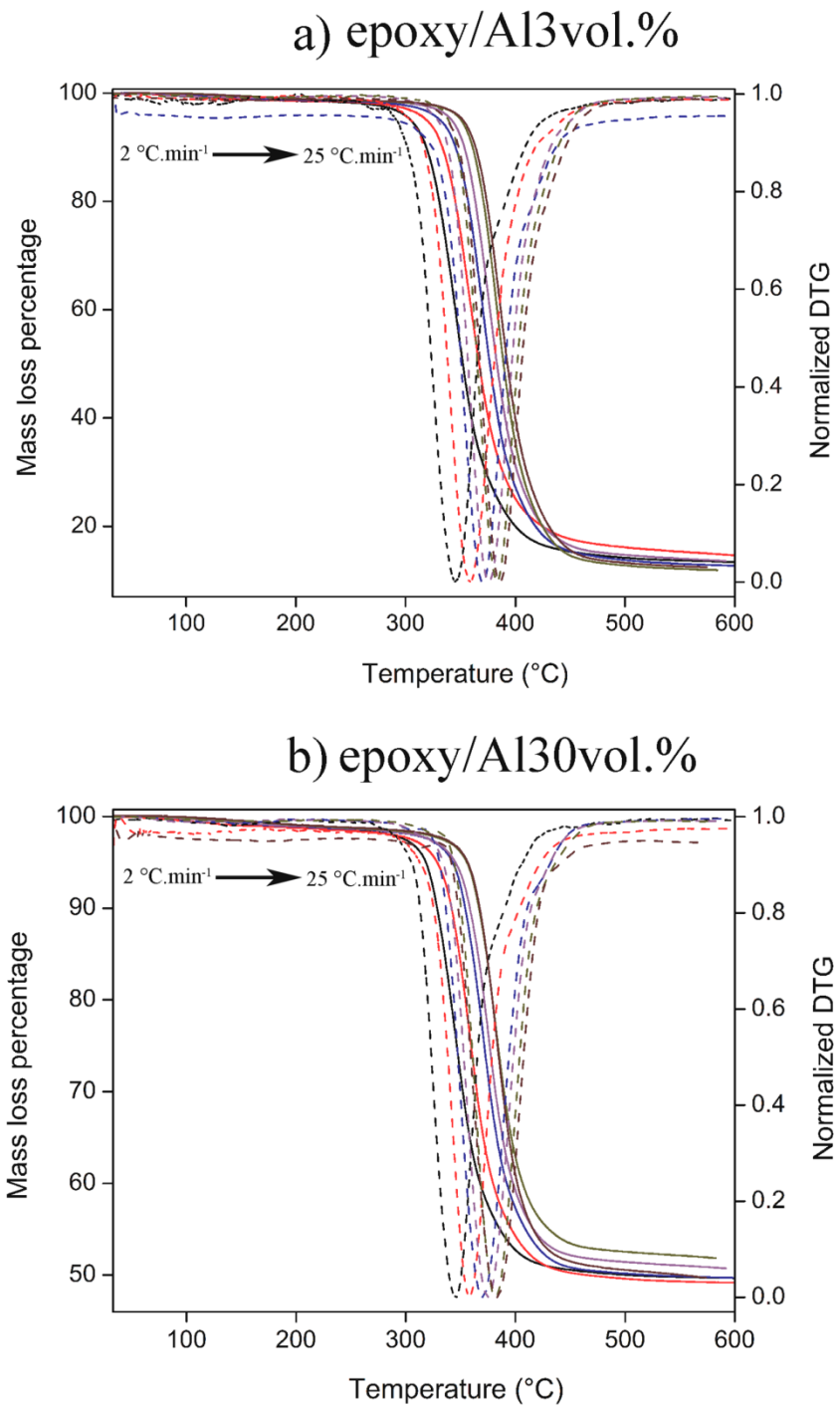

Figure 4.2: TGA and DTG curves of (a) epoxy/Al3vol.% and (b) epoxy/Al30vol.% at different heating rates.

According to Table 4.11, tin shows resistance against the thermal degradation initiation of UFC similar to UFC/Al and UFC/Zn composites, and this resistance seems dependent on tin contents. Figure 4.16 evidences that the second reaction step takes place at comparable temperature ranges in UFC and UFC/Sn composites. However, the third reaction step discernibly shifts to lower temperatures, which is evident from the temperatures of UFC and UFC/Sn composites at maximum reaction rates T_m i.e. $(T_m)_{UFC}$ = 311.52 °C; $(T_m)_{UFC/Sn5vol.\%}$ = 300.7 °C; and $(T_m)_{UFC/Sn35vol.\%}$ = 289.42 °C. This reaction step is more predominantly catalyzed by tin contents. The influence of tin contents on the mentioned degradation step of UFC resin resembles closely with its influence on the principal degradation step of epoxy/Sn composites [182]. The fourth reaction step, on the other hand, shifts partially towards the higher temperatures in the case of UFC/Sn composites, as demonstrated in Figure 4.16/Table 4.11, showing induction of thermal stability by tin contents into UFC matrix [195].

The irregularities in thermal degradation behaviors of UFC/Sn composites due to the nature and the contents of tin are satisfactorily explained on the basis of competitive variations in catalytic activity and heat capacity of tin, as already explained in the previous cases. In this context, the main reason behind the behavior shown by tin in UFC/Sn composites, on one hand, can be its fine catalytic activity at relatively lower temperatures which might diminish at higher temperatures. On the other hand, the heat capacity of tin exhibits converse behavior with temperature. As mentioned earlier, the heat capacity of tin at room temperature is merely 0.228 $J.g^{-1}.K^{-1}$, while its heat capacity at the melting point (232°C) has been reported to be 0.25 $J.g^{-1}.K^{-1}$ [226], causing the thermal stability of UFC/Sn composites to relatively increase particularly at higher filler loadings.

Table 4.12: IPDT values in the case of measured and corrected TG curves for UFC/Sn composites.

Sample	IPDT (°C) from measured TG curves	IPDT (°C) from corrected TG curves
UFC/Sn5vol.%	665	565
UFC/Sn35vol.%	839	600

In the interest of quantitative evaluation of the effect of tin on the inherent thermal stability of UFC, the IPDT parameters of UFC/Sn composites (for both the measured and corrected TG curves) are determined at 20 °C.min^{-1} and shown in Table 4.12. The IPDT results in Table 4.12 illustrate that the net influence of tin on UFC is to induce thermal stability into matrix and this thermal stabilization effect seems the function of tin contents in UFC/Sn composites. Furthermore, thermal stabilization effect induced by tin into UFC matrix seems more significant than that was induced into epoxy matrix [182].

Based on the above discussion and IPDT values of pure UFC and UFC/Sn composites, it is perceivable that the effect of tin on the thermal degradation of UFC is non-uniform, and it might be governed by the net effect of competitive temperature dependent variations in catalytic activity and heat capacity of tin and its contents in composites. In this regard, it is found that tin is capable of significantly increasing the thermal stability of UFC resin, and the thermal stability of resin seems directly related to the quantity of tin in UFC/Sn composites [195]. Additionally, thermal stabilization effect of tin on UFC matrix seems more important than that of epoxy matrix.

4.5. Mutual comparison between thermal degradation behaviors of epoxy/metal and UFC/metal composites

The discussions carried out in the previous sections, regarding the thermal degradation behaviors of epoxy composites filled with aluminum, zinc and tin particles, point out that the nature and contents of metals play a crucial role in defining the thermal degradation behaviors of relevant composites. In accordance with the obtained results, the chemical involvement of the metals in the thermal degradation process of epoxy seems highly improbable. However, the variation of physical properties of metals (predominantly, catalytic activity and specific heat) with temperature might considerably influence the thermal degradation of the resin. It has been observed that at relatively lower temperatures, catalytic activity of metal is more influential, which contributes in accelerating the thermal degradation of epoxy. Briefly speaking, metals tend to facilitate the degradation of epoxy at lower temperatures. At higher temperatures though, the catalytic activity is reduced due to catalyst deactivation, and specific heat of metal becomes more influential, resulting in producing shield against the thermal degradation of epoxy. On the basis of these considerations, a selectivity order of metals can be established taking into account their

potential of accelerating the thermal degradation rate of epoxy. The most likely ascending order of metals to catalyze the thermal degradation of epoxy resin could be:

$$Al < Zn < Sn$$

It is nevertheless worth remarking that at higher temperatures, the order of metals providing resistance against the thermal degradation of epoxy resin is more or less similar to the above mentioned order. This inference has been verified by mutually comparing the integral procedure decomposition temperature (IPDT) values of epoxy/metal composites.

In the case of UFC/metal composites, a critical analysis of the thermal degradation behaviors of UFC composites charged with aluminum, zinc and tin particles point out that the nature and contents of metals (in complementary to the individual structure, nature and properties of UFC matrix) play an integral role in explicating the thermal degradation behaviors of UFC/metal composites. According to the morphological characterization results, metals do not participate in any kind of chemical reaction during the preparation of UFC/metal composites. Although the thermal degradation profiles of UFC/metal composites by TG/DTG analyses suggest that metals might (UFC/Zn composites) or might not (UFC/Al and UFC/Sn composites) alter the thermal degradation behavior of UFC resin which, in the former case, could possibly be an indication of the alternation of degradation pathway of UFC resin by the introduction of metal. Nevertheless, the competitive variations in physical properties of metals including generally catalytic activity and specific heat with temperature might considerably influence the thermal degradation of UFC resin. We find that contrary to epoxy /metal composites, metals provide resistance against the initiation of thermal degradation process of UFC. Nevertheless, by passing this stage, (and similar to epoxy/metal composites), catalytic activity of metal becomes more influential which contributes in accelerating the thermal degradation of UFC. Likewise, at higher temperatures, the catalytic activity is reduced due to catalyst deactivation, and specific heat of metal becomes more influential, resulting in providing shield against the thermal degradation of UFC. It should however be noticed that a selectivity order of metals regarding to their potential of accelerating the thermal degradation of UFC resin could not be established, contrary to epoxy. The reason is that the influences of metals chosen in the present study on UFC resin are not at all straightforward. Despite, a selectivity order of the metals for providing thermal stability to UFC resin can be proposed by taking into account the IPDT considerations, which could be as follows:

Al < Sn < Zn

Hence, within the selected set of metals, zinc possesses highest ability to thermally stabilize the UFC resin, followed by tin and finally aluminum. Under the similar experimental conditions, the thermal stability order of UFC/metal composites differs from epoxy/metal composites.

Taking into account the above considerations, UFC and UFC/metal composites could serve in those industrial applications which demand higher thermal stabilities. This is because UFC has significantly higher thermal stability (IPDT = 547 °C) then epoxy (IPDT = 478 °C) and the studied metals improve the thermal stability of UFC by providing resistance against its thermal degradation. On the other hand, epoxy/metal composites might be employable in those industrial applications where faster thermal degradation rates are required as the studied metals facilitate the thermal degradation of epoxy.

4.6. Conclusion

In this chapter, a detailed account of thermal behaviors of epoxy and UFC composites filled with Al, Zn and Sn particles over long temperature ranges is given and discussed. Thermal analysis results of neat epoxy describe that its thermal degradation follows a quasi-single step thermal degradation process. In addition, the metals might not chemically participate in the thermal degradation of epoxy, which is evident by the similar thermal degradation processes of epoxy and epoxy/metal composites. Although, it has been found that the nature/contents of metals, and particularly variation in physical properties of metals (predominantly catalytic activities and heat capacities of metals) with temperature could strongly affect the thermal degradation behaviors of epoxy/metal composites. As a matter of fact, catalytic activities and heat capacities of the studied metals play a major role in explaining and predicting the thermal degradation behaviors and thermal stabilities of epoxy/metal composites. On the other hand, thermal degradation profile of neat UFC resin demonstrates that its thermal degradation process follows a substantially complicated pathway, comprising various competitive/consecutive reactions. Apparently, aluminum and tin do not chemically participate in the thermal degradation process of UFC, as evidenced by their resembling thermal degradation profiles. Though more probably, zinc chemically involves in the thermal degradation of UFC and tends to alter its thermal degradation pathway. However, despite the influence of individual structure and properties of UFC matrix, the nature/contents of metals and particularly variation in their catalytic activities and heat capacities of metals with temperature, may strongly affect the thermal degradation behaviors of UFC/metal composites. Similar to epoxy/metal composites, catalytic activities and heat capacities of the studied metals play a crucial role in explaining and predicting the thermal degradation behaviors and thermal stabilities of UFC/metal composites. Based on these findings, selectivity orders of metals regarding to their capabilities of thermally accelerating/stabilizing the epoxy/UFC matrices are suggested and their potential industrial applications are stated.

Chapter 5

Kinetics of Thermal Degradation Mechanisms in Polymer (Epoxy, UFC)/Metal (Al, Zn, Sn) Composites

5.1. Introduction

An important application of solid state kinetics is to model the thermal degradation processes taking place in materials over long temperature ranges. Kinetic modeling of thermal degradation processes in materials is undertaken by evaluating their activation parameters (activation energies and pre-exponential factors) in order to analyze the transition states related to processes, and finally their reaction mechanisms [100, 233]. Kinetic parameters are considered invaluable in controlling the processes under consideration for their eventual efficiency optimizations, and predicting thermal stabilities/lifetimes of materials outside the experimental range [101, 107]. It is however worth pointing out that, despite the usefulness of the kinetic parameters of solid state processes, these processes are familiar for their complexities, and even an apparently simple reaction might comprise several steps. It should be noted that certain important efforts have recently been made to kinetically interpret the complicated solid state reaction mechanisms [126, 140] as detailed in **Chapter 2**. The applicability and soundness of those approaches will particularly be taken into consideration in the present chapter.

In the previous chapters, structures and thermal degradation behaviors along with thermal stabilities of epoxy and UFC composites filled with metal particles including, aluminum, zinc, and tin were discussed. This chapter deals with modeling the experimentally obtained thermal degradation behaviors of epoxy/metal and UFC/metal composites by employing solid state kinetics approaches. Kinetic parameters of neat epoxy and UFC resins and their respective composites will be evaluated. The probable thermal degradation mechanisms of resins and their composites will be predicted on the basis of kinetic analysis, and an account of the influence of nature and contents of metals on the thermal degradation mechanism of resins will be given. Finally, the information obtained by structural characterization and thermal degradation of epoxy/metal and UFC/metal composites in the previous chapter will be compared with the information obtained by thermal degradation kinetic analysis of those materials, interpreted, and discussed.

5.2. Thermal degradation kinetics of epoxy and epoxy/metal composites

In order to give kinetic description of the thermal degradation processes taking place in pure epoxy and epoxy/metal composites, their activation energies demand evaluation as an initial condition for their kinetic modeling. For this purpose, isoconversional kinetic analysis is carried

out on the thermoanalytical data of epoxy and epoxy/metal composites (chapter 4). A set comprising differential and integral isoconversional methods can be useful to verify and compare the trend of activation energy with the advancement of reaction [184]. In all the cases, a set of Friedman's linear differential method and linear integral methods of Kissinger-Akahira-Sunose (KAS) and Ozawa-Flynn-Wall (OFW) have been utilized within $\alpha \in [0.05,\ 0.95]$ (except in the case of epoxy/Zn3vol.%, $\alpha \in [0.05,\ 0.8]$ is chosen as ahead 0.8, an intense scattering has been observed), and with an interval $\Delta\alpha = 0.05$. It should also be taken into account that in the case of epoxy/Sn composites, activation energies from KAS, OFW methods have been determined by employing Arshad-Maaroufi's generalized linear isoconversional method (GLIM) [126]. Figure 5.1 and Figure 5.2a-f show respectively the results obtained by applying the selected set of isoconversional methods on pure epoxy, and epoxy/metal composites:

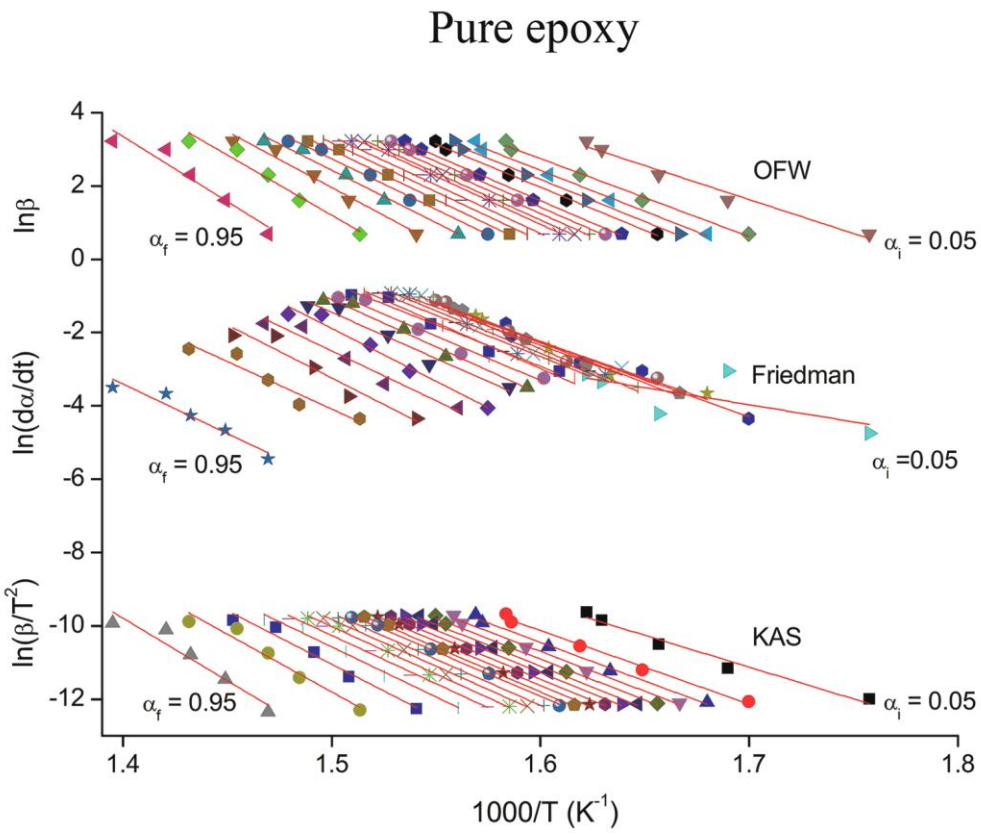

Figure 5.1: Applications of differential and integral isoconversional methods to non-isothermal degradation of pure epoxy.

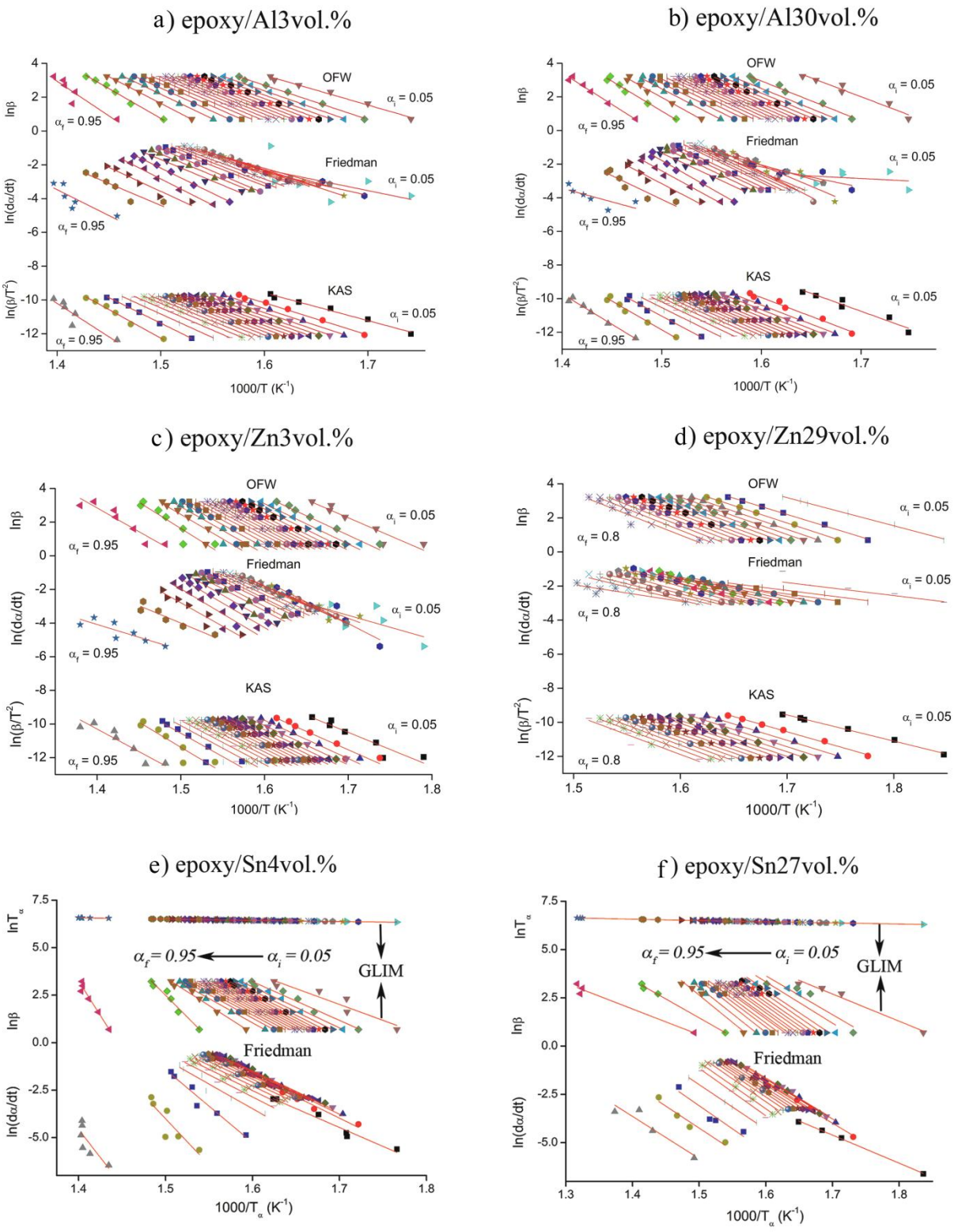

Figure 5.2: Applications of differential and integral isoconversional methods to nonisothermal degradation of epoxy/metal composites.

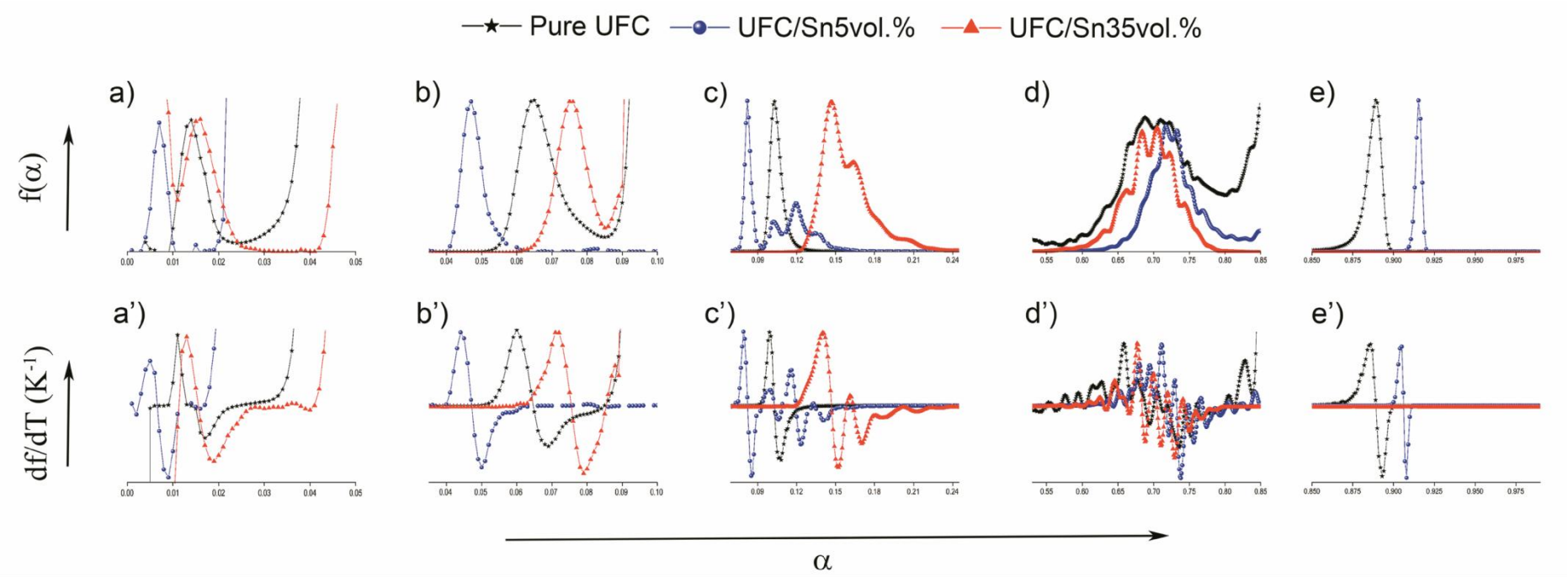

Figure 5.16: a-e) Normalized reaction models of the thermal degradation of pure UFC, UFC/Sn5vol.% and UFC/Sn35vol.%. evaluated by advanced reaction model determination methodology at 20 °C.min^{-1}; a′-e′) Application and normalization of df/dT function on the thermal degradation of pure UFC, UFC/Sn5vol.% and UFC/Sn35vol.%. at 20 °C.min^{-1}

In the last case, the normalized f(α) and df/dT curves of UFC/Sn composites are shown in Figure 5.16 which suggest that the thermal degradation of UFC/Sn composites takes place in multiple steps. Based on the discussed thermal degradation profiles (Chapter 4) and E-α dependencies of UFC/Sn composites, Figure 5.16 can be divided into various regions i.e. Figure 5.16a-e for f(α), and Figure 5.16a′-e′ for df/dT respectively.

Mechanistic information about the thermal degradation processes taking place in UFC and UFC/Sn composites over long temperature ranges can be obtained by comparing Figure 5.16a-e and Figure 5.16a′-e′ with the standard f(α) and df/dT curves already given in Figure 2.1 and Figure 2.5 respectively. Figure 5.16a-a′ shows that the first step, ranging till 5% of conversion degree and comprising dehydration of UFC/Sn composites and some weaker interactions present in their macromolecular structures, follows nucleation/growth phenomenon. The second step ranges between [0.055, 0.4] of 'α' is further divided into two sub-steps as shown in Figure 5.16b-c & 5.16b′- c′ respectively. The first one of the two sub-steps obeys similar mechanism as UFC, however, the second one follows quite different and tin contents-dependent mechanism in comparison with UFC. In the case of UFC/Sn5vol.% composite, the step under consideration follows four reaction pathways i.e. the first one and the third one being nucleation/growth, while second and fourth probably follow nucleation and diffusion respectively. The same step in UFC/Sn35vol.% on the other hand follows two-step pathway. The first one being nucleation/growth and the second one is probably diffusion. The third degradation step corresponds to [0.45, 0.8] of 'α' and is shown in Figure 5.16d-d′. As already discussed previously, this step is considerably complex, comprising various parallel reactions. Figure 5.16d-d′ evidences the higher though resembling reaction complexities of UFC and UFC/Sn composites in the third degradation step. The last step corresponds to 'α' above 0.8, and is associated with the char formation as described in Figure 5.16e-e′. Figure 5.16e-e′ shows that the char formation of UFC and UFC/Sn5vol.% composite can be considered as single step process obeying nucleation/growth phenomenon. Char formation in UFC/Sn35vol.% composite could probably be shifted to lower degrees of conversion by convoluting with the previous degradation step. Likewise, it may contribute in augmenting the thermal stability of the system. The obtained mechanistic information related to thermal degradation of UFC and UFC/Sn composites elucidates that despite of certain complexities induced by tin (particularly diffusion), all the studied materials obey more or less similar thermal degradation mechanisms [195]. Kinetic study

suggests that mechanistic behaviors of UFC/Sn composites seem analogous to epoxy/Sn composites [182].

It is worth noticing that somewhat resembling patterns of the variation in activation energy with the degree of conversion of UFC resin and UFC/metal composites (excluding zinc metal) has already been observed and explicated previously in the case of epoxy resin and epoxy/metal composites. However, a major difference between the E-α dependency patterns of epoxy/metal composites and UFC/metal composites is that the thermal degradation of epoxy/metal composites consists of relatively fewer reaction steps, and therefore their thermal degradation can be kinetically simulated by autocatalytic reaction model SB (m, n) by probably following complex nucleation/growth mechanisms [182-184]. On the other hand, all the studied UFC/metal composites possess significantly intricate reaction profiles with various successive/competing reactions (as elaborated in Chapter 4). The well known reaction model determination approaches thus become invalid in the case of UFC/metal composites' thermal degradation [126]. Moreover, thermal degradation of UFC/metal composites can be satisfactorily divided into four reaction regimes and not the reactions themselves. As the exact number of reactions taking place during the thermal degradation of UFC/metal composites is uncertain and the true nature of reactions regarding to their mutual dependency (which is the fundamental condition for applying the peak deconvolution approach to non-isothermal kinetics) is obscure, hence peak deconvolution is entirely inconvenient [243] in modeling thermal degradation kinetics of UFC/metal composites. It therefore justifies the inevitability and effectiveness of advanced reaction model determination methodology in fairly predicting the reactions mechanisms of complicated multi-step processes taking place in UFC/metal composites [192, 194, 195].

5.4. Conclusion

In the present chapter, an account of the detailed kinetic analysis effectively carried out on the thermoanalytical data of epoxy and UFC resins and their respective composites (filled with aluminum, zinc and tin metals) has been reported. The principal objective of this study was to obtain profound understanding of the thermal degradation behaviors of the resins and their composites discussed in the previous chapter, and to gain insights into their thermal degradation mechanisms by employing solid state kinetic approaches. Thermal degradation kinetics of epoxy and epoxy/metal composites suggests that the thermal degradation processes taking place in

those materials follow quasi-single step processes. Although, metals do not chemically involve in the thermal degradation of epoxy resin as remarked in chapters 3 and 4. This fact has been verified on the basis of their similar E-α dependencies by isoconversional analysis and their similar reaction models. Since, the reaction models of epoxy resin and epoxy/metal composites remain more or less same, the major roles in differentiating between their reaction rates are then played by their activation energies and pre-exponential factors. Generally, the activation energies and pre-exponential factors of the thermal degradation of epoxy/metal composites are therefore worth attributing as quantitative representatives of the catalytic activities of metals in the case thereof.

In the case of UFC and UFC/metal composites, the complex nature of their thermal degradation mechanisms (as discussed in the previous Chapter) is revealed by their variable E-α dependency patterns by employing isoconversional kinetic analysis. Since the activation energies of the composite materials show substantial variations with the degree of reaction advancement, kinetic approaches capable of dealing with single-step processes become inapplicable in the case of UFC and UFC/metal composites. Therefore, advanced reaction determination methodology is employed on the thermoanalytical data of UFC/metal composites in order to probe their reaction mechanisms. Advanced reaction determination methodology not only validates the findings of the previous chapters but also provides interesting and important insights into the reactions mechanisms of UFC/metal composites. For instance, though the thermal degradation profiles (Chapter 4) and the E_α dependencies of UFC and UFC/Al composites by isoconversional analysis are apparently similar, their thermal degradation pathways differ from each other. This point unravels the fact that isoconversional kinetic analysis is merely a necessary but not a sufficient condition for mechanistic predictions by kinetics. In this regard, the df/dT complementary to f(α) shows considerable potential to analyze the complex multi-step processes and predicting their probable reaction mechanisms. Likewise, this study favors the capability of advanced reaction model determination methodology in plausibly coping with the complex condensed phase processes.

Chapter 6

Kinetic approach to degradation mechanisms in polymer solar cells and their accurate lifetime predictions

6.1. Introduction

The previous chapters of the present thesis were devoted to study the thermal degradation processes taking place in polymers and their composites. New approaches have been put forward to kinetically model those processes and to predict their reaction mechanisms. The obtained results have demonstrated that the suggested approaches give plausible description of the mechanisms of thermally stimulated processes occurring in polymer and their composites. It should be recalled that the studied materials (polymers, composites) are of great importance as they find a wide range of industrial applications. One of these important applications is found in the organic photovoltaic (OPV) or polymer solar cells which are deemed as the potential materials for satisfying future energy demands. Thus, the aim of this chapter is to generalize the applicability of the developed kinetic models on the degradation of polymer solar cells under different physical and chemical constraints.

More than eighty five percent of solar cells occupying global photovoltaic market are based so far on crystalline silicon (c-Si) or amorphous silicon (a-Si) [244, 245]. Although the reported efficiencies of such units of commercially available conventional solar panels in the market today are greater than 20%, yet their contribution is minor in satisfying the global energy demand due to the use of expensive and energy demanding processing techniques in their fabrication [246]. For any PV technology to be commercially competing, it must satisfy the stability-efficiency-cost (SEC) demands i.e. the technology must demonstrate high stability and efficiency at minimum costs. The reported efficiencies of solar cells are of course in continuous increase with the development of new conversion systems as shown in the Figure 6.1.

However, it should be noted that among the major challenges being currently encountered by PV technology include:

- Reduction in the cost of solar energy conversion into electricity using cheap materials
- Minimizing the aging observed in these systems (stability/degradation issues)

Accordingly, the OPV cells are the subject of a number of ongoing renewable energy researches due to their low cost technologies for producing large surfaces from the printing industries (inkjet, screen printing, etc.), easy processing, and flexible substrates and energy source [248–255]. Currently these deposit processes are emerging with a very promising attractiveness. The organic/hybrid photovoltaic can access marketable applications thanks to its specificities that are complementary to those of the silicon industry.

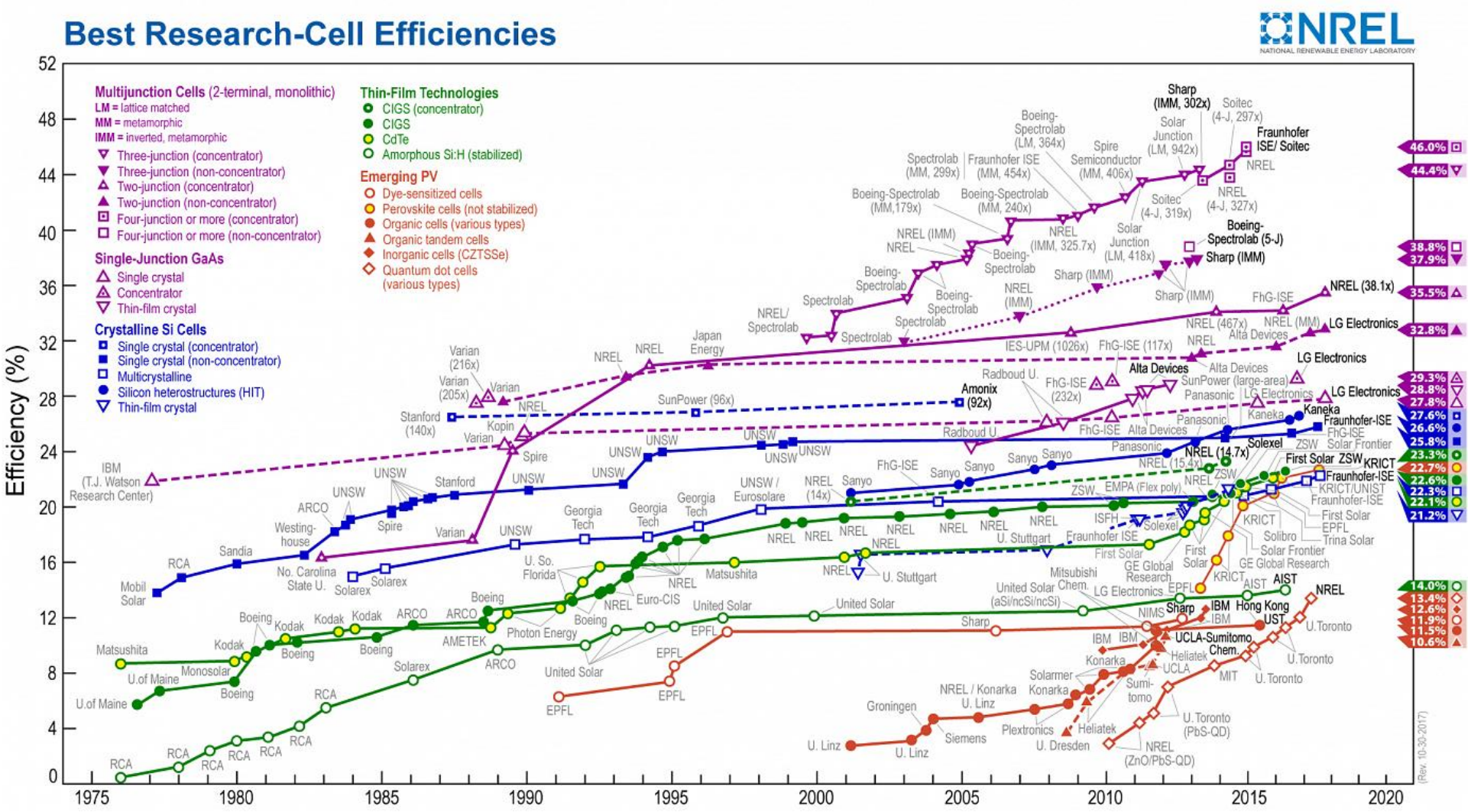

Figure 6.1: Efficiency trend of PV solar cells over time [247].

The reported efficiencies of these kinds of cells comparative to Si-cells are though low today (11.5%), however, an overwhelmingly increasing efficiency trend of these cells is in continuous progress as reported during the past couple of years (see Figure 6.1). Nevertheless, their stability/lifetime (particularly under natural conditions) being one of the burning issues related to the current organic photovoltaics research, needs prompt addressing for their large scale production and commercialization [247, 248, 256]. It should be mentioned here that certain serious efforts have recently been made in order to cope with the stated issue [247, 257-260]. However, a reliable modeling approach based on theoretical underpinning of degradation processes taking place in OPV devices has not yet been suggested. In this regard, an advanced approach comprising a set of theoretical models to simulate the degradation mechanisms in polymer solar cells is put forward in the present work. It is in fact a systematic theoretical approach to kinetically model the potential simultaneous degradation processes taking place at different levels and layer interfaces of the organic solar cells. Briefly, it is an attempt to take into consideration multiple factors contributing to polymer solar cell degradation without focusing on a single one, and to offer a suitable alternative to the accelerated lifetime testing. The efficacy of the suggested kinetic approach will be justified theoretically as well as by practical degradation data of familiar solar energy material/solar cells consisting of, poly(3-hexyl thiophene) (P3HT) polymer film, poly2-methoxy-5-3,7-dimethyloctyloxy-1,4-phenylenevinylene (MDMO-PPV) and 6,6-phenyl C61-butyric acid methyl ester (PCBM) bulk heterojunction solar cell and dye-sensitized solar cells (DSSC), and discussed. Furthermore, on the basis of the suggested kinetic approach, a lifetime prediction formula for polymer solar cells is put forward. The mentioned formula will finally be tested on the dye-sensitized solar cells for predicting their lifetimes. It should be taken into account that the solar cell efficiencies of P3HT:PCBM, MDMO-PPV:PCBM and DSSC solar cells in accordance with literature are, 5.4%, 2.5% and 11-14% respectively [247, 261-263].

6.2. Structure of a polymer solar cell

A polymer solar cell is usually fabricated by dissolving polymers into organic solvents, which are then transferred to a substrate by printing or coating methods. The materials are added in layers in a certain order to construct a solar cell stack. The materials required in the solar cell stack are; a central active/light absorbing layer which transforms the striking photons into

excitonic bound electron-hole, a selective charge transport layer on each side of the active layer, allowing only the passage of either electrons (electron transport layer or briefly ETL) or holes (hole transport layer or simply HTL), and finally two electrodes for extracting the charges from the solar cell, with at least one of the electrodes having a requirement of transparency such that the light can pass through and arrive at the active layer [264]. The structure of a simple organic solar cell is described in Figure 6.2.

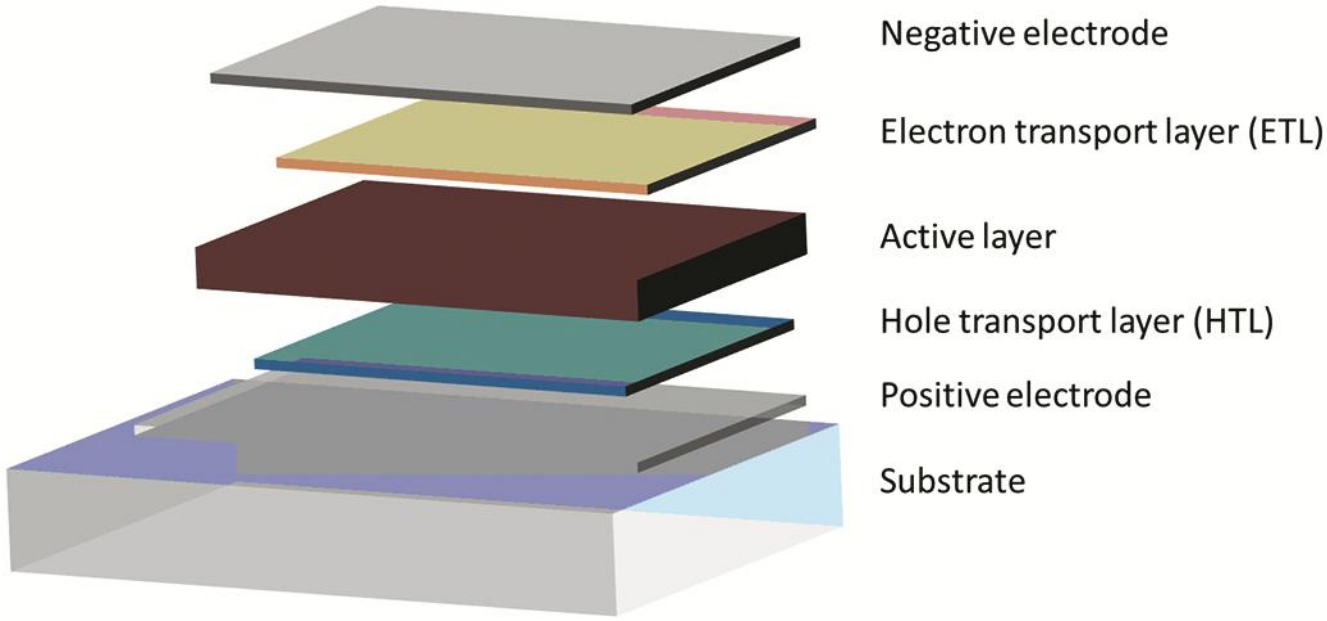

Figure 6.2: The layers of an organic solar cell [265].

Polymer solar cells are often divided into two categories based upon the solar cell stack geometry; a normal and an inverted geometry. The definition of the two geometries lies within the direction of the charge flow. In a normal geometry solar cell, the substrate and the transparent electrode on it is the positive electrode, with the light passing through the substrate and this electrode before being absorbed in the active layer. The top electrode is then the negative electrode. In the inverted geometry, the two electrodes and the charge selective layers are switched around, such that the transparent electrode at the substrate is the negative electrode, with a ETL layer between it and the active layer, while the top electrode is the positive electrode with a HTL layer between it and the active layer.

A polymer solar cell contains also an active layer which further consists of two components. A donor which absorbs the light and an acceptor which extracts the electron from the excitonic

bound electron hole, resulting in an electron traveling through the acceptor phase of the active layer and a hole traveling through the donor phase. For the mentioned phenomenon to be effective, the low lifetime of an exciton in the donor materials demands a donor-acceptor boundary at which the exciton can be broken within approximately 10 nm. In addition, since the holes and electrons have to travel out of the active layer towards the electrodes, the domains of donor and acceptor needs to be connected in an interconnected network allowing both the efficient dissociation of the excitons and the efficient transport of the charge carriers to the respective electrodes.

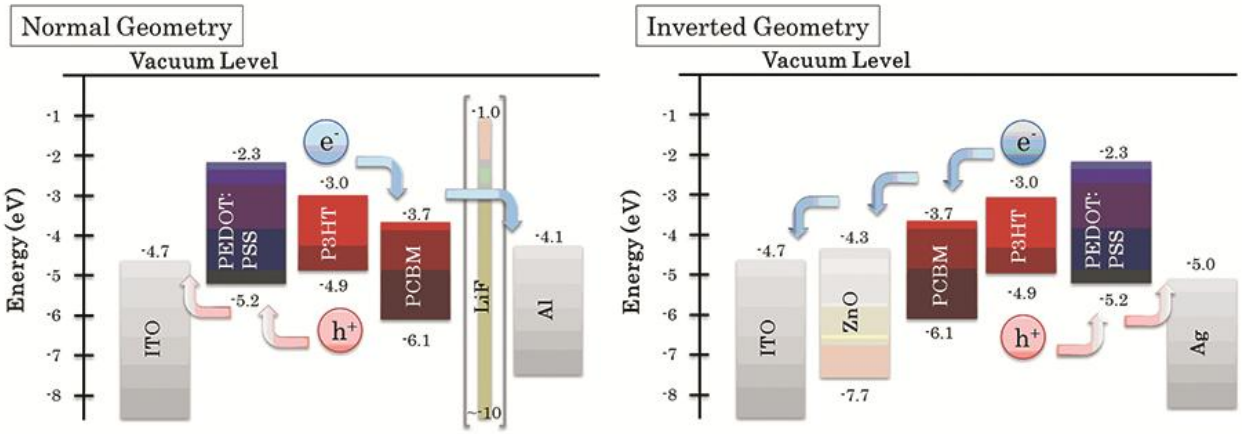

Figure 6.3: Energy levels associated with the normal and inverted geometry solar cells [265].

The transport layers (Figure 6.3) comprise materials with the capability of transferring either the electrons or the holes resulting from a suitable positioning of the energy levels. Examples of hole transport materials include, the polymer based Poly(3,4-ethylenedioxythiophene):Polystyrene sulfonate (PEDOT:PSS; see Annex C) and a metal oxide such as molybdenum oxide (MoOx). Examples of often used electron transport layers are lithium floride (LiF), calcium (Ca) and metal oxides such as zinc oxide (ZnO) and titanium oxide (TiO). The most commonly used electrode material (Figure 6.3) is indium tin oxide (ITO), due to a high optical transmission or for its optical transparency combined with a low electrical resistance. The main issue with the selection of electrodes is to find electrodes with a suitable energy level and with one of the electrodes being transparent to allow sufficient light to enter the solar cell (ITO). PEDOT:PSS is a material that has started to become popular as use as an electrode, since it can

be doped to allow conductivities of more than 500 $S.cm^{-1}$ with a transmission of >80%. The doped PEDOT:PSS solutions tend to allow easier fabrication on flexible substrates, since the polymer based films have a better tolerance towards bending compared to an ITO electrode.

During the polymer solar cell fabrication, the substrates used for supporting the layered solar cell stack, can be divided into two distinct groups: glass and plastics. The two most commonly used types being floated glass substrates with ITO transparent electrodes used in lab scale production and flexible PET (polyethylene terephthalate) foil used in upscaling focused on manufacturing, where the transparent electrodes are either ITO as for the glass substrates [265] or some other potential nanomaterials-based printed transparent electrodes including carbon nanotubes (CNTs), graphene, metal nanowires (MNWs), etc. [266]

The major reasons behind the degradation of the active components, oxidation of electrodes, and delamination of the layers in the fabricated OPV devices include exposure to moisture, oxygen, or ultraviolet radiation (will be detailed in the upcoming section). The optimal solution of such an issue would be to protect the device against the mentioned environments which can be effectively achieved by encapsulating the OPV device with a high energy barrier material. The encapsulant material must be capable of reducing the ingress of moisture, oxygen as well as remain resistant to UV radiation [267]. The conventional encapsulant material is glass, tough it is brittle, heavy, and not suitable for large area and large-scale processing, leading to detrimental effect on the main features and advantages of organic solar devices [268]. Thus, it is unsuitable for being used as an encapsulant. Hence, an easily processable, monolithic, flexible, high vapor and gas barrier material, which can conform into various surfaces and shapes, is desirable ideally as an OPV encapsulant [269]. These characteristics are prtly satisfied by materials like, ethylene vinyl acetate (EVA), poly(ethylene terephthalate) (PET), poly(ethylene naphthalate) (PEN), etc. though they are confronted with various challenges [270, 271]. Quest for an appropriate encapsulant with most of the mentioned characteristics is another important subject of ongoing PV researches.

6.3. Degradation sources/mechanisms in a polymer solar cell

Mainly, the polymer solar cells are known to degrade on their exposure to humidity, oxygen, ultraviolet (UV) illumination, and temperature [272, 273]. UV constitutes approximately 5% of solar tressterial radiations. Although this fraction seems insignificant, yet being highly energetic,

long-term exposure of polymer solar cell to direct UV is a major cause of its damaging [270]. All these factors make the intrinsic lifetimes of OPV devices (without encapsulation) extremely short [274]. Their limited lifetime is in fact a result of multitude of the processes taking place in them (often) simultaneously. Some well familiar degradation mechanisms involve: diffusion of molecular oxygen and water into the device, degradation of interfaces, Photo/thermal degradation of the active material, inter-layer and electrode diffusion, electrode reaction with the organic materials, morphological changes, and macroscopic changes such as delamination, formation of particles, bubbles, and cracks [248, 256, 275–283]. A schematic diagram of the mentioned degradation mechanisms is shown in Figure 6.4 by considering a bulk heterojunction polymer solar cell. It is noteworthy that the OPV degradation may occur during fabrication, operation and/or storage. Moreover, the OPV degradation processes may not necessarily follow similar reaction rates. It is hard initially to identify OPV degradation mechanisms, and therefore discrete analysis of the influence of each aging parameter on OPV degradation is recommended (as will be detailed in the next sections). Even more challenging is to quantitatively model those mechanisms and their relative contributions towards the entire degradation phenomenon [284].

Irrespective of the climatic conditions, the physical and/or chemical degradation modes of (flexible) OPVs devices can be categorized into two main classes:

- Intrinsic degradation because of the variations in the characteristics of the interface between the stack layers and due to internal modification of the employed materials.
- Extrinsic degradation caused by the variations in the cell behavior due to external factors such as, water, oxygen, electromagnetic radiations (UV, visible light, IR, etc.) and temperature.

The latter is strongly linked to the quality and stability in properties of the encapsulation system, namely the barrier, the substrate and the type of edge sealing used. Some of the failure modes of OPV devices under the influence of external factors are demonstrated in Table 6.1. It is worth mentioning that active layer is principally vulnerable to extrinsic degradation. In Table 6.1, certain external factors may show inter-dependencies. For instance, illumination may cause an increase of the cell temperature. These two factors facilitate the diffusion of the oxygen and water, which eventually leads to the oxidization mechanism [278].

The slopes of the straight lines at different temperatures are in fact the rate constants as shown in Figure 6.14c (slope = k_x = a). By knowing the rate constants at different temperatures and activation energy, the pre-exponential factors can be determined, which are pasted in Table 6.7. Substituting the obtained kinetic parameters into Eq. (6.50) yields the following kinetic expression:

$$x \approx 3.1\times10^{15} \exp(-137,000 / RT_h)t_x \tag{6.51}$$

Eq. (6.51) is capable of kinetically describing the thermally stimulated short circuit current density of DSSC at higher temperatures. It is noticeable that although the activation parameters are comparable over the whole experimental range, the reaction mechanism of thermally stimulated short circuit current density of DSSC varies from linear at lower temperatures to zero order at higher temperatures.

During the kinetic modeling of various polymer solar cell degradation processes (discussed above), it has been observed that the agreement between theoretical models and experimental data starts diminishing at higher temperatures. It may possibly be due to the involvement of additional phenomena contributing into solar cell degradation at higher temperatures. One important phenomenon is blend phase separation associated particularly with the bulk heterojunction polymer solar cells [308, 313]. Although participation of blend phase separation into degradation of solar cell could be insignificant at lower temperatures, yet it might become worth taking into consideration at higher temperatures (probably due to diffusion which enhances with temperature), as can be remarked in Figure 6.11. On the basis of the results obtained in the present study, it is recommended to carry out the temperature acceleration tests on properties (of)/processes in polymer solar cells at relatively lower temperature ranges, say within [25 °C, 65 °C] in order to adequately model its degradation kinetics. Nevertheless, as can be seen the agreement between experiment and theoretical approach is good taking into account the external effects (environmental, photodegradation, temperature).

6.7.3. Lifetime prediction of dye-sensitized solar cells (DSSCs)

Aiming at predicting the reliable lifetime of DSSC whose kinetics of thermally accelerated short circuit current density and photodegradation have been demonstrated in the previous section, the kinetics of the rest of processes contributing to DSSC degradation (in conformity

with Eq. (6.26)) need modeling. It is noteworthy that in the case of DSSC, moisture can slightly increase the power output, though it may negatively influence the long-term stability of the cell. H.-L. Lu et al. [314] suggested a descending order of water isotopes according to their effects on the degradation rate of DSSC as following:

$$H_2O > D_2O > H_2{}^{18}O$$

Nevertheless, it has recently been demonstrated that DSSC solar cells can be effectively protected against long-term degradation caused by moisture, by introducing hydrophilic silica nanoparticles into its electrolytes [315]. Under these conditions, Eq. (6.26) can take the following form:

$$\frac{1}{t_{1/2}} = \frac{1}{(t_x)_{1/2}} + \frac{1}{(t_z)_{1/2}} \tag{6.52}$$

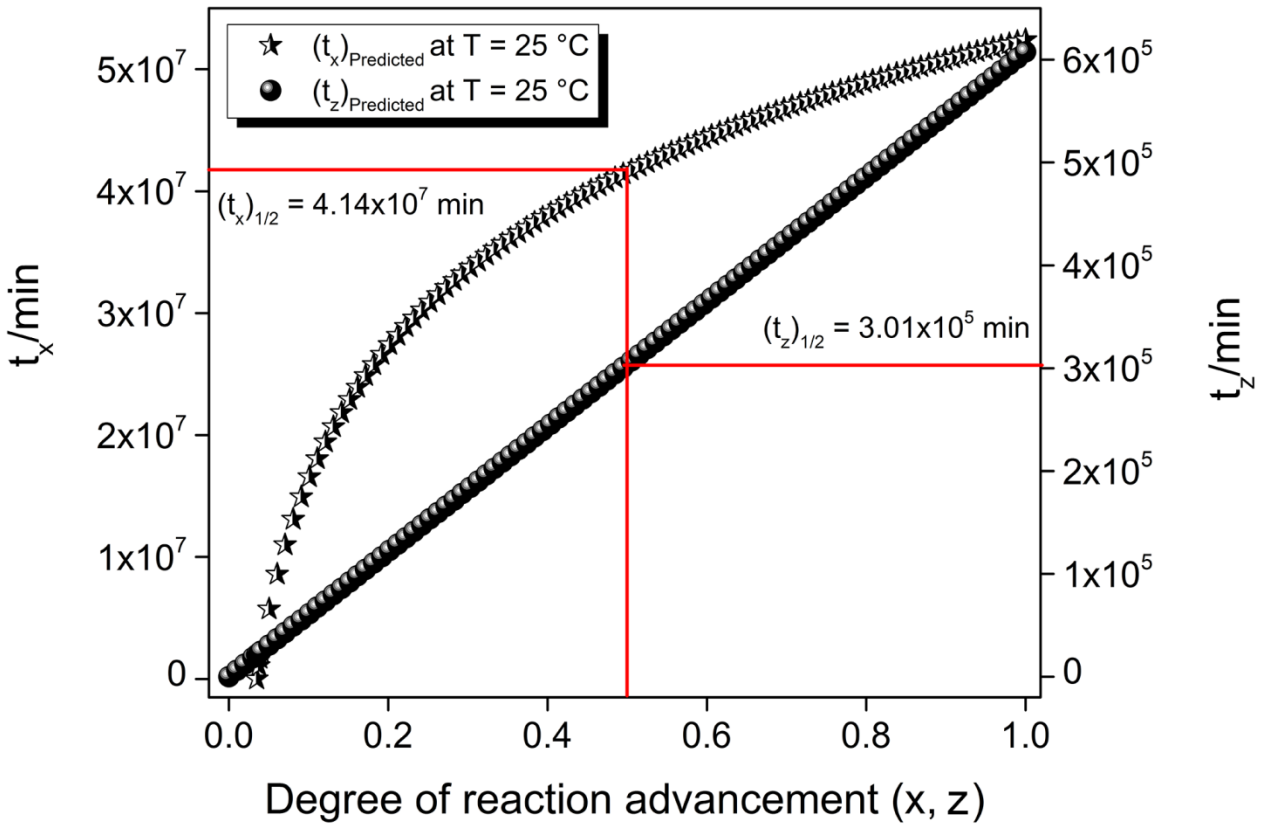

Figure 6.15: Lifetime prediction of DSSC at room temperature.

For predicting the lifetime of DSSC at room temperature conditions, stability/degradation curves of DSSC are predicted at 25 °C by employing Eqs. (6.42) and (6.49) and the obtained results are shown in Figure 6.15:

In Figure 6.15, the predicted half life of DSSC solar cell with the structure suggested by L. Ciammaruchi et al. [311] and D. Bari et al. [312] at room temperature in relation to thermally stimulated short circuit current density is 4.14×10^{7} min (≈ 79 years). On the other hand, in reference to thermally accelerated photodegradation, the same cell has a half life of 3.01×10^{5} min (≈ 7 months). By employing Eq. (6.52), the effective half life of solar cell obtained is approximately 7 moths. Physically, it means that evolution of thermally accelerated short circuit current density of DSSC under pure thermal stresses is an extremely slow process, while this cell is highly vulnerable to thermally accelerated photodegradation. It might be due to a significant difference in the activation energies of thermally induced short circuit current density and thermally accelerated photodegradation of DSSC, as elaborated in sections 6.5.4 and 6.7.1. Actually, brisk degradation of such DSSCs under UV light is known in the literature [316, 317]. Important breakthroughs are being reported in the literature to cope with the stated DSSC issue; among them is the most recently proposed idea of photo-electrochemical cells capable of operating in the dark [299, 318].

Although the suggested kinetic approach is proven to be efficacious on limited number of kinetic datasets, it might effectively be generalized on the temperature acceleration of variation in short circuit current density, oxygen diffusion and photoreactions taking place in polymer solar materials, P3HT:PCBM solar cells and dye-sensitized solar cells [260, 278, 287, 306, 319-323]. The reason is that the kinetic curves in the mentioned studies [260, 278, 287, 306, 319-323] (transformable to curves similar to those shown in Figure 6.7a′-c′/Figure 6.8b demonstrate thermally stimulated/accelerated processes. In general, thermally stimulated/accelerated structural/phase transformations in condensed phase are known to follow activation phenomena. Those phenomena can be plausibly modeled by Arrhenius type relations or their modified forms. Likewise, the processes considered in the mentioned studies might be satisfactorily modeled by applying the proposed approach [299].

6.8. Conclusion

In the light of results and discussion, following concluding points are made:

- Certain crucial flaws have been pointed out in the temperature accelerated lifetime testing (ALT) of polymer solar cells. As an alternative, an advanced approach to predict accurate lifetimes of polymer solar cells has been put forward which takes into account systematic kinetic modeling of various possible degradation processes in polymer solar cells. This approach states that the lifetimes of polymer solar cells are governed by the relative contributions of individual degradation processes under natural weathering. In case if the degradation rates of various processes taking place in polymer solar cells differ widely, the fastest degradation process more probably controls the cell lifetime. It means that the fastest degradation process might be the main reason of cell failure and hence demand particular attention. In this regard, prediction of accurate lifetime of a solar cell on the basis of temperature stimulation/acceleration of merely a single property of material (as usually employed in the accelerated lifetime measurement test) is doubtful. This is because the rates of different degradation processes taking place in a solar cell may not only differ from each other, but also show dependence on the nature of materials employed into it. The advanced method developed in this piece of research therefore strongly emphasizes (on) and recommends the kinetic modeling of individual processes occurring in polymer solar cells in order to estimate the trustworthy lifetimes of solar cells under natural weathering conditions.
- The suggested kinetic approach has shown fair agreement with the experimental data of thermally accelerated current density of bulk heterojunction (MDMO-PPV:PCBM BHJ solar cell) solar cell, oxygen uptake of P3HT polymer film, and photodegradation of DSSC solar cell. The mechanistic information related to the mentioned polymer degradation phenomena has been interpreted and discussed.
- The lifetime determination formula based on the suggested kinetic approach has been tested on dye-sensitized solar cell and its half life at room temperature is predicted.
- The kinetic approach proposed in the present study can especially be helpful in verifying the reliability/replicability of the experimental data-sets and the possible mechanistic variations with, say, temperature.

- It has been noticed that the degradation mechanisms in polymer solar cells might not correspond to the familiar condensed phase mechanisms. The suggested kinetic approach may therefore propose new reaction models capable of dealing with the degradation mechanisms of polymer solar cells.
- The proposed method depicts flexibility, in a sense that it may either be applied to individual components of polymer solar cell (vulnerable to weathering phenomenon) or the whole integrated product. In addition, although basically suggested for polymer solar cells, this approach can effectively be generalized on other known kinds of solar cells. Thus, it is capable of contributing in the advancement of renewable and sustainable energy research, and it may find applications in commercializing organic solar cells.

Chapter 7

Kinetics of Crystallization Processes in Amorphous Materials

7.1. Introduction

Amorphous or non-crystalline materials have random distributions of atoms/molecules with the absence of crystal structures [324]. These materials can be categorized into several categories namely, polymers, alloys, glassy materials, and inorganic materials which have no long-range order (<10 Å) and high viscosity greater than 10^{13} Poise, are the most typical amorphous materials [325-327]. Although, the regular arrangement resulting from the distribution over long distances of a repeating atomic arrangement (which is characteristic of a crystal) is missing in glasses, yet often a short-range order is evidenced in glasses [328]. Crystallization in an amorphous material usually involves simultaneous nucleation and growth of crystallites [329]. Crystallization is initiated by crystal nucleation. Nucleation may occur spontaneously or it may be induced artificially. It is not always possible, however, to decide whether a system has nucleated of its own accord or whether it has done so under the influence of some external stimulus [330]. The nucleation either occurs without the involvement of a foreign substance in the interior of the parent phase which is called "homogeneous or primary nucleation" or with the contact of the parent phase with a foreign substance that acts as a preferred nucleation site which is called "heterogeneous or secondary nucleation". The nucleation process is followed by the growth of the crystal nuclei to macroscopic dimensions, which is known as "crystal growth" [331]. Study of crystallization processes in amorphous materials finds numerous applications in optics, electronics, opto-electronics, biology, geology and atmospheric physics [332]. Profound insights into mechanisms of crystallization processes in amorphous materials can be helpful in the control and optimization of those processes aiming at their eventual applications. Kinetic analysis, in this regard, plays a vital role in modeling the nucleation/growth phenomena taking place in amorphous materials.

The kinetic study of crystallization describes a characteristic sigmoidal behavior of time 't' dependence of the crystallized fraction 'α' which is usually explained by Johnson-Mehl-Avrami-Erofeev-Kolmogorov, JMAEK or simply JMA equation [112], as given below:

$$\alpha = 1 - \exp(-(kt)^p) \tag{7.1}$$

Where, *'k'* is the temperature dependent rate constant and *'p'* is the Avrami exponent which controls the nucleation rate and/or dimensionality of crystal growth [333]. Differentiation of Eq. (7.1) under constant conditions of temperature generates the following rate equation:

$$\frac{d\alpha}{dt} = kp(1-\alpha)\{-\ln(1-\alpha)\}^{1-1/p} \tag{7.2}$$

Eq. (7.2) is often used for the description of thermoanalytical crystallization data. Nevertheless, it should be noticed that the validity of the JMA equation is based on the following assumptions [334]:

- Crystallization occurs under isothermal conditions.
- Homogeneous nucleation or heterogeneous nucleation at randomly dispersed second-phase particles.
- Growth rate of new phase is controlled by temperature and does not depend upon time
- Growing crystals show high isotropy.
- Fair completion of nucleation before the commencement of growth process [335].

Yet, it has been pointed out that the validity of the JMA equation can be extended to non-isothermal kinetics if the crystallization rate is defined only by temperature and does not depend on the previous thermal history [336]. The applicability of JMA model in crystallization kinetics is generally estimated by Malék's reaction model determination methodology using *z(α)* function which is defined in the following equation:

$$z(\alpha) \approx \pi(x)(d\alpha / dt)T / \beta \tag{7.3}$$

Where, *'π(x)'* is an approximation of the temperature integral [120] (as expressed in Eq. (2.15) and detailed in section 2.2.1 of **Chapter 2**), and *'β'* is the heating rate. The maximum of the *z(α)* function α_p^{∞} must achieve a value close to 0.632, in order to satisfy the validity condition for JMA model (See **Chapter 2**). If α_p^{∞} attains a significantly lower value then the JMA model couldn't be applicable. In this case, the two parameter autocatalytic Šestak-Berggren SB (m, n) model [83, 117] can be used for the satisfactory description of crystallization processes:

$$f(\alpha) = (\alpha)^m(1-\alpha)^n \tag{7.4}$$

The SB (m, n) reaction model is an empirical model and in fact, it includes the JMA model as a special case which plausibly explains the kinetics of crystallization processes occurring in amorphous materials [239, 240, 334]. However, trouble with this SB (m, n) model is that the physical meanings of its parameters have not yet been fully understood [182]. Both the JMA and SB (m, n) models have the capability to model the kinetics of crystallization in amorphous

materials, though an explicit mathematical relationship between them both is unclear [239]. In this frame of reference, in one hand, this chapter presents a particular application of advanced reaction model determination methodology in solid state kinetics [126] to simulate the kinetics of crystallization processes in amorphous materials. On the other hand, it addresses the fundamental questions lying in the kinetic modeling of crystallization processes occurring in amorphous materials including:

- What could possibly be the relationship between the reaction model parameters of JMA and SB (m, n) models i.e. p, m & n?
- If it exists, what are the phenomenological limits of that relationship?
- How m and n are related to the nucleation and growth morphologies of the newly formed crystalline structures?

7.2. Theoretical basis of crystallization kinetics

7.2.1. Classical basic crystallization kinetics theories

Crystallization kinetics in materials is usually studied by differential scanning calorimetry (DSC) under either isothermal or non-isothermal conditions. The term degree of conversion is substituted by crystallization fraction in isothermal 'α_t' or non-isothermal 'α_T' experimental conditions and is evaluated by the following relations [154, 337]:

In non-isothermal crystallization kinetics,

$$\alpha_T = \frac{\Delta H_T}{\Delta H_{Total}} = \frac{\int_{T_0}^{T} \left(\frac{dH}{dT}\right) dT}{\int_{T}^{T_\infty} \left(\frac{dH}{dT}\right) dT} \tag{7.5}$$

In isothermal crystallization kinetics,

$$\alpha_t = \frac{\Delta H_t}{\Delta H_{Total}} = \frac{\int_{t_0}^{t} \left(\frac{dH}{dt}\right) dt}{\int_{t}^{t_\infty} \left(\frac{dH}{dt}\right) dt} \tag{7.6}$$

Where, T_0, T & T_∞ and t_0, t & t_∞ are the onset, arbitrary and end crystallization temperatures/times respectively in a DSC run; dH is the heat released in an infinitesimally small temperature or time interval dT or dt respectively.

The term activation energy of crystallization processes has been criticized in the literature in regard to being a single energy barrier [338]; despite, it is emphasized that it should be an effective value (an average activation energy taking into account the individual energies of all the elementary reaction steps involved in the crystallization process). Therefore, in crystallization kinetics case, basic kinetic equation can be written in the following format:

$$\frac{d\alpha}{dt} = A\exp(-E/RT)\,f(\alpha) \tag{7.7}$$

Eq. (7.7) is the fundamental kinetic equation for crystallization processes comprising *A* as the pre-exponential factor, *E* as the activation energy for the crystallization, and *f(α)* is a function of crystallization fraction that can be called the crystallization model. Physically, *A* describes the frequency(ies) of vibration(s) of activated complex(es); *E* is the effective value of the energy barriers of various elementary reaction steps involved in a crystallization process, and *f(α)* is capable of presenting the information about the crystallization mechanism. As mentioned earlier, the crystallization model may satisfactorily be described by either JMA or SB (m, n) models. The reliability of the parameters of these models is investigated in the next section.

7.2.2. A new kinetic approach for predicting reaction mechanisms of crystallization processes

Arshad and Maaroufi [126] have put forward an advanced reaction model determination methodology taking into account the variable activation energy concept in order to kinetically interpret the thermally induced condensed phase processes (See, **Chapter 2** for details). In their approach, they exploit a modified Arrhenius equation which includes variable activation energy and pre-exponential factor as given in Eq. (7.8):

$$\frac{d\alpha}{dt} = A_0\,(T/T_0)^n \exp(-E_\alpha/RT)\,f(\alpha) \tag{7.8}$$

Where, *'A_0'* is the value of pre-exponential factor at initial temperature *'T_0'* and *'n'* is a numerical constant. Usually, $n \in [0,\ 1]$ but it may have positive values other than mentioned in the interval and it can even be a negative number [143, 154], as elaborated in **Chapter 2**.

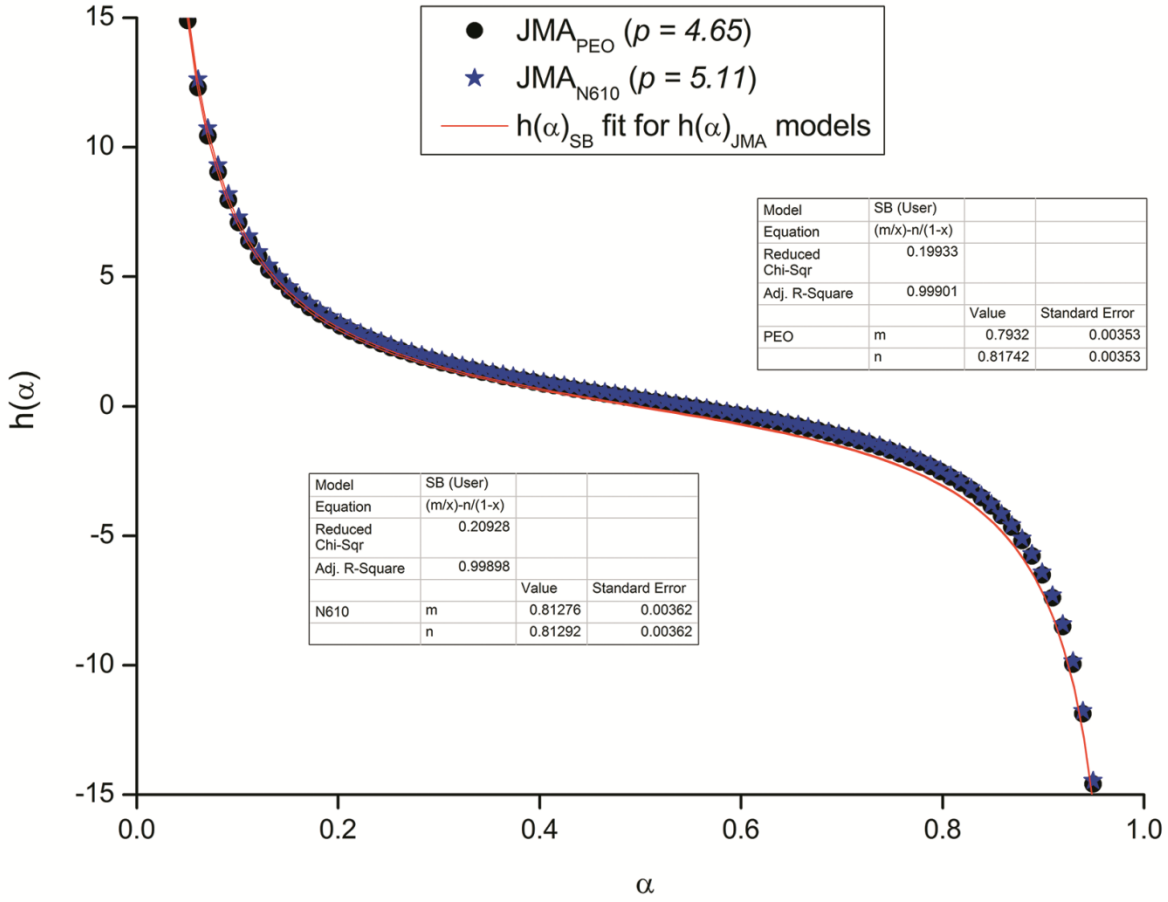

Figure 7.5: Crystallization parameters of JMA model for polyethylene oxide and Nylon (6, 10) [350], simulated by SB model parameters.

It is worth noticing that the suggested relationship fits well on the crystallization of the considered polymers excluding polyethylene oxide and Nylon (6, 10). In fact, the *p* values for polyethylene oxide and Nylon (6, 10) polymers, when simulated by SB model parameters as shown in Figure 7.5, depict deviation from the phenomenological relationship limits between both the models as demonstrated in Table 7.3. It is more likely that the crystallization mechanisms shown by both the polymers are not standard and probably more complicated.

While applying Eq. (7.16) to the experimental thermoanalytical data available in the literature, a point must be noted that the proposed relationship is absolute and the obtained results could differ slightly due to the data handing and treatment, say noise, numerical differentiation and/or integration, etc.

In addition to the above considerations, an interesting phenomenon is observed when *h(α)* expression for JMA model is simulated within the interval $p \in (0, 1)$. It is revealed that the behavior shown by JMA model in this interval with relatively higher values of JMA exponent closely resembles with the behaviors of diffusion models. The *h(α)* expressions for diffusion models are given in Table 7.7 and are graphically shown in Figure 7.6.

Table 7.7: *h(α)* expressions for well known diffusion models [126, 154, 239].

Reaction Model	Notation	*f(α)*	*h(α)*
1D-Diffusion	*D1*	*1/2α*	*-1/α*
2D-Diffusion	*D2*	*-1/ln(1-α)*	$1/\ln(1-\alpha)^{1-\alpha}$
3D-Diffusion (Jander's Equation)	*D3*	$\frac{3(1-\alpha)^{2/3}}{2\left\{1-(1-\alpha)^{1/3}\right\}}$	$-\frac{2}{3}\left[\frac{1}{1-\alpha}+\frac{1}{2(1-\alpha)^{2/3}\left\{1-(1-\alpha)^{1/3}\right\}}\right]$
3D-Diffusion (Ginstling Equation)	D4	$\frac{3}{2\left\{(1-\alpha)^{-1/3}-1\right\}}$	$-\frac{1}{3}\left[\frac{1}{\left\{(1-\alpha)^{-1/3}-1\right\}(1-\alpha)^{4/3}}\right]$

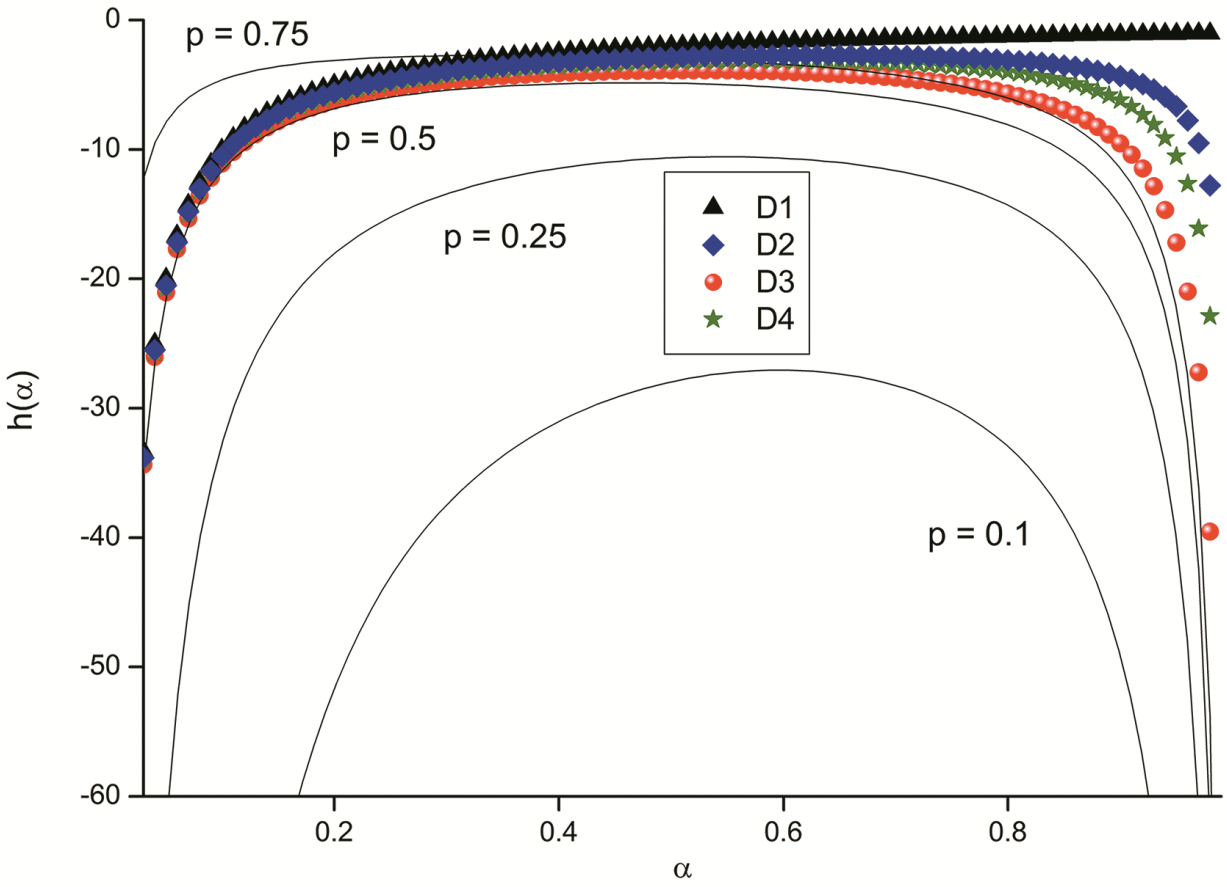

Figure 7.6: Comparison of *h(α)* expressions for JMA as $p \in (0, 1)$ and diffusion models [239].

It can be observed in Figure 7.6 that only the Jander's three dimensional diffusion (D3) model shows (up to certain extent) an agreement with JMA model for $p \approx 0.5$ in $\alpha \in [0, 0.5]$ and for $p \approx 0.75$ in $\alpha \in [0.5, 1]$. Though, the diffusion behavior shown by JMA model seems substantially complicated and might not be attributed to the well known diffusion models.

7.5. Conclusion

In this chapter, a new kinetic approach has been suggested to simulate the kinetics of crystallization in materials in general and in amorphous materials in particular, by employing the advanced reaction model determination methodology. On the basis of this approach, an explicit relationship between Johnson-Mehl-Avrami and Šesták-Berggren models has been developed that holds in the crystallization kinetics of amorphous materials. The validity conditions of the proposed relationship along with its phenomenological limits are also discussed. The values of the two parameters of empirical SB (m, n) model are related to the nucleation and growth dimensionality of known crystallization mechanisms with the help of JMA model. The suggested relationship has been effectively tested on the crystallization processes in various kinds of amorphous materials including; glasses alloys and polymers. Furthermore, this chapter sheds light on the finding that JMA model is not merely restricted to the phase transformations following nucleation/growth mechanism but also the relatively higher values of JMA exponents in the interval (0, 1) might also explain the solid state processes analogous to diffusion.

References

[1] P.J. Flory, Principles of Polymer Chemistry, 16th ed., Cornell University Press, New York, 1995.
[2] C. Vasile, G.E. Zaikov, New Trends in Natural and Synthetic Polymer Science, Nova Science Publishers, New York, 2006.
[3] J.-P. Pascault, H. Sautereau, J. Verdu, R.J.J. Williams, Thermosetting Polymers, Marcel Dekker, New York, 2002.
[4] J.K. Fink, A Concise Introduction to Additives for Thermoplastic Polymers, John Wiley and Sons, Salem, Massachusetts, 2010.
[5] K.A. Bhowmick, Current Topics in Elastomers Research, CRC Press, Boca Raton, 2008.
[6] http://www.docbrown.info/page04/OilProducts07.htm, last retrieved on November 26, 2018.
[7] https://igcseandialchemistry.com/addition-polymers/, last retrieved on November 26, 2018.
[8] D.W. Van Krevelen, K. Te Nijenhuis, Properties of Polymers: Their correlation with chemical structure, their numerical estimation and prediction from additive group, 4th ed., Elsevier B.V., Oxford, 2009.
[9] https://byjus.com/chemistry/nylon-fabric-and-polyester-fibres/, last retrieved on November 26, 2018.
[10] https://en.wikipedia.org/wiki/Epoxide, last retrieved on November 26, 2018.
[11] M.A. Boyle, C.J. Martin, J.D. Neuner, ASM Handbook: Epoxy Resins; Composites, Vol. 21, ASM Int., Ohio, 2001, p.78-89.
[12] S.T. Cholake, M.R. Mada, R.K.S Raman, Y. Bai, X. Zhao, S. Rizkalla, S. Bandyopadhyay, Defence Sci. J. 64 (2014) 314-321.
[13] J.H. Laza, C.A. Julian, E.M. Larrauri, M. Rodriguez, M.H. Leon, Polymer 40 (1999) 35-45.
[14] J. Wan, Z.-Y. Bu, C.-J. Xu, B.-G Li and H. Fan, Thermochim. Acta 519 (2011) 72–82.
[15] B. Meyer, Urea-Formaldehyde Resins, Addison-Wesley, Reading, Massachusetts, 1979.
[16] E. Lokensgard, Industrial Plastics: Theory and Applications, 5th ed., Delmar, New York, 2008.
[17] D. Levendis, A. Pizzi, A. Ferg, Holzforschung 46 (1992) 263–269.
[18] M.A. Hubbe, O.J. Rojas, L.A. Lucia, M. Sain, BioResources 3 (2008) 929–980.
[19] A.S. Singha, V.K. Thakur, Polym. Compos. 31 (2010) 459–470.
[20] H. Zhang, J. Zhang, S. Song, G. Wu, J. Pu, BioResources 6 (2011) 4430–4438.
[21] A.H. Basta, H.E. Saied, J.E. Winandy, R. Sabo, J. Polym. Enviorn. 19 (2011) 405–412
[22] K.K. Chawla, Fibrous Materials, 2nd ed., Cambridge University Press, Alabama, 2005.
[23] M. Elices, Structural Biological Materials, Pergamon Press, Amsterdam, 2000.
[24] S.A. Wainwright, W. D. Biggs, J. D. Currey, J. M. Gosline, Mechanical Design in Organisms, Princeton University Press, Princeton, New Jersey, 1982.
[25] K.K. Chawla, J. Miner. Met. Mater. Soc. 57 (2005) 47–47.
[26] A. Eitan, K. Jiang, D. Dukes, R. Andrews, L.S. Schadler, Chem. Mater. 15 (2003) 3198-3201.
[27] S.K. Bhattacharya, A.C.D. Chaklader, Polym. Plast. Technol. Eng. 19 (1982) 21–51.
[28] R. Strumpler, J. Glatz-Reichenbach, J. Electroceram. 3 (1999) 329–346.
[29] F. Carmona, Physica A 157 (1989) 461–469.
[30] H.Q. Pham, M.J. Marks, Encyclopedia of Polymer Science and Technology, John Wiley & Sons, New York, 2004.
[31] S.K. Bhattacharya, Metal-filled Polymers: Properties and Applications, Marcel Dekker, New-York, 1986.
[32] W. B. Genetti, W. L. Yuan, B. P. Grady, E. A. O'rear, C. L. Lai, D. T. Glatzhofer, J. Mater. Sci. 33 (1998) 3085–3093.
[33] A. Maaroufi, K. Haboubi, A. El Amarti, F. Carmona, J. Mater. Sci. 39 (2004) 265–270.
[34] J. Delmonte, Metal/Polymer Composites, Springer, New York, 1990.
[35] Y. Zarea, I. Shabanib, Mater. Sci. Eng. C 60 (2016) 195–203.
[36] V.E. Gul, Structure and Properties of Conducting Polymer Composites, VSP, Utrecht, 1996.
[37] X. S. Yi, G. Wu, Y. Pan, Polym. Int. 44 (1997) 117–124.

[38] C. Muñoz, G. Steinthal, S. Sunshine, Sensor Rev. 19 (1999) 300–305.
[39] D. Mottahed, Polym. Eng. Sci. 40 (2000) 61–69.
[40] B.S. Villacorta, T.H. Hubing, A.A. Ogale, Compos. Sci. Tech. 89 (2013) 158–166.
[41] D.M.B. Battelle, Polym. Eng. Sci. 17 (1977) 842–847.
[42] V.I. Roldughin, V.V. Vysotskii, Prog. Org. Coats. 39 (2000) 81–100.
[43] G. Bierwagen, R. Fishman, T. Storsved, J. Johnson, Prog. Org. Coat. 35 (1999) 1–9.
[44] K. Falconer, Fractal Geometry; Mathematical Foundations and Applications, 2nd Ed., John Wiley & Sons, West Sussex, England, 2004.
[45] D. Stauffer, A. Aharonay, Introduction to Percolation Theory, 2nd Ed., Taylor & Francis, London, 1992.
[46] V.I. Selyakov, V.V. Kadet, Percolation Models for Transport in Porous Media, Springer, Dordrecht, 2006.
[47] P.J. Brigandi, J.M. Cogen, R.A. Pearson, Polym. Eng. Sci. 54 (2014) 1–16.
[48] J. Gurland, Trans. Metall. Soc. 236 (1966) 642–646.
[49] A. Malliaris, D.T. Turner, J. Appl. Phys. 42 (1971) 614–618.
[50] G. Pinto, A. Jiménez-Martín, Polym. Comp. 22 (2001) 65–70.
[51] A. Maaroufi, G. Pinto, I. Paz, J. Appl. Polym. Sci. 98 (2005) 990–996.
[52] G. Pinto, A.K. Maaroufi, J. Appl. Polym. Sci. 96(6) (2005) 2011–2015.
[53] E. Bruneel, A.J. Ramirez-Cuesta, I.V. Driessche, S. Hoste, Phys. Rev. B 61 (2000) 9176–9180.
[54] F.F.T. Araujo, H.M. Rosenberg, J. Phys. D: Appl. Phys. 9 (1976) 665–675.
[55] V. Kurnoskin, Polym. Compos. 14 (1993) 481–490.
[56] S.-G. Hong, Macromol. Mat. Eng. 215 (1994) 161–173.
[57] S.-G. Hong, J.-S. Tsai, Macromol. Mat. Eng. 276/277 (2000) 59–65.
[58] Z. Zhang, C. P. Wong, J. App. Polym. Sci. 86 (2002) 1572–1579.
[59] J.V.D. Brand, S.V. Gils, P.C.J. Beentjes, H. Terryn, V. Sivel, J.H.W. de Wit, Prog. Org. Coats. 51 (2004) 339–350.
[60] M. Aufray, A.A. Roche, Int. J. Adhes. Adhes. 27, 387–393 (2007).
[61] P. Mohan, J. App. Polym. Sci. 116 (2010) 3271–3277.
[62] M. El Homrany, A. Maaroufi, R. Benavente, J. M. Pereña, G. Pinto, M. Halim, J. App. Polym. Sci. 118 (2010) 3701–3706.
[63] K. Haboubi, Preparation and study of the electrical, thermal and thermo-mechanical behaviors of polymers filled with conducting particles (in French), Abdel Malek Essaadi University, Tetouan (Moroco), 2004.
[64] A.S. Luyt, J.A. Molefi, H. Krump, Polym. Degrad. Stab. 91 (2006) 1629–1636.
[65] W. Zhou, D. Yu, J. App. Polym. Sci. 118 (2010) 3156–3166.
[66] G. Pinto, A.K. Maaroufi, Polym. Compos. 26(3) (2005) 401–406.
[67] G. Pinto, A.K. Maaroufi, R. Benavente, J.M. Pereña, Polym. Compos. 32(2) (2011) 193–198.
[68] G. Pinto, A.K. Maaroufi, Polym. Compos. 33(12) (2012) 2188–2194.
[69] R. Tomovska, A. Agirre, A. Veloso, J.R. Leiza, Reference Module in Chemistry, Molecular Sciences and Chemical Engineering: Characterization Techniques for Polymeric Materials, Elsevier, Waltham, Massachusetts, 2014.
[70] P.J. Goodhew, J. Humphreys, R. Beanland, Electron Microscopy and Analysis, Taylor & Francis, New York, 2001.
[71] V. Kazmiruk, Scanning Electron Microscopy, InTech, Shanghai, 2012.
[72] Y. Waseda, E. Matsubara, K. Shinoda, X-Ray Diffraction Crystallography, Springer, New York, 2011.
[73] V.R. Gowariker, N.V. Viswanathan, J. Sreedhar, Polymer Science, New Age Int., New Delhi, 2012.
[74] https://www.doitpoms.ac.uk/tlplib/polymers/crystalline.php, last retrieved on November 26, 2018.
[75] www.icdd.com, last retrieved on November 27, 2018.
[76] R. Bhargava, S. Wang, J.L. Koening, Advances in Polymer Science: FTIR Microspectroscopy of polymeric systems, Vol. 163, Springer, 2003, p. 137-191.

[77] L.H. Lee, Characterization of Metal and Polymer Surfaces: Metal Surfaces, Academic Press, New York, 1977.
[78] D.I. Bower, W.F. Maddams, The Vibrational Spectroscopy of Polymer, Cambridge University Press, UK, 1989.
[79] J.L. Koenig, Rapra Review Reports: Infrared and Raman Spectroscopy of Polymers, Rapra Technology, UK, 2001.
[80] P. Zhang, J. He, X. Zhou, Polym. Test. 27 (2008) 153–157.
[81] O. Winther-Jensen, R. Vijayaraghavan, J. Sun, B. Winther-Jensen, D.R. MacFarlane, Chem. Commun. 21 (2009) 3041–3043.
[82] http://www.imperial.ac.uk/vibrational-spectroscopy-and-chemical-imaging/research/complex-materials/, last retrieved on November 26, 2018.
[83] J. Šesták, Science of Heat and Thermophysical Studies: A Generalized Approach to Thermal Analysis, Elsevier B.V., Amsterdam, 2005.
[84] P. Gabbott, Principles and Applications of Thermal Analysis, Wiley-Blackwell, Oxford, 2007.
[85] A.W. Coats, J.P. Redfern, Analyst, 88 (1963) 906–924.
[86] J. Šesták, Thermophysical Properties of Solids, Their Measurements and Theoretical Analysis, Elsevier, Amsterdam, 1984.
[87] S. Vyazovkin, Characterization of Materials; Thermogravimetric Analysis, 2nd ed., John Wiley & Sons, New Jersey, 2012.
[88] https://www.labcompare.com/169-Thermogravimetric-Analyzer-TGA-Analyzer/9818903-Q500-Thermogravimetric-Analyzer/#productdetails, last retrieved on November 26, 2018.
[89] H.M. Gajiwala, R. Zand, Polymer 41 (2000) 2009–2015.
[90] Z. Tao, J. Jin, S. Yang, D. Hu, G. Li, J. Jiang, J. Macromol. Sci. B 48 (2009) 1114–1124.
[91] X. Liu, W. Yu, J. Appl. Polym. Sci. 99 (2006) 937–944.
[92] B. Wunderlich, Thermal Analysis, Academic Press, New York, 1990.
[93] J.A. Dean, The Analytical Chemistry Handbook, McGraw Hill, New York, 1995.
[94] E. Pungor, A Practical Guide to Instrumental Analysis, CRC Press, Boca Raton, 1995.
[95] D.A. Skoog, F.J. Holler, T.A. Nieman, Principles of Instrumental Analysis, 5th ed., Brooks Cole, New York, 1998.
[96] M.J. O'Neill, Anal. Chem. 36 (1964) 1238–1245.
[97] http://pslc.ws/macrog/dsc.htm, last retrieved on November 26, 2018.
[98] B. Wunderlich, Macromolecular physics: crystal melting, Vol. 3, Academic Press, New York, 1980, p. 366.
[99] W.S. Kloss, Differential Thermal Analysis: Application and Results in Mineralogy, Springer, Berlin, 1974.
[100] M.E. Brown, P.K. Gallagher, Handbook of Thermal Analysis and Calorimetry; Recent Advances, Techniques and Applications, Elsevier, B.V., Amsterdam, 2008.
[101] S. Vyazovkin, Isoconversional Kinetics of Thermally Stimulated Processes, Springer, New York, 2015.
[102] M.E. Brown, M. Maciejewski, S. Vyazovkin, etal. Thermochim. Acta 355 (2000) 125-143.
[103] M. Maciejewski, Thermochim. Acta 355 (2000) 145-154.
[104] S. Vyazovkin, Thermochim. Acta 355 (2000) 155-163.
[105] A.K. Burnham, Thermochim. Acta 355 (2000) 165-170.
[106] B. Roduit, Thermochim. Acta 355 (2000) 171-180.
[107] S. Vyazovkin, A.K. Burnham, J.M. Craido, L.A. Pérez-Maqueda, C. Popescu, N. Sbirrazzuoli, Thermochim. Acta 520 (2011) 1-19.
[108] M. Bertmer, R.C. Nieuwendaal, A.B. Barnes, S.E. Hayes, J. Phys. Chem. B 110 (2006) 6270–6273.
[109] P.W.M. Jacobs, F.C. Tompkins, Classification and theory of solid reactions. In W.E. Garner (ed.), Chemistry of the solid state, Academic Press, New York, 1955, pp. 184.
[110] M.E. Brown D. Dollimore, A.K. Galwey, Theory of solid state reaction kinetics. In C. F. H. Tipper (ed.), Comprehensive Chemical kinetics, Elsevier, Amsterdam, 1980.

[111] A. Khawam, D.R. Flanagan, J. Pharm. Sci. Volume 95 (2006) 472–498.
[112] M. Fanfoni, M. Tomellini, Il Nuovo Cimento 20 (1998) 1171–1182.
[113] F. Booth, Trans. Faraday Soc. 44 (1948) 796–801.
[114] A. Khawam, D.R. Flanagan, J. Phys. Chem. B, 110 (2006) 17315–17328.
[115] Ginstling, B.I. Brounshtein, J. Appl. Chem. USSR 23 (1950) 1327–1338.
[116] W.Z. Jander, Anorg. Allg. Chem. 163 (1927) 1–30.
[117] J. Sestak, G. Berggren, Thermochim. Acta 3 (1971) 1–12.
[118] P.W.M. Jacobs, F.C. Tompkins, Chemistry of the Solid State, Academic Press, New York, 1955. or Bagdassarian, C. Acta Physicochim. U.S.S.R. 1945, 20, 441
[119] H. L. Friedman, J. Polym. Sci. 6 (C) (1965) 183–195.
[120] J. H. Flynn, Thermochim. Acta 300 (1997) 83–92.
[121] J. Cai, F. Yao, W. Yi, F. He, AIChE J. 52 (2006) 1554–1557.
[122] T. Ozawa, Bull. Chem. Soc. Jpn. 38 (1965) 1881–1886.
[123] J. H. Flynn, L.A. Wall, J. Polym. Sci. Part C: Polym. Lett. 4 (1966) 323–328.
[124] T. Sunose, T. Akahira, Res. Report: Chiba Inst. Technol. (Sci. Technol.) 16 (1971) 22–31.
[125] M.J. Starink, Thermochim. Acta 404 (2003) 163–176.
[126] M.A. Arshad, A. Maaroufi, Thermochim. Acta 585 (2014) 25–35.
[127] S. Vyazovkin, D. Dollimore, J. Chem. Inf. Comput. Sci. 36 (1996) 42–45.
[128] S. Vyazovkin, J. Comp. Chem. 18 (1997) 393–402.
[129] S. Vyazovkin, J. Comput. Chem. 22 (2001) 178–183.
[130] A.W. Coats, J.P. Redfern, Nature 201 (1964) 68–69.
[131] A.W. Coats, J.P. Redfern, J. Polym. Sci. Part C: Polym. Lett. 3 (1965) 917–920.
[132] J. Màlek, Thermochim. Acta 200 (1992) 257–269.
[133] J. Malek, T. Mitsuhashi, J.M. Criado, J. Mat. Res. 16 (2001) 1862–1871.
[134] G.I. Senum and R.T. Yang, J. Therm. Anal. 11 (1977) 445–447.
[135] P.E. Sánchez-Jiménez, L.A. Pérez-Maqueda, A. Perejón and J.M. Criado, J. Phys. Chem. A 2010 (114) 7868–7876.
[136] P.E. Sánchez-Jiménez, L.A. Pérez-Maqueda, A. Perejón, J.M. Criado, Thermochim. Acta 552 (2013) 54–59.
[137] S. Vyazovkin, C.A. Wight, Annu. Rev. Phys. Chem. 48 (1997) 125–149.
[138] S. Vyazovkin, New J. Chem. 24 (2000) 913–917.
[139] S. Vyazovkin, Int. Rev. Phys. Chem. 19 (2000) 45–60.
[140] G. Tan, Q. Wang, H. Zheng, J. Phys. Chem.- A 115(22) (2011) 5517–5524.
[141] D.M. Kooij, Z. Phys. Chem., 12 (1893) 155–161.
[142] S.O. Ajadi, S.S. Okoya, Int. Comm. Heat Mass Transfer 31 (2004) 143–150.
[143] R.W. Carr, Modeling of Chemical Reactions, Elsevier B.V., Amsterdam, 2007.
[144] A.K. Burnham, R.L. Braun, Energ. Fuel 13 (1999) 1–22.
[145] E. Segal, Thermochim. Acta, 42 (1980) 357–361.
[146] M. Balarin, Phys. Stat. Sol. 54(2) (1979) K137–K140.
[147] D. Dollimore, G.A. Gamlen, T.J. Taylor, Thermochim. Acta, 54 (1982) 181–186.
[148] M.J. Dresser, T.E. Madey, T.J. Yates, Surf. Sci. 42 (1974) 533–551.
[149] H. Ibach, W. Erley, H. Wagner, Surf. Sci. 92 (1980) 29–42.
[150] J.M. Soler, N. Garcia, Surf. Sci. 124 (1983) 563–570.
[151] R.M. German, Sintering Theory and Practice, John Wiley, New York, 1996.
[152] M.A. Arshad, A. Maaroufi, G. Pinto, S. El-Barkany, A. Elidrissi, Bull. Mater. Sci. 39 (2016) 1609–1618.
[153] M.A. Arshad, A. Maaroufi, MOJ Polym. Sci. 1(3) (2017) 120–125.
[154] M.A. Arshad, A. Maaroufi, Rev. Adv. Mater. Sci. 51 (2017) 177.
[155] J. Fan, J. Zeng, Appl. Math. Comput. 219 (2013) 9438–9446.
[156] J.M. Criado, L.A. Pérez-Maqueda, P.E. Sánchez-Jiménez, J. Therm. Anal. Calorim. 82 (2005) 671–675.

[157] N. Sbirrazzuoli, Thermochim. Acta, 564 (2013) 59–69.
[158] S. Vyazovkin, Thermochim. Acta 397 (2003) 269–271.
[159] S. Vyazovkin, Phys. Chem. Chem. Phys. 18 (2016) 18643–18656.
[160] Acton, Numerical Methods That Work, 2nd ed., Math. Assoc. Amer., Washington DC, 1990.
[161] J. Sarada, K.V. Nagaraja, Appl. Math. Comput. 217 (2011) 5612-5621.
[162] B. Janković, Colloid Polym. Sci. 296 (2018) 1459–1477.
[163] F. Ouanji, M. Khachani, S. Arsalane, M. Kacimi, M. Halim, A. El Hamidi, Monatsh. Chem. 147 (2016) 1693–1702.
[164] H. Ebrahimzade, G.R. Khayati, M. Schaffie, Trans. Nonferrous Met. Soc. China 28 (2018) 1265–1274.
[165] H. Ebrahimzade, G.R. Khayati, M. Schaffie, Adv. Powder Technol. 28 (2017) 2779–2786.
[166] M. Koniorczyk, P. Konca, Int. J. Therm. Sci. 122 (2017) 124–132.
[167] M. Dahhou, M. El Moussaouiti, A. Benlalla, A. El Hamidi, M. Taibi, M.A. Arshad, Waste Biomass Valor. 7 (2016) 1177–87.
[168] S. Thomas, K. Joseph, S.K. Malhotra, K. Goda, M.S. Sreekala, Polymer Composites, V1: Macro- and Microcomposites, Wiley-VCH Verlag Gmbh & co. Weinheim, 2012.
[169] D.L. Deborah, Chung, Composite Materials Science and Applications, 2nd ed., Springer-Verlag, London, 2010.
[170] N. Boumedienne, Y. Faska, A. Maaroufi, G. Pinto, L. Vicente, R. Benavente, Phys. Chem. Solids 104 (2017) 185–191.
[171] M.A. Arshad, A. Maaroufi, Soc. Plast. Eng., 2018. DOI: 10.2417/spepro.006991
[172] M.A. Arshad, A. Maaroufi, Soc. Plast. Eng., 2015. DOI: 10.2417/spepro.006183
[173] A.J. McNamara, Y. Joshi, Z. M. Zhang, Int. Jrnl. Therm. Sci. 62 (2011) 2–11.
[174] D. Angmo, F.C. Krebs, J. App. Polym. Sci. 129 (2013) 1–14.
[175] B.P. Rand, H. Richter, Organic Solar Cells: Fundamentals, Devices, and Upscaling, Taylor & Francis, Florida, 2014.
[176] N.N. Greenwood, A. Earnshaw, Chemistry of the Elements, 2nd ed., Butterworth-Heinemann, Oxford, 1997.
[177] R. Mihai, N. Sofian, D. Rusu, Polym. Test. 20 (2001) 409–417.
[178] M. Rusu, M. Dărăngă, N. M. Sofian, D.L. Rusu, Mat. Plast. 35 (1998) 15.
[179] B. Pradhan, S. K. Majee, S. K. Batabyal, A.J. Pal, J. Nanosci. Nanotechnol. 7 (2007) 4534–4539.
[180] J.T. Seil, T.J. Webster, Zinc oxide nanoparticle and polymer antimicrobial biomaterial composites, Proceedings of the 2010 IEEE 36th Annual Northeast Bioengineering Conference, (2010) 1–2.
[181] P.J. Smith, Chemistry of Tin, Springer, Dordrecht, 1998.
[182] M.A. Arshad, A. Maaroufi, R. Benavente, G. Pinto, Polym. Compos. 38 (2017) 1529–1540.
[183] M.A. Arshad, A. Maaroufi, R. Benavente, J.M. Pereña, G. Pinto, Polym. Compos. 34 (2013) 2049–2060.
[184] M. A. Arshad, A. Maaroufi, R. Benavente, G. Pinto, J. Mater. Environ. Sci. 5 (2014) 1342-1354.
[185] Th.V. Kosmidou, A.S. Vatalis, C.G. Delides, E. Logakis, P. Pissis, G.C. Papanicolaou, Express Polym. Lett. 2 (2008) 364–372.
[186] S.F. Bartolucci, J. Paras, M.A. Rafiee, J. Rafiee, S. Lee, D. Kapoor, N. Koratk, Mater. Sci. Eng. A 528 (2011) 7933–7937.
[187] C. Yao, W. Chen, W. Gao, Surf. Coat. Tech. 219 (2013) 126–130.
[188] L.Y. Beaulieu, S.D. Beattie, T.D. Hatchard, and J.R. Dahn, J. Electrochim. Soc. 150 (2003) A419–A424.
[189] Y. Ngono, Y. Maréchal, N. Mermilliod, J. Phys. Chem. B 103 (1999) 4979–4985.
[190] G. Bouvet, N. Dang, S. Cohendoz, X. Feaugas, S. Mallarino, S. Touzain, Prog. Org. Coat. 96 (2016) 32–41.
[191] H.-C. Lu, Y.-C. Peng, M.-Y. Lin, S.-L. Chou, J.-I. Lo, B.-M. Cheng, Opt. Photon. J. 3 (2013) 25–28.
[192] M.A. Arshad, A. Maaroufi, R. Benavente, G. Pinto, J. Appl. Polym. Sci. 134 (2017) 1–13.

[193] I.A. Hakim, S.L. Donaldson, N.G. Meyendorf, C.E. Browning, Mater. Sci. App. 8 (2017) 170–187.
[194] M.A. Arshad, A. Maaroufi, R. Benavente, G. Pinto, J. Mat. Sci. Mat. Electron. 28 (2017) 11832–11845.
[195] M.A. Arshad, A. Maaroufi, R. Benavente, G. Pinto, Polym. Compos. 39 (2018) 4341–4354.
[196] S. Park, J.O. Baker, M.E. Himmel, P.A. Parilla, D.K. Johnson, Biotechnol. Biofuels 3 (2010) 1–10.
[197] E. Roumeli, E. Papadopoulou, E. Pavlidou, G. Vourlias, D. Bikiaris, K.M. Paraskevopoulos, K. Chrissafis, Thermochim. Acta 527 (2012) 33–39.
[198] I.M. Arafa, M.M. Fares, A.S. Braham, Eur. Polym. J. 40 (2004) 1477–1487.
[199] V. Jovanovic´, S. Samarzija-Jovanovic´, B. Petkovic´, Z. Milic´evic´, G. Markovic´, M. Marinovic´-Cincovic´, Polym. Compos. 2018, accepted manuscript. DOI: 10.1002/pc.24849
[200] S.S. Jada, J. Appl. Polym. Sci. 35 (1988) 1573–1592.
[201] H. Yang, R. Yan, H. Chen, D.H. Lee, C. Zheng, Fuel 86 (2007) 1781–1788.
[202] F. Xu, J.X. Sun, R. Sun, P. Fowler, M.S. Baird, Ind. Crop. Prod. 23 (2006) 180–193.
[203] B.C. Smith, Infrared spectral interpretation: a systematic approach, CRC Press, Boca Raton, 1998.
[204] M.O. Edoga, Leonardo Elect. J. Pract. Tehnol. 9 (2006) 63–80.
[205] S. Samarzija-Jovanovic, V. Jovanovic, S. Konstantinovic, G. Markovic, M. Marinovic-Cincovic, J. Therm. Anal. Calorim. 104 (2011) 1159–1166.
[206] S. Vyazovkin, K. Chrissafis, M.L.D. Lorenzo, N. Koga, M. Pijolat, B. Roduit, N. Sbirrazzuoli, J.J. Suñol, Thermochim. Acta 590 (2014) 1–23.
[207] A.A. Joraid , I.M.A. Alhosuini, Thermochim. Acta 595 (2014) 28–34.
[208] J.M. Criado, P.E. Sánchez-Jiménez, L.A. Pérez-Maqueda, J. Therm. Anal. Calorim. 92 (2008) 199–203.
[209] Z. Shuping, W. Yulong, Y. Mingde L. Chun, T. Junmao, Bioresour. Technol. 101 (2010) 359–365
[210] S.C. Lin, B.J. Bulkin, E.M. Pearce, J. Polym. Sci. A Polym. Chem. 17 (1979) 3121–3148.
[211] J.C. Paterson-Jones, J. Appl. Polym. Sci. 19 (1975) 1539–1547.
[212] D.P. Bishop, D.A. Smith, J. Appl. Polym. Sci. 14 (1970) 205–223.
[213] J.M. Stuart, DA. Smith, J. Appl. Polym. Sci. 9 (1965) 3195–3214.
[214] D. Puglia, L.B. Manfredi, A. Vazquez, J.M. Kenny, Polym. Degrad. Stab. 73 (2001) 521–527.
[215] B.-L. Denq, W.-Y. Chiu, K.-F. Lin, M.-R.S Fu, J. App. Polym. Sci. 81 (2001) 1161–1174.
[216] M.V.S. Murty, E.A. Grulke, D. Bhattachatyya, Polym. Degrad. Stab. 61 (1998) 421–430.
[217] P.-Y. Kuo, L. A. Barros, Y.-C. Sheen, M. Sain, J. S. Y. Tjong, N. Yan, J. Anal. App. Pyrol. 117 (2016) 199–213.
[218] C.D. Doyle, Anal. Chem. 33 (1961) 77–79.
[219] M.D. Argyle, C.H. Bartholomew, Catalysts 5 (2015) 145–269.
[220] C.H. Bartholomew, Appl. Catal. A 212 (2001) 17–60.
[221] Y. Takahashi, T. Azumi, Y. Sekine, Thermochim. Acta 139 (1989) 133–137.
[222] S. Enthaler, ACS Catal. 3 (2013) 150–158.
[223] F. Grønvold, S. Stølen, Thermochim. Acta 395 (2002) 127–131.
[224] H. Nishida, T. Mori, S. Hoshihara, Y. Fan, Y. Shirai, T. Endo, Polym. Degrad. Stab. 81 (2003) 515–523.
[225] H. Dong, A.P. Esser-Kahn, P.R. Thakre, J.F. Patrick, N.R. Sottos, S.R. White, J.S. Moore, ACS Appl. Mater. Interfaces 4 (2012) 503–509.
[226] T.W. Chapman, Mater. Sci. Eng. 1 (1966) 65–69.
[227] K. Siimer, T. Kaljuvee, P. Christjanson, I. Lasn, J. Therm. Anal. Calorim. 84 (2006) 71–77.
[228] C. Camino, C. Operti, L. Trossarelli, Polym. Degrad. Stab. 5 (1983) 161–172.
[229] T. Zorba, E. Papadopoulou, A. Hatjiissaak, K.M. Paraskevopoulos, K Chrissafis, J. Therm. Anal. Calorim. 92 (2008) 29–33.
[230] S. Spoljaric, K.K. Wong, M. Pannirselvam, G.J. Griffin, R.A. Shanks, S. Setunge, Chemeca 41 (2013) 805–811.
[231] V. Malmeev, S. Bourbigot, J. Yvon, J. Anal. Appl. Pyrol. 80 (2007) 151–165.
[232] V. Malmeev, S. Bourbigot, M.L. Bras, J. Yvon, Chem. Eng. Sci. 61 (2006) 1276–1292.

[233] M.E. Brown, Introduction to Thermal Analysis, 2nd ed., Kluwer, Dordrecht, 2001.
[234] D. Rosu, C.N. Cascaval, F. Mustata, C. Ciobanu, Thermochim. Acta 383 (2002) 119–127.
[235] J. Luo, K. Ying, J. Bai, Signal Process. 85 (2005) 1429–1434.
[236] J. Wan, B.G. Li, H. Fan, Z.Y. Bu, C.J. Xu, Thermochim. Acta 511 (2010) 51–58.
[237] S. Montserrat, J. Malek, P. Colomer, Thermochim. Acta 313 (1998) 83–95.
[238] K. Chrissafis, K.M. Paraskevopoulos, D. Bikiaris, Thermochim. Acta 505 (2010) 59–68.
[239] M.A. Arshad, A. Maaroufi, J. Non-Cryst. Solids 413 (2015) 53–58.
[240] P. Simon, Thermochim. Acta 520 (2011) 156–157.
[241] M.E. Brown, Thermochim. Acta 300 (1997) 93–106.
[242] H. Dong, Y. Li, J. Zhang, L. Liu, L. Cao, P. Ming, W. Liu, C. Zhang, L. Liu, H. Wei, RSC Adv. 6 (2016) 65533–65540.
[243] A. Perejon, P.E. Sanchez-Jimenez, J.M. Criado, L.A. Perez-Maqueda, J. Phys. Chem. B 115 (2011) 1780–1791.
[244] Y. Sun, W. Zhang, H. Chi, Y. Liu, C.L. Hou, D. Fang, Renew. Sust. Energ. Rev. 43 (2015) 973–980.
[245] J.-S. Cho, S. Baek, S.-H. Park, J.H. Park, J. Yoo, K.H. Yoon, Sol. Energ. Mater. Sol. Cells 102 (2012) 50–57.
[246] P.G.V. Sampaioa, M.O.A. González, Renew. Sust. Energ. Rev. 74 (2017) 590–601.
[247] https://www.nrel.gov/pv/accelerated-testing-analysis.html, last retrieved on November 26, 2018.
[248] H. Cao, W. He, Y. Mao, X. Lin, K. Ishikawa, J.H. Dickerson, W.P. Hess, J. Power Sources 264 (2014) 168–183.
[249] L. Hu, F. Wu, C. Li, A. Hu, X. Hu, Y. Zhang, L. Chen, Y. Chen, Macromolecules 48 (2015) 5578–5586.
[250] F. Meyer, Prog. Polym. Sci. 47 (2015) 70–91.
[251] C.E. Small, S.-W. Tsang, S. Chen, S. Baek, C.M. Amb, J. Subbiah, J.R. Reynolds, F. So, Adv. Energy Mat. 3 (2013) 909–916.
[252] A.J. Moule, Curr. Opin. Solid State Mater. Sci. 14 (2010) 123–130.
[253] M. Helgesen, S. Sondergaard, F.C. Krebs, J. Mater. Chem. 20 (2010) 36–60.
[254] V. Svrcek, H. Fujiwara, M. Kondo, Acta Mater. 57 (2009) 5986–5995.
[255] C.J. Brabec, S.N. Sariciftci, Monatsh. Chem. 132 (2001) 421–431.
[256] F.C. Krebs (Guest Ed.), Special issue entitled, "Degradation and stability of polymer and organic solar cells", Sol. Energ. Mater. Sol. Cells 92 (2008) 685–820.
[257] M.O. Reese, S.A. Gevorgyan, M. Jørgensen, et al. Sol. Energ. Mater. Sol. Cells 95 (2011) 1253–1267.
[258] S.A. Gevorgyan, N. Espinosa, L. Ciammaruchi, et al., Adv. Energy Mat. 6 (2016) 1600910.
[259] J. Kettle, V. Stoichkov, D. Kumar, M. Corazza, S.A. Gevorgyan, F.C. Krebs, Sol. Energ. Mater. Sol. Cells 167 (2017) 53–59.
[260] L. Torto, A. Rizzo, A. Cester, N. Wrachien, L. Passarini, F.C. Krebs, M. Corazza, S.A. Gevorgyan, Analysis of electrical and thermal stress effects on PCBM:P3HT solar cells by photocurrent and impedance spectroscopy modeling, IEEE International Reliability Physics Symposium (2017), DOI: 10.1109/IRPS.2017.7936274.
[261] P. R. Berger, M. Kim, J. Renew. Sustain. Ener. 10 (2018) 013508.
[262] D. Chi, S. Qu, Z. Wang, J. Wang, J. Mater. Chem. C 2 (2014) 4383–4387.
[263] C.-P. Lee, C.-T. Li, K.-C. Ho, Mater. Today 20 (2017) 267–283.
[264] G. Li, R. Zhu, Y. Yang, Nat. Photonics 6 (2012) 153–161.
[265] http://plasticphotovoltaics.org/lc/lc-polymersolarcells/lc-layer.html, last retrieved on July 19, 2018.
[266] W. Cao, J. Li, H. Chen, J. Xue, J. Photon. Energy 4 (2014) 040990.
[267] G. Dennler, C. Lungenschmied, H. Neugebauer, N.S. Sariciftci, A. Labouret, J. Mater. Res. 20 (2005) 3224–3233.
[268] F.C. Krebs, Sol. Energ. Mater. Sol. Cells 90 (2006) 3633–3643.

[269] S. Seethamraju, P.C. Ramamurthy, G. Madras, Encapsulation for Improving the Efficiencies of Solar Cells. In D.J. Lockwood (Ed.), Materials and Processes for Solar Fuel Production, Springer, New York, 2014, pp. 23.
[270] M. Jørgensen, K. Norrman, F.C. Krebs, Sol. Energ. Mater. Sol. Cells 92 (2008) 686–714.
[271] S. Jiang, K. Wang, H. Zhang, Y. Ding, Q. Yu, Macromol. React. Eng. 9 (2015) 522–529.
[272] Q.L. Song, Appl. Phys. Lett. 89 (2006) 251118.
[273] S. Schäfer, A. Petersen, T.A. Wagner, R. Kniprath, D. Lingenfelser, A. Zen, et al., Phys. Rev. B 83 (2011) 165311.
[274] C. Deibel, V. Dyakonov, Rep. Prog. Phys. 73 (2010) 096401.
[275] E.B.L. Pedersen, T. Tromholt, M.V. Madsen, A.P.L. Böttiger, M. Weigand, F.C. Krebs, J.W. Andreasen, J. Mater. Chem. C 2 (2014) 5176-5182.
[276] I.F. Dominguez, A. Distler, L. Luer, Adv. Energy Mater. 7 (2016) 1601320.
[277] P.A. Troshin, Org. Photonics Photovolt. 3 (2015) 161–182.
[278] V.I. Madogni, B. Kounouhewa, A. Akpo, M. Agbomahéna, S.A. Hounkpatin, C.N. Awanou, Chem. Phys. Lett. 640 (2015) 201–214.
[279] A. Rivaton, A. Tournebize, J. Gaume, P.-O. Bussiere, J.-L. Gardette, S. Therias, Polym. Int. 63 (2014) 1335–1345.
[280] N. Grossiord, J.M. Kroon, R. Andriessen, P.W.M. Blom, Org. Electron. 13 (2012) 432–456.
[281] F.C. Krebs, Stability and degradation of organic and polymer solar cells, Wiley, New York, 2012.
[282] A. Manor, E.A. Katz, T. Tromholt, F.C. Krebs, Adv. Energy Mater. 1 (2011) 836–843.
[283] K. Norrman, M.V. Madsen, S.A. Gevorgyan, F.C. Krebs, J. Am. Chem. Soc. 132 (2010) 16883–16892.
[284] F.C. Krebs, S.A. Gevorgyan, J. Alstrup, J. Mater. Chem. 19 (2009) 5442-5451.
[285] R.D. Bettignies, J. Leroy, M. Firon, C. Sentein, Synth. Met. 156 (2006) 510–513.
[286] S. Schuller, P. Schilinsky, J. Hauch, C.J. Brabec, App. Phys. A 79 (2004) 37–40.
[287] I. Visoly-Fisher, A. Mescheloff, M. Gabay, C. Bounioux, L. Zeiri, M. Sansotera, A.E. Goryachev, A. Braun, Y. Galagan, E.A. Katz, Sol. Energ. Mater. Sol. Cells 134 (2015) 99–107.
[288] J. Adams, G.D. Spyropoulos, M. Salvador, N. Li, S. Strohm, L. Lucera, S. Langner, F. Machui, H. Zhang, T. Ameri, M.M. Voigt, F.C. Krebs, C.J. Brabec, Energ. Environ. Sci. 8 (2015) 169–176.
[289] I. Cardinaletti, J. Kesters, S. Bertho, B. Conings, F. Piersimoni, J. D'Haen, L. Lutsen, M. Nesladek, B.V. Mele, G.V. Assche, K. Vandewal, A. Salleo, D. Vanderzande, W. Maes, J.V. Manca, J. Photon. Energy 4 (2015) 040997.
[290] J. Kesters, P. Verstappen, J. Raymakers, W. Vanormelingen, J. Drijkoningen, J. D'Haen, J. V. Manca, L. Lutsen, D.J.M. Vanderzande, W. Maes, Chem. Mater. 27 (2015) 1332–1341.
[291] M. Corazza, F.C. Krebs, S.A. Gevorgyan, Sol. Energ. Mater. Sol. Cells 143 (2015) 467–472.
[292] N. Bristow, J. Kettle, J. Renew. Sust. Energy 7 (2015) 013111.
[293] J. Kesters, S. Kudret, S. Bertho, N.V. den Brande, M. Defour, B.V. Mele, H. Penxten, L. Lutsen, J. Manca, D. Vanderzande, W. Maes, Org. Electron. 15 (2014) 549–562.
[294] A. Dupuis, P. Wong-Wah-Chung, A. Rivaton, J.-L. Gardette, Polym. Degrad. Stab. 97 (2012) 366–374.
[295] O. Haillant, D. Dumbleton, A. Zielnik, Sol. Energ. Mater. Sol. Cells 95 (2011) 1889–1895.
[296] T.J. McMahon, Prog. Photovolt.: Res. Appl. 12 (2004) 235–248.
[297] O. Haillant, Sol. Energ. Mater. Sol. Cells 95 (2011) 1284–1292.
[298] M. Vasquez, I. Rey-Stolle, Prog. Photovolt.: Res. Appl. 16 (2008) 419–433.
[299] M.A. Arshad, A. Maaroufi, J. Power Sources 391 (2018) 134–147.
[300] A. Mahmoudloo, S. Ahmadi-Kandjani, App. Phys. A 119 (2015) 1523–1529.
[301] V. Dyakonov, App. Phys. A 79 (2004) 21–25.
[302] F. Jesnsen, Qual. Reliab. Eng. Int. 1 (1985) 13–17.

[303] H.C. Weerasinghe, S.E. Watkins, N. Duffy, D.J. Jones, A.D. Scully, Sol. Energ. Mater. Sol. Cells 132 (2015) 485–491.
[304] M.A. Arshad, A. Maaroufi, Physica B 545 (2018) 465–474.
[305] Y. Zhou, W. Lin, F. Yang, Chem. Phys. 441 (2014) 23–29.
[306] H. Hintz, H.-J. Egelhaaf, L. Luer, J. Hauch, H. Peisert, T. Chass, Chem. Mater. 23 (2011) 145–154.
[307] D. Wenger, V.L. Malinovskiia, R. Haner, Chem. Commun. 47 (2011) 3168–3170.
[308] B. Conings, S. Bertho, K. Vandewal, A. Senes, J. D'Haen, J. Manca, R.A.J. Janssen, Appl. Phys. Lett. 96 (2010) 163301.
[309] https://apps.automeris.io/wpd/, last retrieved on November 26, 2018.
[310] O. Stern, M. Volmer, Physik. Zeitschr 20 (1919) 183–188.
[311] L. Ciammaruchi, S. Penna, A. Reale, T.M. Brown, A.D. Carlo, Microelectron. Reliab. 53 (2013) 279–281.
[312] D. Bari, N. Wrachien, R. Tagliaferro, S. Penna, T.M. Brown, A. Reale, et al., Microelectron. Reliab. 51 (2011) 1762–1766.
[313] J.U. Lee, J.W. Jung, J.W. Jo, W.H. Jo, J. Mater. Chem. 22 (2012) 24265–24283.
[314] H.-L. Lu, T.F.-R. Shen, S.-T. Huang, Y.-L. Tung, T.C.-K. Yang, Sol. Energ. Mater. Sol. Cells 95 (2011) 1624–1629.
[315] O. Moudam, A. El Gamouz, Org. Electron. 36 (2016) 7–11.
[316] A. Cester, N. Wrachien, M. Bon, G. Meneghesso, R. Bertani, R. Tagliaferro, et al., Degradation mechanisms of dye-sensitized solar cells: Light, bias and temperature effects, IEEE International Reliability Physics Symposium (2015).
DOI:10.1109/IRPS.2015.7112716
[317] J. Gong, K. Sumathy, Q. Qiao, Z. Zhou, Renew. Sust. Energ. Rev. 68 (2017) 234–246.
[318] Q. Tang, J. Wang, B. He, P. Yang, Nano Energy 33 (2017) 266–271.
[319] N. Li, J. D. Perea, T. Kassar, M. Richter, T. Heumueller, G.J. Matt, et al., Nat. Commun. 8 (2017) 14541.
[320] S. Shoaee, J.R. Durrant, J. Mater. Chem. C 3 (2015) 10079–10084.
[321] J. Gorenflot, M.C. Heiber, A. Baumann, J. Lorrmann, M. Gunz, A. Kampgen, et al., J. App. Phys. 115 (2014) 144502.
[322] A. Seemann, T. Sauermann, C. Lungenschmied, O. Armbruster, S. Bauer, H.-J. Egelhaaf et al., Solar Energy 85 (2011) 1238–1249.
[323] S.E. Koops, P.R.F. Barnes, B.C. O'Regan, J.R. Durrant, J. Phys. Chem. C 114 (2010) 8054 –8061.
[324] M.A. Omar, Elementary Solid State Physics: Principles and Applications, Addison-Wesley, Boston, 1993.
[325] R.H. Doremus, Glass science, Wiley, New York, 1973.
[326] K.A. Jackson, Kinetic Processes: Crystal Growth, Diffusion, and Phase Transitions in Materials, Wiley-VCH, Weinheim, 2004.
[327] J. Park, Bioceramics: Properties, Characterizations, and Applications, Springer, New York, 2009.
[328] C.B. Carter, M.G. Norton, Ceramic Materials Science and Engineering, Springer, New York, 2007.
[329] H. Yinnon, D.R. Uhlmann, J. Non-Cryst. Solids 54 (1983) 253-275.
[330] J.W. Mullin, Crystallization, Butterworth- Heinemann, London, 2001.
[331] J.A. Kalb, Crystallization Kinetics. In S. Raoux, M. Wuttig, Phase Change Materials: Science and Applications, Springer, New York, 2009, pp. 125-148.

[332] J.Malek, J. Shanelova, Crystallization Kinetics in Amorphous and Glassy Materials. In J. Sestak, P. Simon (Edts.), Thermal analysis of Micro, Nano- and Non-Crystalline Materials, Springer, Dordrecht, 2012, pp. 291.
[333] J. Wu, Y. Pan, J. Huang, J. Pi, Thermochim. Acta 552 (2013) 15-22.
[334] J. Malek, Thermochim. Acta 355 (2000) 239-253.
[335] M.C. Weinberg, J. Non-Cryst. Solids 127 (1991) 151-158.
[336] D.W. Henderson, J. Therm. Anal. 15 (1979) 325-331.
[337] F. Shehzad, S.P. Thosmas, M.A. Al-Harthi, Thermochim. Acta 589 (2014) 226-234.
[338] S Vyazovkin, N Sbirrazzuoli, Macromol. Rapid. Commun. 25 (2004) 733-738.
[339] A.K. Jena, M.C. Chaturvedi, Phase Transformations in Materials, Prentice Hall, New Jersey, 1992.
[340] A.H. Ammar, A.M. Farid, A.A.M. Farag, J. Non-Cryst. Solids, 434 (2016) 85-91.
[341] C. Helbert, E. Touboul, S. Perrin, L. Carraro, M. Pijolat, Chem. Eng. Sci. 59 (2004) 1393-1401.
[342] J. Militky, J. Sestak, J. Therm. Anal. Calorim. 127 (2016) 1131-1133.
[343] H.W. Choi, Y.H. Kim, Y.H. Rim, Y.S. Yang, Phys. Chem. Chem. Phys. 15 (2013) 9940-9946.
[344] G.M. Shashidhara, S.H.K. Devi, S. Preethi, Polym. Sci. Ser. A 55 (2013) 393-403.
[345] B. Deb, A. Ghosh, Europhys. Lett. 95 (2011) 26002.
[346] R. Svoboda, J. Malek, J. Non-Cryst. Solids 358 (2012) 276-284.
[347] P. Pustkova, D. Svadlak, J. Shanelova, J. Malek, Thermochim. Acta 445 (2006) 116-120.
[348] J. Malek, E. Cernoskova, R. Svejka, J. Sestak, G. Van der Plaats, Thermochim. Acta 280/281 (1996) 353-361.
[349] T. Car, N. Radic, J. Ivkov, E. Babic, A. Tonejc, Appl. Phys. A 68 (1999) 69-73.
[350] K.P. Chuah, S.N. Gan, K.K. Chee, Polymer, 40 (1999) 253-259.
[351] A.L. Greer, N. Mathur, Nature 437 (2005) 1246–1247.
[352] K. Russew, L. Stojanova, Properties and Applications of Amorphous Metallic Alloys. In Glassy Metals, Springer, Berlin, 2016, pp. 217.
[353] A.L. Greer, Metall. Mater. Trans. A 27 (1996) 549–555.

General Conclusion

The present thesis reports a multidisciplinary research work on the following subjects/domains:

- Structures and thermal degradation mechanisms in polymer composites filled with metal particles,
- Kinetic and mechanisms of thermally activated condensed phase processes,
- Renewable and sustainable energy: Organic photovoltaics,
- Kinetics of crystallization in amorphous materials

In the first part, formation, structural analysis and kinetics of the thermal degradation mechanisms carried out on the insulating and conducting epoxy and urea-formaldehyde cellulose (UFC) composites filled with Al, Zn and Sn particles have been reported. Structural characterizations of epoxy/metal and UFC/metal composites by SEM-EDX, XRD and FTIR analyses suggest that the composites are fairly homogeneous and the polymer-metal interphases existing in the composites are more probably of physical nature. Reaction profiles of the thermal degradation processes taking place in the polymer/metal composites elucidate that epoxy/metal composites probably follow single-step processes, while UFC/metal composites pursue complex multi-step processes comprising various consecutive/competitive processes. Kinetics modeling on the thermoanalytical data of polymer/metal composites verifies the information obtained from their reaction profiles. It has been demonstrated that the thermal degradation of epoxy/metal composites can be satisfactorily modeled by Šestak-Berggren model suggesting autocatalytic mechanisms for epoxy/metal composites. In addition, thermal degradation mechanism of epoxy is found to remain unaltered by the nature and contents of the metals. On the other hand, kinetic analysis on the thermoanalytical data of UFC/metal composites reveals that predominantly, the thermal degradation of UFC/metal composites follow complicated multi-step nucleation/growth mechanisms. Contrary to epoxy/metal composites, thermal degradation of UFC resin shows strong dependence on the nature and contents of metals. It should however be noticed that despite of differing reaction profiles/degradation mechanisms, thermal degradation behaviors of epoxy/metal and UFC/metal composites can be fairly explicated by the temperature dependence of heat capacities and catalytic activities of metals in the composites.

The second part is associated principally with the manipulation of the complexity of condensed phase processes. One of the important issues in solid state kinetics has been associated with determining the reaction models of processes under variable activation energy conditions. A new reaction model determination methodology based on the concept of variable activation energy is

therefore put forward in the present research. The suggested methodology is capable of simulating not only single-step but also multi-step processes and it has been found effective in isothermal as well as non-isothermal kinetics. The efficacy of the suggested methodology and some of its important applications on various emerging research areas are considered.

The third part contributes in renewable and sustainable energy research with special regard to organic photovoltaics. In this part, certain crucial flaws in the well-known temperature accelerated lifetime testing of polymer solar cells are pointed out. Alternatively, an advanced method to predict lifetimes of polymer solar cells has been proposed which takes into account systematic kinetic modeling of various possible degradation processes in polymer solar cells. The suggested kinetic approaches have been substantiated by modeling thermally accelerated current density of MDMO-PPV:PCBM bulk heterojunction and DSSC solar cells, oxygen uptake of P3HT polymer film, and photodegradation of DSSC solar cell. Moreover, lifetime of DSSC has been effectively predicted by the advanced method. Briefly, the suggested kinetic approaches to degradation mechanisms in polymer solar cells are capable of responding to some of the critical challenges being faced by the organic photovoltaics domain today, and they might play an important role in the commercialization of organic photovoltaic devices. Although basically suggested for polymer solar cells, this method could likely be generalized on the other kinds of solar cells.

In the fourth part, a new kinetic modeling method to simulate the crystallization processes occurring in amorphous materials is proposed. On the basis of this method, an explicit relationship between two well familiar crystallization reaction models i.e. Johnson-Mehl-Avrami and Šesták-Berggren models is developed. The validity conditions of the proposed relationship along with its phenomenological limits are also discussed. The values of the two parameters of empirical SB (m, n) model have been attributed to the nucleation and growth dimensionality of known crystallization mechanisms. The suggested method/relationship has been effectively tested on crystallization processes in polymeric materials, alloys and glasses.

On the whole, the research conducted in the present thesis contributes significantly (and is of equal interest) to academia and industry.

Conclusion Générale

La présente thèse porte sur un travail de recherche multidisciplinaire concernant les sujets/domaines suivants:

- Les structures et les mécanismes de dégradation thermique dans les composites polymères chargés de particules métalliques,
- La cinétique et les mécanismes des processus thermiquement activés de la phase condensée,
- Les énergies renouvelables et durables: photovoltaïque organique,
- La cinétique de cristallisation dans les matériaux amorphes

Dans la première partie, nous avons discuté de la formation, de l'analyse structurale et de la cinétique des mécanismes de dégradation thermique mis en œuvre sur les composites isolants et conducteurs à base d'époxyde et d'urée-formaldéhyde-cellulose (UFC) remplis de particules d'Al, Zn et Sn. Les caractérisations structurales qui ont été effectuées sur les composites époxyde/métal et UFC/métal par les analyses MEB-EDAX, DRX et IRTF suggèrent que les composites sont assez homogènes et que les interphases polymère-métal existant dans les composites sont plus probablement de nature physique. Les profils de réaction des processus de dégradation thermique se produisant dans le composite polymère/métal indiquent clairement que les composites époxyde/métal suivent probablement des processus en une seule étape, tandis que les composites UFC/métal suivent des processus complexes multi-étape comprenant divers processus consécutifs/compétitifs. La modélisation cinétique des données thermo-analytiques des composites polymère/métal vérifie les informations obtenues à partir de leurs profils de réaction. Il a été démontré que la dégradation thermique des composites époxyde/métal peut être modélisée d'une manière satisfaisante par le modèle de Šestak-Berggren suggérant des mécanismes auto-catalytiques pour ces composites. De plus, il apparaît que le mécanisme de dégradation thermique de l'époxyde reste indifférent par rapport à la nature et le contenu en métaux. D'autre part, l'analyse cinétique des données thermo-analytiques des composites UFC/métal révèle que, de manière prédominante, la dégradation thermique des composites UFC/métal suit des mécanismes compliqués de nucléation/croissance en plusieurs étapes. Contrairement aux composites époxyde/métal, la dégradation thermique de la résine UFC montre une forte dépendance à la nature et au contenu en métaux. Toutefois, il convient de noter que, malgré les différences dans les profils de réaction/mécanismes de dégradation, les comportements de dégradation thermique des composites époxyde/métal et UFC/métal peuvent être expliqués de manière équitable par la dépendance en fonction de la température des capacités thermiques et des activités catalytiques des métaux dans les composites.

La seconde partie consiste à saisir la complexité des processus en phase condensée. Un des problèmes majeurs de la cinétique de l'état solide est lié à la détermination des modèles de

réaction de processus dans des conditions d'énergie d'activation variables. A cet effet, une nouvelle méthodologie de détermination du modèle de réaction basée sur le concept d'énergie d'activation variable est donc proposée dans la présente recherche. La méthodologie suggérée est capable de simuler non seulement des processus en une seule étape mais également des processus multi-étape. Elle s'est avérée efficace dans les cinétiques isothermes et non isothermes. L'efficacité de la méthodologie suggérée et certaines de ses applications importantes dans divers domaines de recherche émergents sont pris en considération.

La troisième partie contribue à la recherche sur les énergies renouvelables et durables en accordant une attention particulière au photovoltaïque organique. Dans cette partie, certains défauts cruciaux dans des tests bien connus sur la durée de vie thermiquement accélérée des cellules solaires polymères ont été décelés. On a également proposé une méthode avancée pour prédire la durée de vie des cellules solaires polymères, cette méthode prend en compte la modélisation cinétique systématique de divers processus de dégradation possibles dans les cellules solaires polymères. Les approches cinétiques suggérées ont été vérifiées par la modélisation de la densité du courant thermiquement accélérée de l' hétérojonction massive de MDMO-PPV: PCBM et des cellules solaires DSSC, de l'absorption d'oxygène par le film polymère P3HT et de la photodégradation de la cellule solaire DSSC. En outre, la méthode avancée a permis de prédire efficacement la durée de vie du DSSC. En bref, les approches cinétiques suggérées pour les mécanismes de dégradation des cellules solaires polymères sont capables de répondre à certains défis critiques auxquels est confronté le domaine de la photovoltaïque organique, et elles pourraient jouer un rôle important dans la commercialisation des dispositifs photovoltaïques organiques. Bien qu'elle soit fondamentalement suggérée pour les cellules solaires polymères, cette méthode pourrait probablement être généralisée à d'autres types de cellules solaires.

Dans la quatrième partie, une nouvelle méthode de modélisation cinétique pour simuler les processus de cristallisation intervenant dans les matériaux amorphes est proposée. Sur la base de cette méthode, une relation explicite est développée entre deux modèles de réaction de cristallisation bien connus, à savoir les modèles de Johnson-Mehl-Avrami et de Šesták-Berggren. Les conditions de validité de la relation proposée ainsi que ses limites phénoménologiques sont également discutées. Les valeurs des deux paramètres du modèle empirique SB (m, n) ont été attribuées à la dimensionnalité de la nucléation et de la croissance des mécanismes de cristallisation connus. La méthode/relation suggérée a été efficacement testée sur des procédés de cristallisation dans des matériaux polymères, des alliages et des verres.

Dans l'ensemble, la recherche effectuée dans la présente thèse contribue de manière significative (et présente un intérêt égal) à la fois au milieu académique et industriel.

Annex A

Theoretical h(α) expressions for condensed phase reaction models

Annex A1: *h(α)* Expression for Reaction Order (RO) Model

The general expression for RO model is given as following:

$$f(\alpha) = (1-\alpha)^n \tag{A11}$$

Differentiation of Eq. (A11) with respect to *'α'* yields the following equation:

$$f'(\alpha) = -n(1-\alpha)^{n-1} \tag{A12}$$

Therefore, the *h(α)* function is described as;

$$h(\alpha) = \frac{f'(\alpha)}{f(\alpha)} = \frac{-n}{1-\alpha} \tag{A13}$$

Annex A2: *h(α)* Expression for Jhonson-Mehl Avrami (JMA) Model

The general expression for JMA model is described in Eq. (A21):

$$f(\alpha) = m(1-\alpha)\{-\ln(1-\alpha)\}^{1-1/m} \tag{A21}$$

Differentiating Eq. (A21) with respect to *'α'* provides the Eq. (A22) as following:

$$f'(\alpha) = m\left(\frac{1-1/m}{\ln(1/1-\alpha)} - 1\right)\{\ln(1/1-\alpha)\}^{1-1/m} \tag{A22}$$

The *h(α)* function is then expressed as:

$$h(\alpha) = \frac{f'(\alpha)}{f(\alpha)} = \frac{\left(\frac{1-1/m}{\ln(1/1-\alpha)} - 1\right)}{1-\alpha} \tag{A23}$$

Annex A3: *h(α)* Expression for One Dimensional Diffusion (D1) Model

The D1 reaction model may be described in the following way,

$$f(\alpha) = \frac{1}{2\alpha} \tag{A31}$$

Differentiating Eq. (A31) with respect to *'α'* yields:

$$f'(\alpha) = -\frac{1}{2\alpha^2} \tag{A32}$$

h(α) function takes the following form:

$$h(\alpha)=\frac{f'(\alpha)}{f(\alpha)}=-\frac{1}{\alpha} \tag{A33}$$

Annex A4: *h(α)* Expression for Two Dimensional Diffusion (D2) Model

The two-dimensional diffusion model is usually expressed as following;

$$f(\alpha)=-\frac{1}{\ln(1-\alpha)} \tag{A41}$$

Differentiation of Eq. (A41) with respect to *'α'* gives:

$$f'(\alpha)=-\frac{1}{(1-\alpha)\{\ln(1-\alpha)\}^2} \tag{A42}$$

The *h(α)* expression for D2 model is shown in Eq. (A43):

$$h(\alpha)=\frac{f'(\alpha)}{f(\alpha)}=\frac{1}{(1-\alpha)\ln(1-\alpha)}=\frac{1}{\ln(1-\alpha)^{1-\alpha}} \tag{A43}$$

Annex A5: *h(α)* Expression for Jander's Diffusion (D3) Model

Jander's three-dimensional diffusion model (D3) is generally expressed as:

$$f(\alpha)=\frac{3(1-\alpha)^{2/3}}{2\{1-(1-\alpha)^{1/3}\}} \tag{A51}$$

Differentiating Eq. (A51) with respect to *'α'* gives:

$$f'(\alpha)=-\frac{3(1-\alpha)^{2/3}}{2\{1-(1-\alpha)^{1/3}\}}\left[\frac{\frac{2\{1-(1-\alpha)^{1/3}\}}{3(1-\alpha)}+\frac{1}{3(1-\alpha)^{2/3}}}{1-(1-\alpha)^{1/3}}\right] \tag{A52}$$

The *h(α)* expression for D2 model is given in Eq. (A53):

$$h(\alpha)=\frac{f'(\alpha)}{f(\alpha)}=-\frac{2}{3}\left[\frac{1}{1-\alpha}+\frac{1}{2(1-\alpha)^{2/3}\{1-(1-\alpha)^{1/3}\}}\right] \tag{A53}$$

Annex A6: *h(α)* Expression for Ginstling-Brounshtein Diffusion (D4) Model

Ginstling-Brounshtein's three dimensional diffusion model (D4) is expressed as following:

$$f(\alpha) = \frac{3}{2\left\{(1-\alpha)^{-1/3} - 1\right\}} \tag{A61}$$

Differentiating Eq. (A61) with respect to *'α'* yields:

$$f'(\alpha) = -\frac{1}{2}\left[\frac{1}{\left\{(1-\alpha)^{-1/3} - 1\right\}^2 (1-\alpha)^{4/3}}\right] \tag{A62}$$

Therefore,

$$h(\alpha) = \frac{f'(\alpha)}{f(\alpha)} = -\frac{1}{3}\left[\frac{1}{\left\{(1-\alpha)^{-1/3} - 1\right\}(1-\alpha)^{4/3}}\right] \tag{A63}$$

Annex 7: *h(α)* Expression for Šesták–Berggren SB (*m, n*) Model

SB (*m*, *n*) model is mathematically represented as following:

$$f(\alpha) = (\alpha)^m (1-\alpha)^n \tag{A71}$$

Differentiation of Eq. (A71) with respect to *'α'* gives:

$$f'(\alpha) = (\alpha)^m (1-\alpha)^n \left\{\frac{m}{\alpha} - \frac{n}{1-\alpha}\right\} \tag{A72}$$

The *h(α)* expression for SB (*m*, *n*) model is given below in Eq. (A73):

$$h(\alpha) = \frac{f'(\alpha)}{f(\alpha)} = \frac{m}{\alpha} - \frac{n}{1-\alpha} \tag{A73}$$

Annex 8: *h(α)* Expression for Power Law (Pr) Model

General form of power law is given below:

$$f(\alpha) = r(\alpha)^{(1-1/r)} \tag{A81}$$

Derivative of Eq. (A81) with respect to *'α'* provides,

$$f'(\alpha) = r(1-1/r)(\alpha)^{-1/r} \tag{A82}$$

The *h(α)* expression for power law is given as following:

$$h(\alpha) = \frac{f'(\alpha)}{f(\alpha)} = \frac{(1-1/r)}{\alpha} \tag{A83}$$

Annex B

XRD Analysis Reports of Polymer (Epoxy, UFC)/Metal (Al, Zn, Sn) Composites by PANalytical X'Pert Pro Software

XRD analysis report of epoxy/Al3vol.% composite

X-ray diffractogram of epoxy/Al3vol.%:

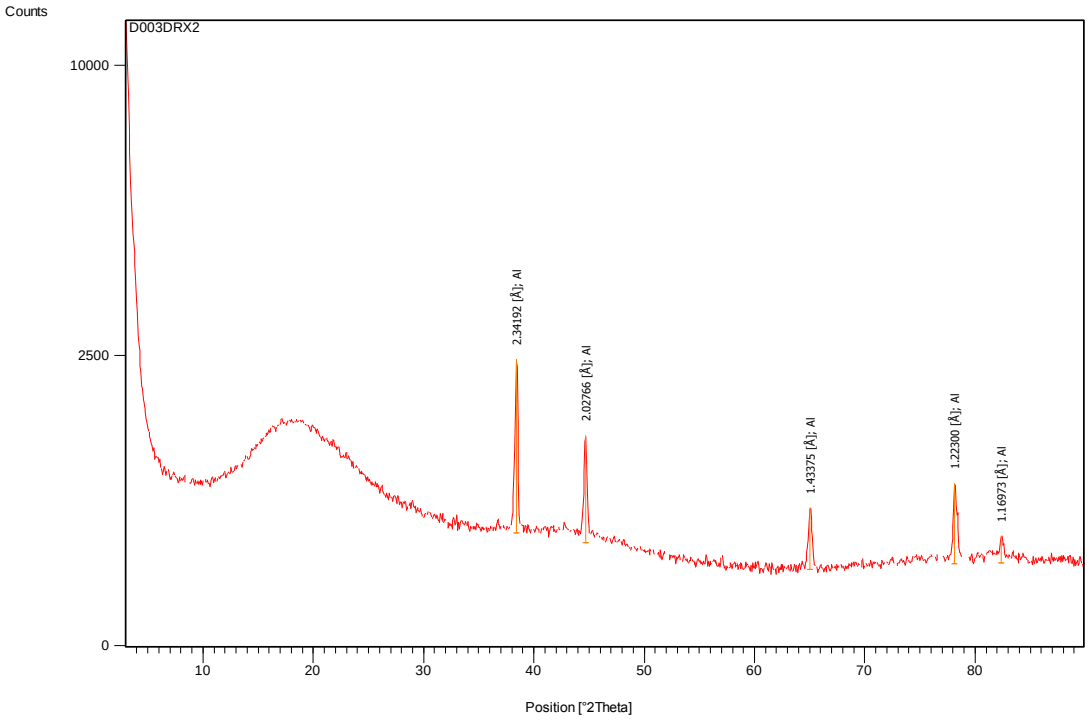

Peak List:

Pos. [°2Th.]	Height [cts]	FWHM [°2Th.]	d-spacing [Å]	Rel. Int. [%]	Tip width [°2Th.]	Matched by
38.4392	2068.10	0.1978	2.34192	100.00	0.2373	03-065-2869
44.6933	1000.22	0.1978	2.02766	48.36	0.2373	03-065-2869
65.0556	395.58	0.2637	1.43375	19.13	0.3165	03-065-2869
78.1542	583.82	0.3956	1.22300	28.23	0.4747	03-065-2869
82.3754	157.37	0.3216	1.16973	7.61	0.3859	03-065-2869

Plot of Identified Phases:

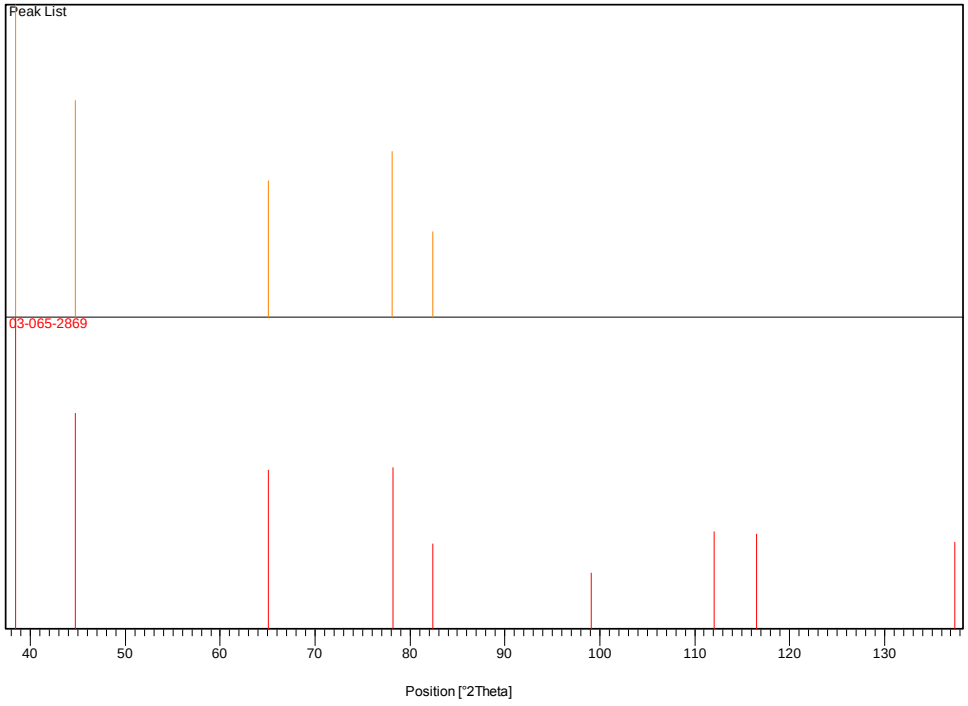

Identified Patterns List:

Visible	Ref. Code	Score	Compound Name	Displacement [°2Th.]	Scale Factor	Chemical Formula
*	03-065-2869	84	Aluminum	0.000	0.834	Al

XRD analysis report of epoxy/Al30vol.% composite

X-ray diffractogram of epoxy/Al30vol.%:

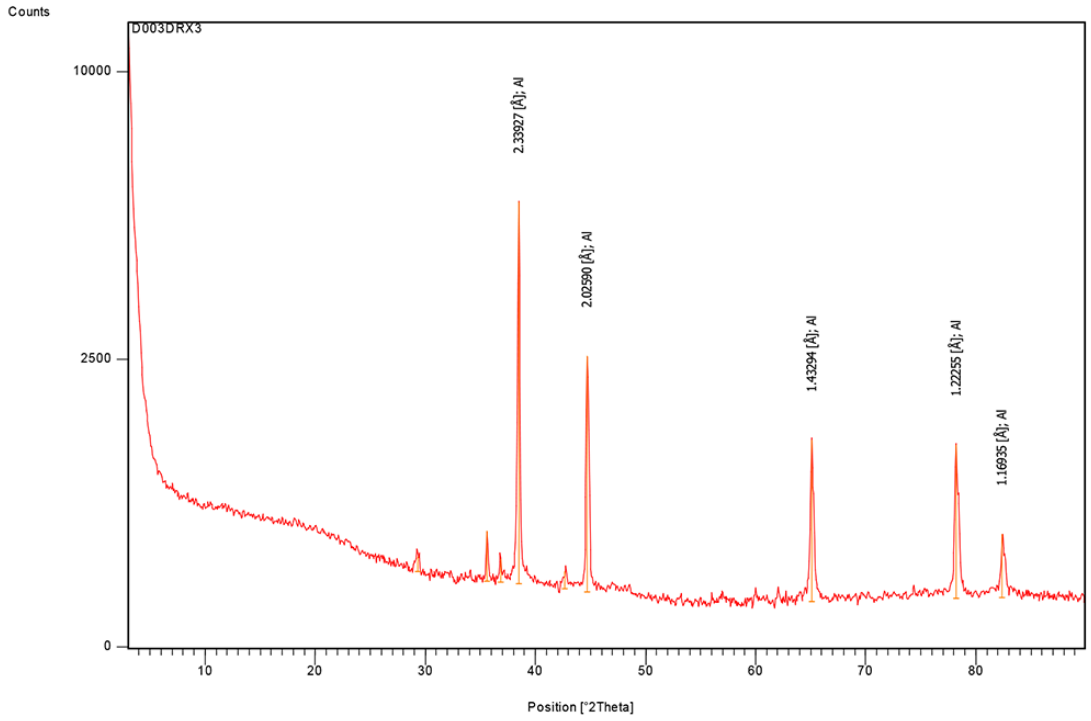

Peak List:

Pos. [°2Th.]	Height [cts]	FWHM [°2Th.]	d-spacing [Å]	Rel. Int. [%]	Tip width [°2Th.]	Matched by
38.4845	5873.44	0.2637	2.33927	100.00	0.3165	01-089-3657
42.6567	71.67	0.3956	2.11963	1.22	0.4747	
44.7342	2460.22	0.1978	2.02590	41.89	0.2373	01-089-3657
65.0968	1229.75	0.3296	1.43294	20.94	0.3956	01-089-3657
78.1884	1161.55	0.3296	1.22255	19.78	0.3956	01-089-3657
82.4076	306.39	0.4020	1.16935	5.22	0.4824	01-089-3657

Plot of Identified Phases:

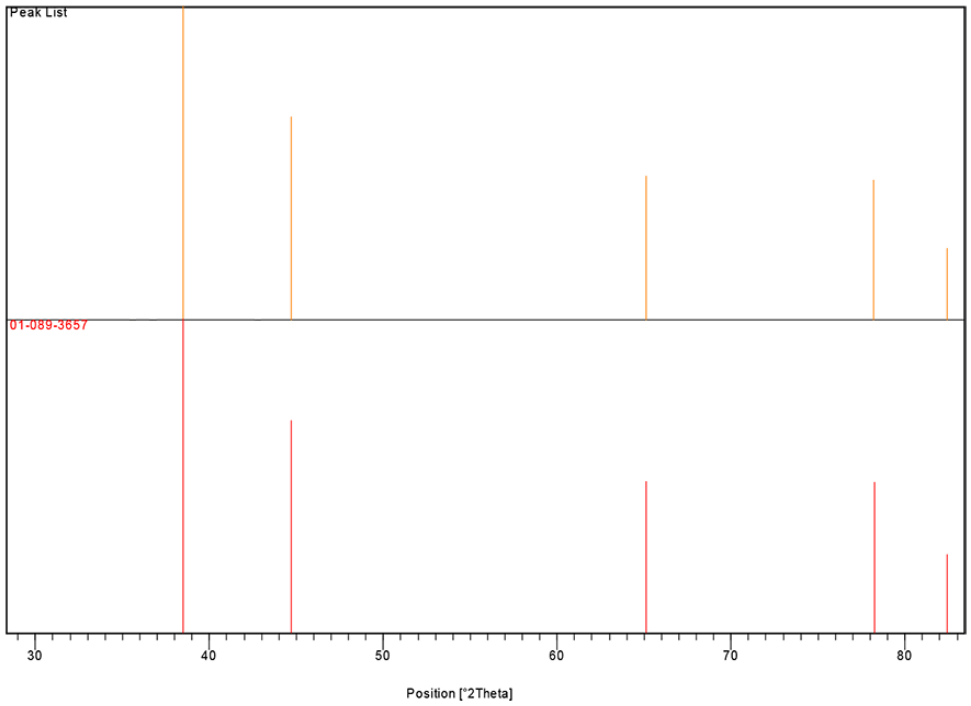

Identified Patterns List:

Visible	Ref. Code	Score	Compound Name	Displacement [°2Th.]	Scale Factor	Chemical Formula
*	01-089-3657	80	Aluminum	0.000	0.998	Al

XRD analysis report of epoxy/Zn3vol.% composite

X-ray diffractogram of epoxy/Zn3vol.%:

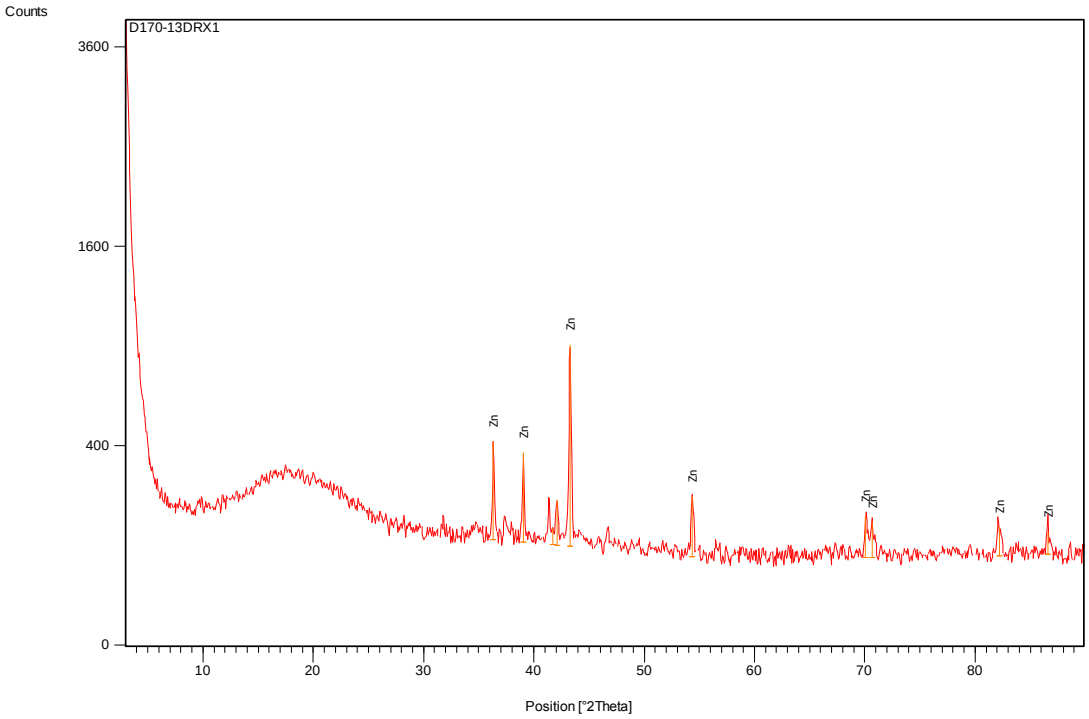

Peak List:

Pos. [°2Th.]	Height [cts]	FWHM [°2Th.]	d-spacing [Å]	Rel. Int. [%]	Tip width [°2Th.]	Matched by
36.3368	305.03	0.2637	2.47245	37.54	0.3165	03-065-3358
39.0496	268.42	0.1978	2.30671	33.04	0.2373	03-065-3358
41.7265	38.18	0.7911	2.16471	4.70	0.9494	
42.0824	111.53	0.1978	2.14722	13.73	0.2373	
43.2878	812.46	0.1978	2.09019	100.00	0.2373	03-065-3358
54.3791	145.65	0.1978	1.68719	17.93	0.2373	03-065-3358
70.0659	90.34	0.2637	1.34299	11.12	0.3165	03-065-3358
70.6850	75.00	0.0900	1.33273	9.23	0.1080	03-065-3358

82.1886	61.36	0.3956	1.17288	7.55	0.4747	03-065-3358
86.6420	46.55	0.4824	1.12275	5.73	0.5789	03-065-3358

Plot of Identified Phases:

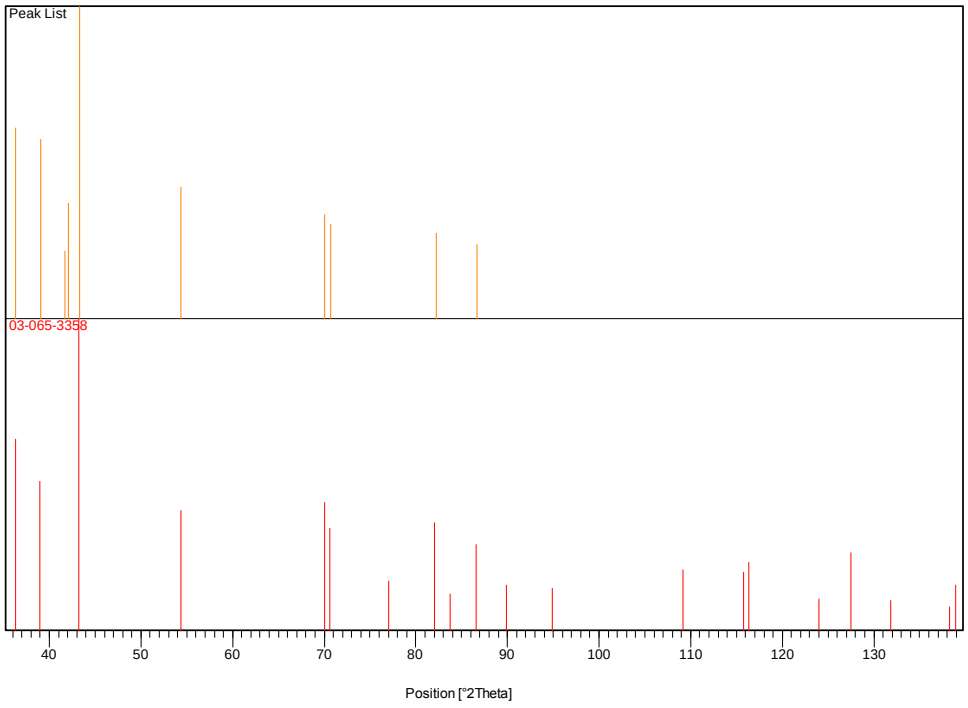

Identified Patterns List:

Visible	Ref. Code	Score	Compound Name	Displacement [°2Th.]	Scale Factor	Chemical Formula
*	03-065-3358	84	Zinc	0.000	0.956	Zn

XRD analysis report of epoxy/Zn29vol.% composite

X-ray diffractogram of epoxy/Zn29vol.%:

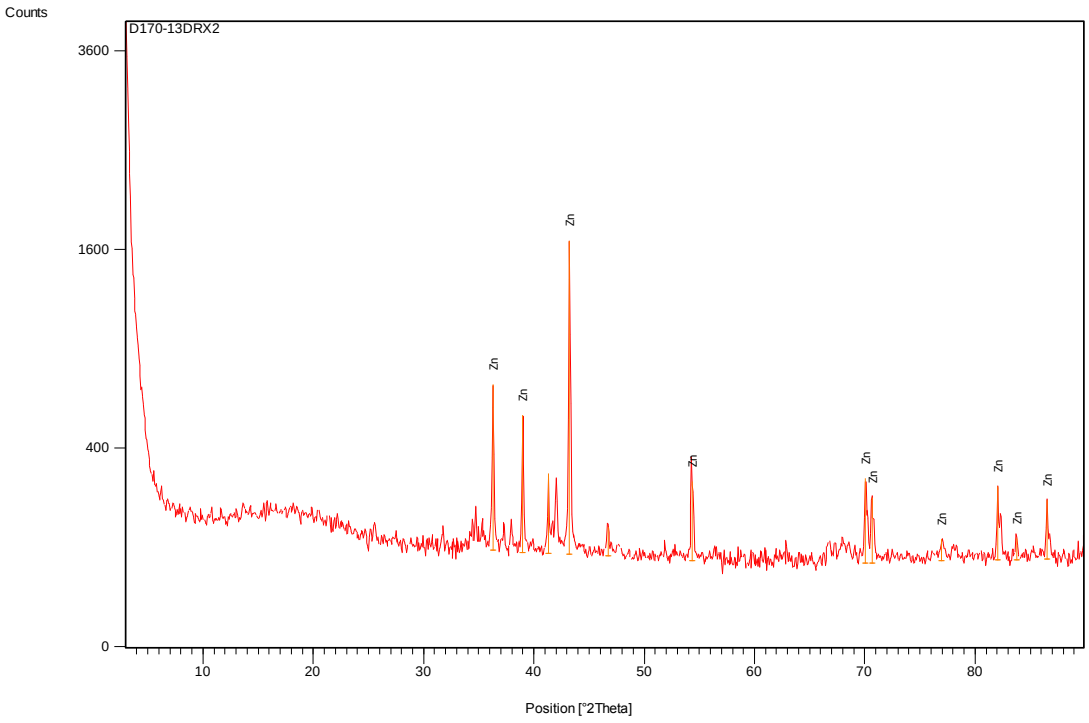

Peak List:

Pos. [°2Th.]	Height [cts]	FWHM [°2Th.]	d-spacing [Å]	Rel. Int. [%]	Tip width [°2Th.]	Matched by
36.2962	606.87	0.1978	2.47512	38.23	0.2373	03-065-5973
38.9985	453.69	0.1978	2.30962	28.58	0.2373	03-065-5973
41.3141	216.50	0.1978	2.18536	13.64	0.2373	
43.2319	1587.61	0.1978	2.09276	100.00	0.2373	03-065-5973
46.7091	61.82	0.3956	1.94475	3.89	0.4747	
54.3407	202.74	0.1978	1.68829	12.77	0.2373	03-065-5973
70.0687	218.37	0.2637	1.34294	13.75	0.3165	03-065-5973
70.6490	153.33	0.1978	1.33332	9.66	0.2373	03-065-5973

76.9830	44.00	0.0900	1.23865	2.77	0.1080	03-065-5973
82.0362	184.06	0.1978	1.17468	11.59	0.2373	03-065-5973
83.7500	43.00	0.0900	1.15495	2.71	0.1080	03-065-5973
86.5010	140.00	0.2412	1.12421	8.82	0.2894	03-065-5973

Plot of Identified Phases:

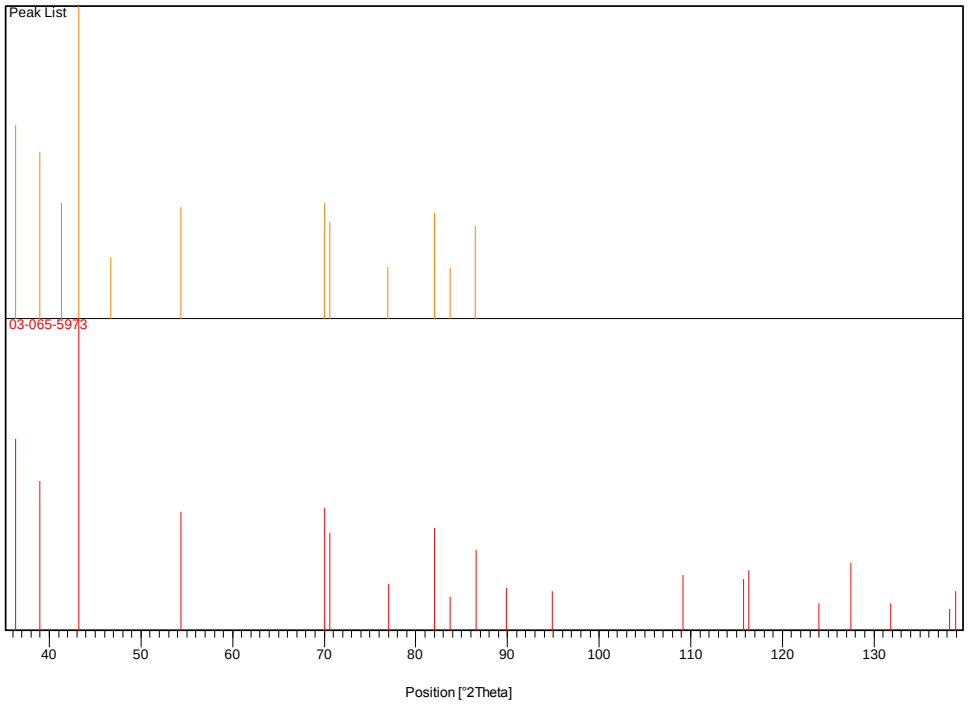

Identified Patterns List:

Visible	Ref. Code	Score	Compound Name	Displacement [°2Th.]	Scale Factor	Chemical Formula
*	03-065-5973	80	Zinc	0.000	1.030	Zn

XRD analysis report of epoxy/Sn4vol.% composite

X-ray diffractogram of epoxy/Sn4vol.%:

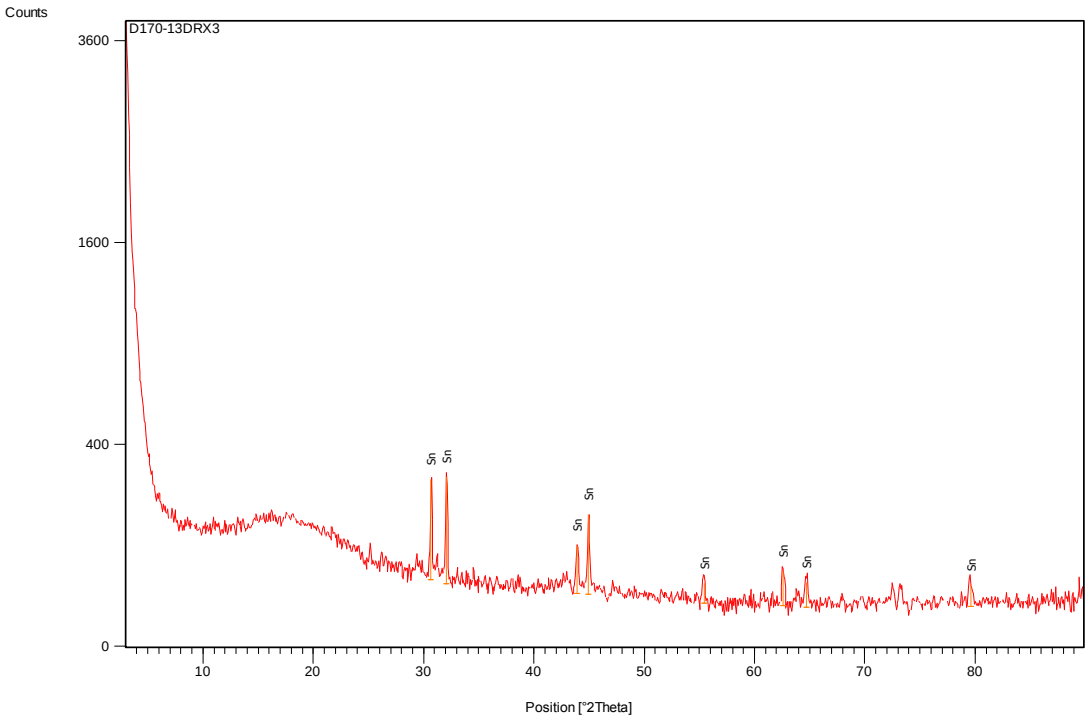

Peak List:

Pos. [°2Th.]	Height [cts]	FWHM [°2Th.]	d-spacing [Å]	Rel. Int. [%]	Tip width [°2Th.]	Matched by
30.6855	230.92	0.1978	2.91368	94.57	0.2373	01-089-2958
32.0821	244.18	0.1978	2.78996	100.00	0.2373	01-089-2958
43.9412	71.89	0.1978	2.06061	29.44	0.2373	01-089-2958
44.9657	144.35	0.1978	2.01601	59.12	0.2373	01-089-2958
55.4760	21.00	0.0900	1.65640	8.60	0.1080	01-089-2958
62.6121	39.99	0.2637	1.48369	16.38	0.3165	01-089-2958
64.7299	24.82	0.7911	1.44017	10.16	0.9494	01-089-2958
79.6318	21.22	0.4824	1.20299	8.69	0.5789	01-089-2958

Plot of Identified Phases:

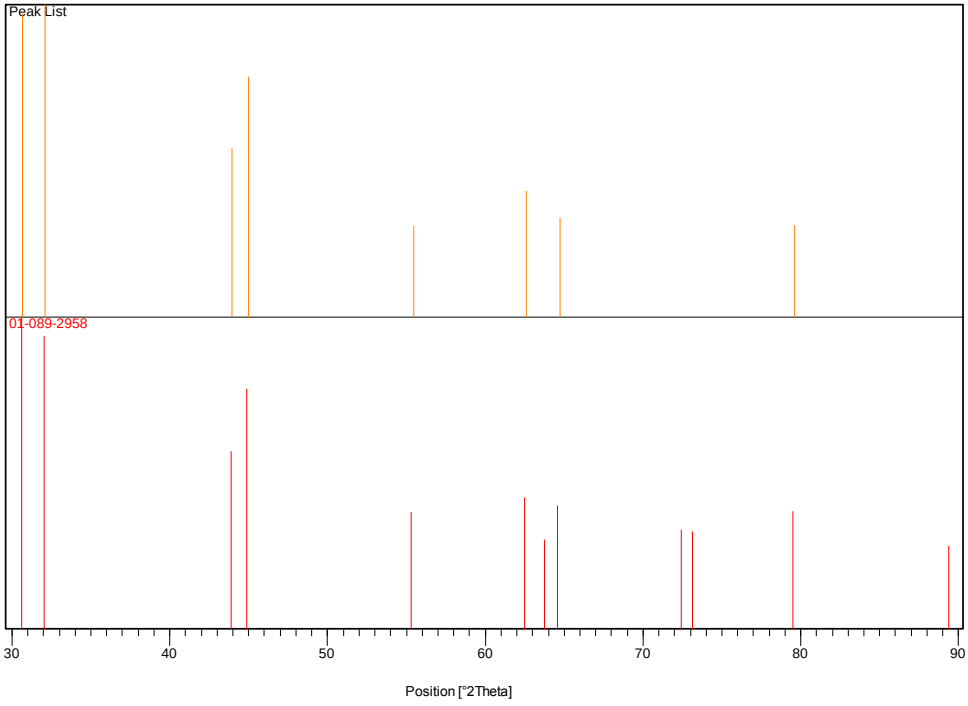

Identified Patterns List:

Visible	Ref. Code	Score	Compound Name	Displacement [°2Th.]	Scale Factor	Chemical Formula
*	01-089-2958	70	Tin metallic, syn	0.000	0.366	Sn

XRD analysis report of epoxy/Sn27vol.% composite

X-ray diffractogram of epoxy/Sn27vol.%:

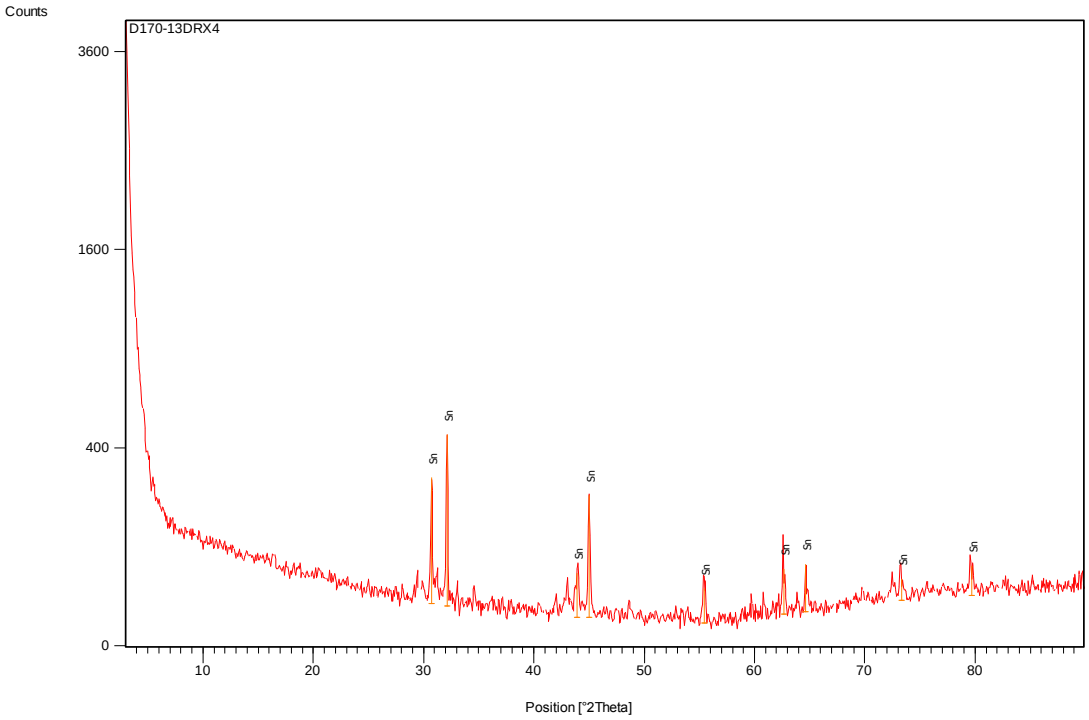

Peak List:

Pos. [°2Th.]	Height [cts]	FWHM [°2Th.]	d-spacing [Å]	Rel. Int. [%]	Tip width [°2Th.]	Matched by
30.7149	272.73	0.1978	2.91096	62.12	0.2373	01-086-2265
32.1099	439.05	0.1319	2.78761	100.00	0.1582	01-086-2265
43.9204	46.38	0.3956	2.06154	10.56	0.4747	01-086-2265
45.0068	223.47	0.1978	2.01427	50.90	0.2373	01-086-2265
55.4695	28.41	0.2637	1.65658	6.47	0.3165	01-086-2265
62.6340	50.03	0.2637	1.48322	11.40	0.3165	01-086-2265
64.6352	56.13	0.1978	1.44205	12.78	0.2373	01-086-

						2265
73.3321	24.92	0.3956	1.29103	5.68	0.4747	01-086-2265
79.6699	39.74	0.6432	1.20251	9.05	0.7718	01-086-2265

Plot of Identified Phases:

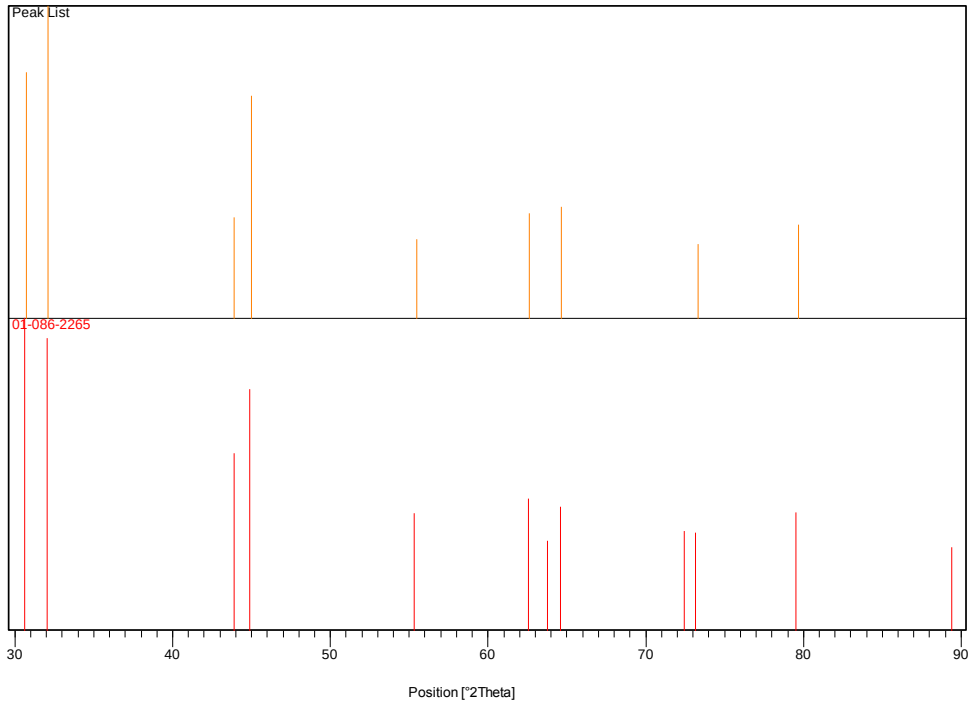

Identified Patterns List:

Visible	Ref. Code	Score	Compound Name	Displacement [°2Th.]	Scale Factor	Chemical Formula
*	01-086-2265	51	Tin metallic, syn	0.000	0.308	Sn

XRD analysis report of UFC/Al5vol.% composite

X-ray diffractogram of UFC/Al5vol.%:

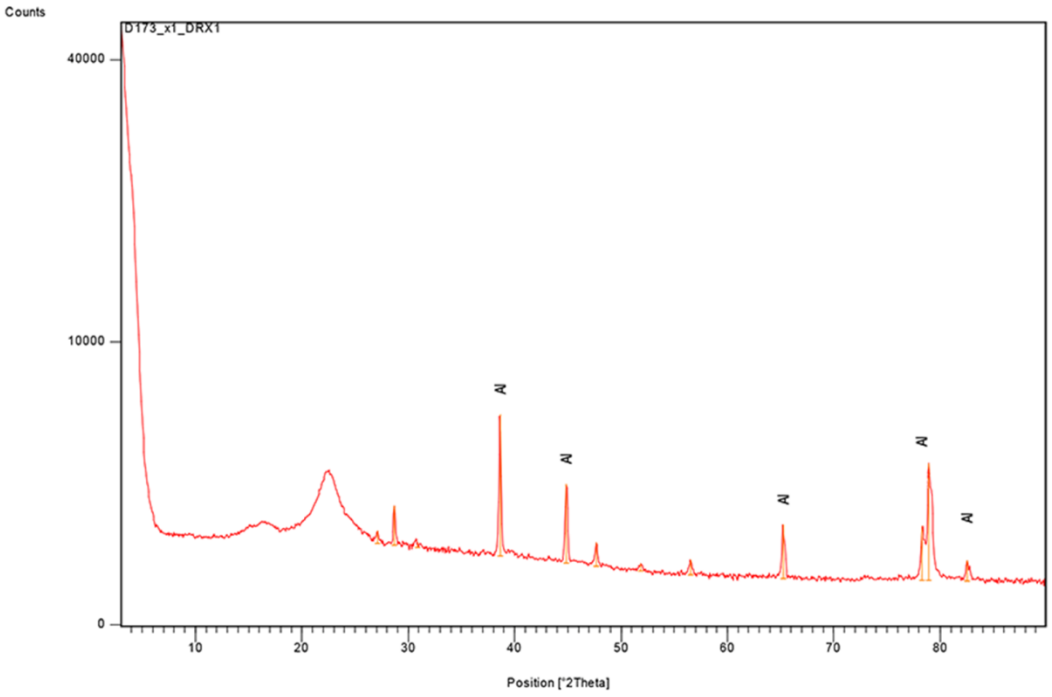

Peak List:

Pos. [°2Th.]	Height [cts]	FWHM [°2Th.]	d-spacing [Å]	Rel. Int. [%]	Tip width [°2Th.]	Matched by
28.6911	970.78	0.2637	3.11151	19.68	0.3165	
38.6278	4931.61	0.1978	2.33092	100.00	0.2373	00-001-1180
44.8786	1983.71	0.1978	2.01972	40.22	0.2373	00-001-1180
47.6829	410.01	0.1978	1.90728	8.31	0.2373	
51.8570	96.10	0.3956	1.76315	1.95	0.4747	
56.5253	213.76	0.2637	1.62812	4.33	0.3165	
65.2271	976.22	0.3296	1.43039	19.80	0.3956	00-001-1180

78.3139	959.73	0.1978	1.22090	19.46	0.2373	00-001-1180
82.5060	271.20	0.4020	1.16821	5.50	0.4824	00-001-1180

Plot of Identified Phases:

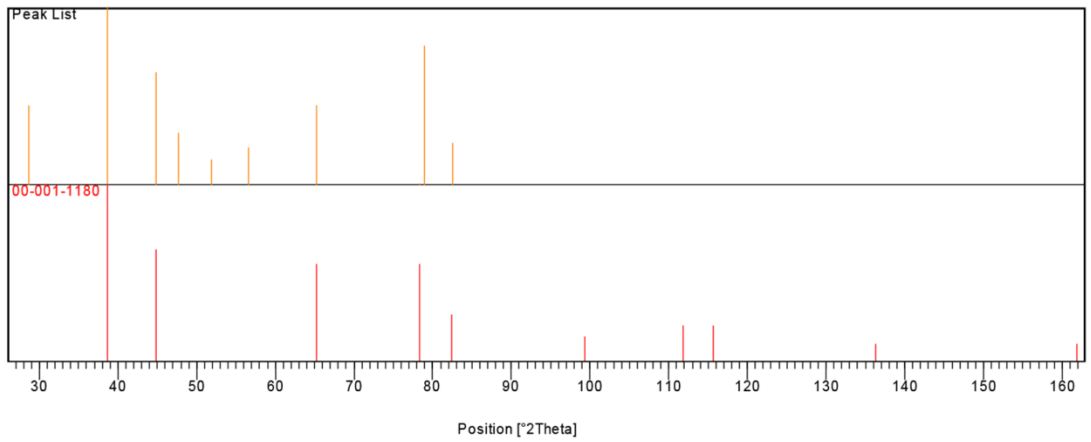

Identified Patterns List:

Visible	Ref. Code	Score	Compound Name	Displacement [°2Th.]	Scale Factor	Chemical Formula
*	00-001-1180	68	Aluminum	0.000	0.504	Al

XRD analysis report of UFC/Al55vol.% composite

X-ray diffractogram of UFC/Al55vol.%:

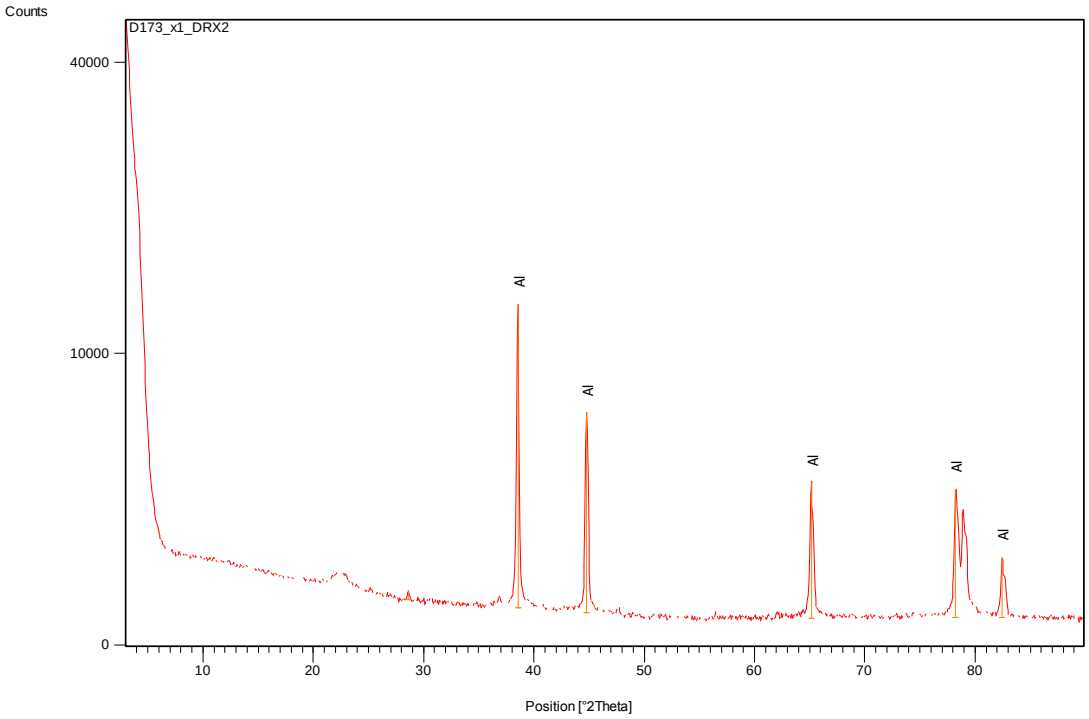

Peak List:

Pos. [°2Th.]	Height [cts]	FWHM [°2Th.]	d-spacing [Å]	Rel. Int. [%]	Tip width [°2Th.]	Matched by
28.5993	100.92	0.1978	3.12129	0.75	0.2373	
38.5391	13530.65	0.2637	2.33608	100.00	0.3165	00-004-0787
44.7843	6235.12	0.2637	2.02375	46.08	0.3165	00-004-0787
65.1454	3044.99	0.3296	1.43199	22.50	0.3956	00-004-0787
78.2393	2788.70	0.3296	1.22188	20.61	0.3956	00-004-0787
82.4453	823.11	0.3216	1.16891	6.08	0.3859	00-004-0787

Plot of Identified Phases:

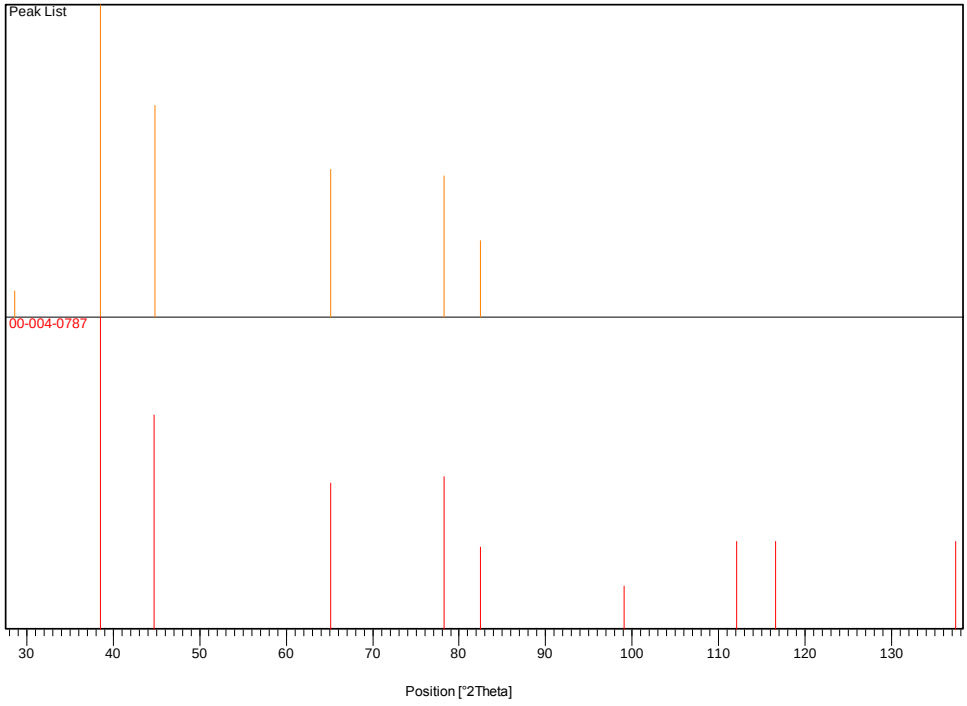

Identified Patterns List:

Visible	Ref. Code	Score	Compound Name	Displacement [°2Th.]	Scale Factor	Chemical Formula
*	00-004-0787	91	Aluminum, syn	0.000	0.995	Al

XRD analysis report of UFC/Zn5vol.% composite

X-ray diffractogram of UFC/Zn5vol.%:

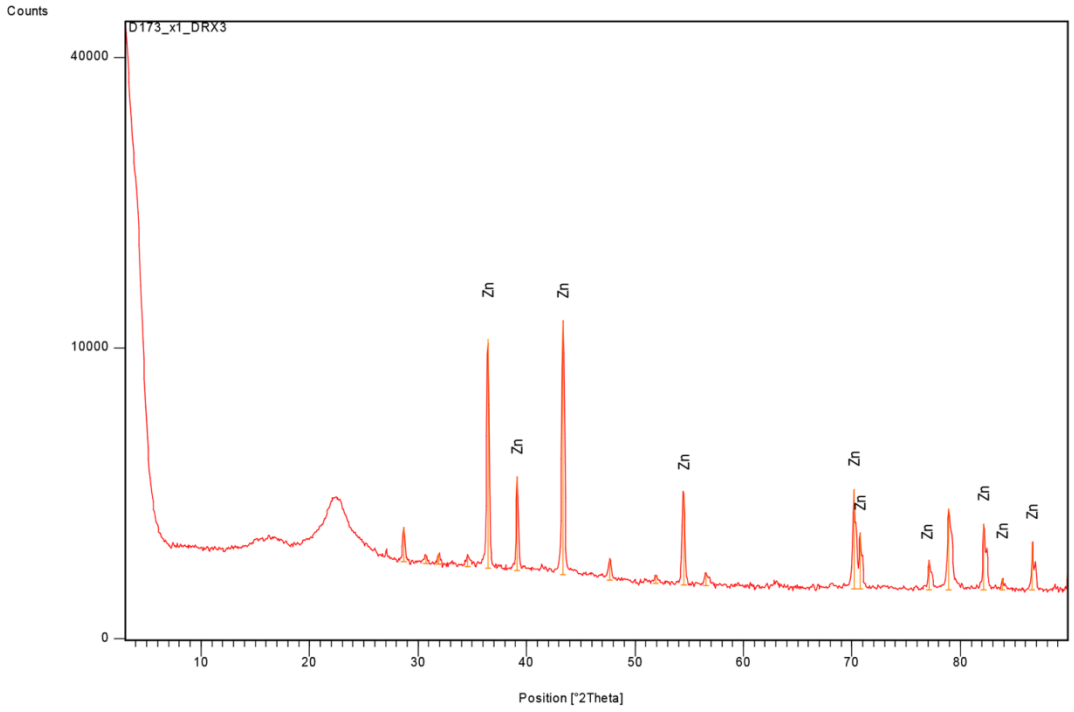

Peak List:

Pos. [°2Th.]	Height [cts]	FWHM [°2Th.]	d-spacing [Å]	Rel. Int. [%]	Tip width [°2Th.]	Matched by
28.6906	768.06	0.1978	3.11157	6.73	0.2373	
36.4478	10014.17	0.1978	2.46518	87.69	0.2373	03-065-5973
39.1550	2524.90	0.1978	2.30074	22.11	0.2373	03-065-5973
43.3826	11419.97	0.2637	2.08584	100.00	0.3165	03-065-5973
47.7026	336.99	0.1978	1.90654	2.95	0.2373	
54.4785	2174.49	0.2637	1.68435	19.04	0.3165	03-065-5973
70.1731	2337.40	0.2637	1.34120	20.47	0.3165	03-065-5973
70.7758	1015.19	0.1978	1.33125	8.89	0.2373	03-065-5973
77.1184	424.31	0.2637	1.23682	3.72	0.3165	03-065-

						5973
78.9310	1690.66	0.3296	1.21290	14.80	0.3956	
82.1664	1272.41	0.1978	1.17314	11.14	0.2373	03-065-5973
83.8529	147.03	0.1978	1.15379	1.29	0.2373	03-065-5973
86.6274	801.99	0.2412	1.12290	7.02	0.2894	03-065-5973

Plot of Identified Phases:

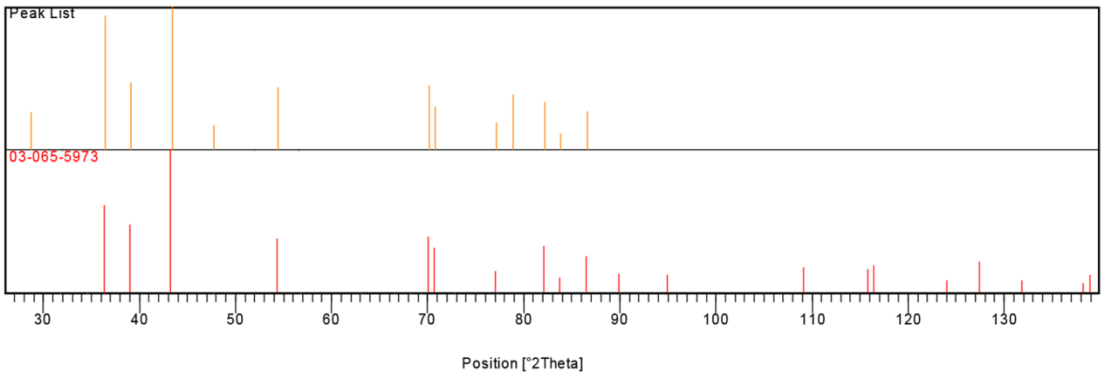

Identified Patterns List:

Visible	Ref. Code	Score	Compound Name	Displacement [°2Th.]	Scale Factor	Chemical Formula
*	03-065-5973	54	Zinc	0.000	0.328	Zn

XRD analysis report of UFC/Zn37vol.% composite

X-ray diffractogram of UFC/Zn37vol.%:

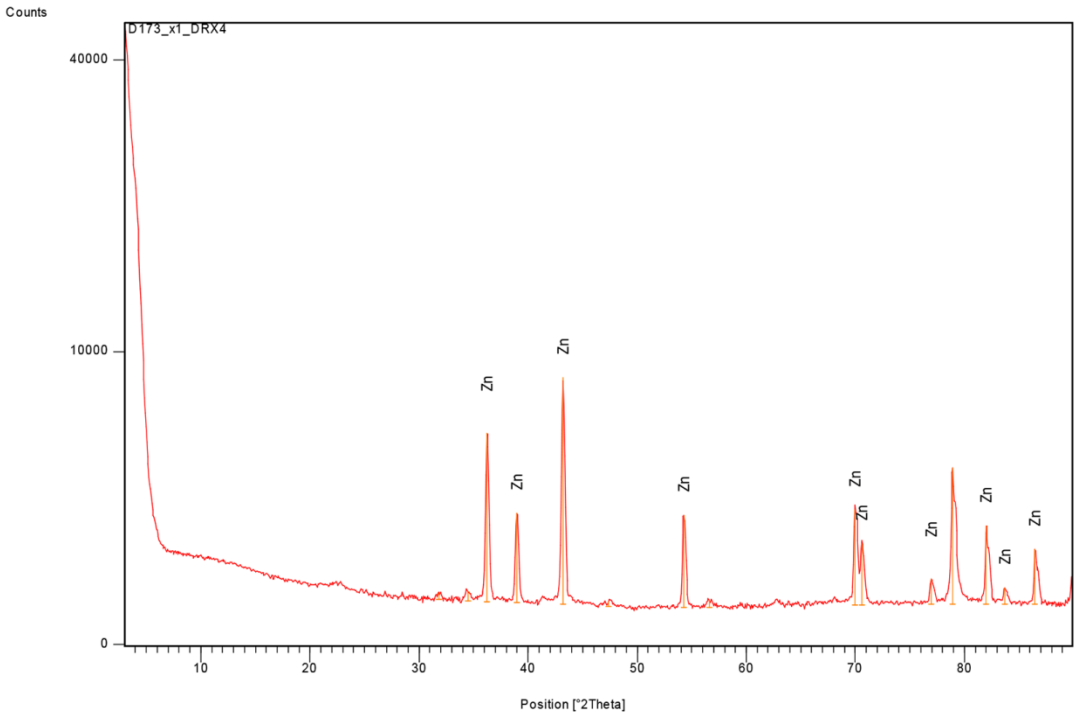

Peak List:

Pos. [°2Th.]	Height [cts]	FWHM [°2Th.]	d-spacing [Å]	Rel. Int. [%]	Tip width [°2Th.]	Matched by
36.2546	5001.96	0.2637	2.47786	61.39	0.3165	00-004-0831
38.9809	1801.52	0.2637	2.31062	22.11	0.3165	00-004-0831
43.1898	8147.38	0.3296	2.09470	100.00	0.3956	00-004-0831
47.3536	44.73	0.7911	1.91977	0.55	0.9494	
54.2735	1791.06	0.2637	1.69022	21.98	0.3165	00-004-0831
70.0064	1946.43	0.3296	1.34398	23.89	0.3956	00-004-0831
70.6274	995.29	0.3296	1.33368	12.22	0.3956	00-004-0831
76.9532	306.86	0.3956	1.23906	3.77	0.4747	00-004-0831
78.9023	3464.41	0.2637	1.21327	42.52	0.3165	

82.0156	1444.85	0.3296	1.17492	17.73	0.3956	00-004-0831
83.7133	177.94	0.2637	1.15536	2.18	0.3165	00-004-0831
86.4846	863.59	0.2412	1.12438	10.60	0.2894	00-004-0831

Plot of Identified Phases:

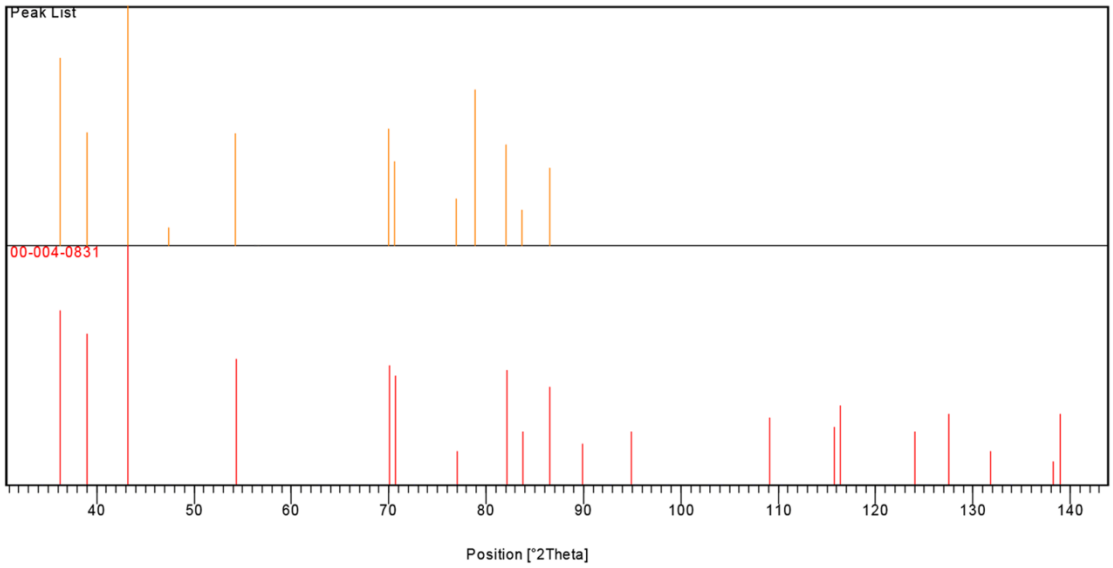

Identified Patterns List:

Visible	Ref. Code	Score	Compound Name	Displacement [°2Th.]	Scale Factor	Chemical Formula
*	00-004-0831	84	Zinc, syn	0.000	0.706	Zn

XRD analysis report of UFC/Sn5vol.% composite

X-ray diffractogram of UFC/Sn5vol.%:

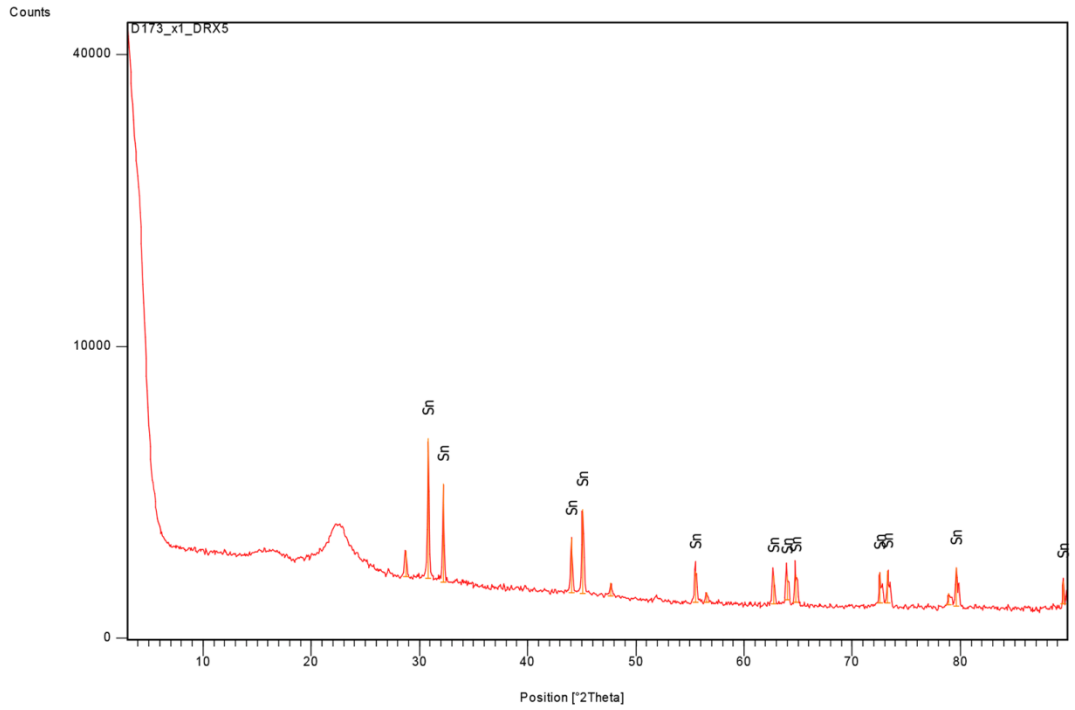

Peak List:

Pos. [°2Th.]	Height [cts]	FWHM [°2Th.]	d-spacing [Å]	Rel. Int. [%]	Tip width [°2Th.]	Matched by
28.7267	447.08	0.1978	3.10774	10.52	0.2373	
30.8222	4250.72	0.1978	2.90106	100.00	0.2373	01-089-4898
32.2045	2420.85	0.1978	2.77963	56.95	0.2373	01-089-4898
44.0584	931.51	0.1978	2.05540	21.91	0.2373	01-089-4898
45.0957	1697.62	0.1978	2.01050	39.94	0.2373	01-089-4898
47.7089	147.37	0.1978	1.90630	3.47	0.2373	
55.5334	360.55	0.2637	1.65482	8.48	0.3165	01-089-4898
56.5489	90.16	0.1978	1.62750	2.12	0.2373	
62.7123	313.53	0.1978	1.48156	7.38	0.2373	01-089-4898

63.9879	268.35	0.1978	1.45507	6.31	0.2373	01-089-4898
64.7794	321.62	0.2637	1.43919	7.57	0.3165	01-089-4898
72.5412	358.35	0.3296	1.30314	8.43	0.3956	01-089-4898
73.2813	382.51	0.3296	1.29180	9.00	0.3956	01-089-4898
78.9380	98.74	0.3956	1.21281	2.32	0.4747	
79.6071	452.93	0.1978	1.20429	10.66	0.2373	01-089-4898
89.4926	237.60	0.2412	1.09422	5.59	0.2894	01-089-4898

Plot of Identified Phases:

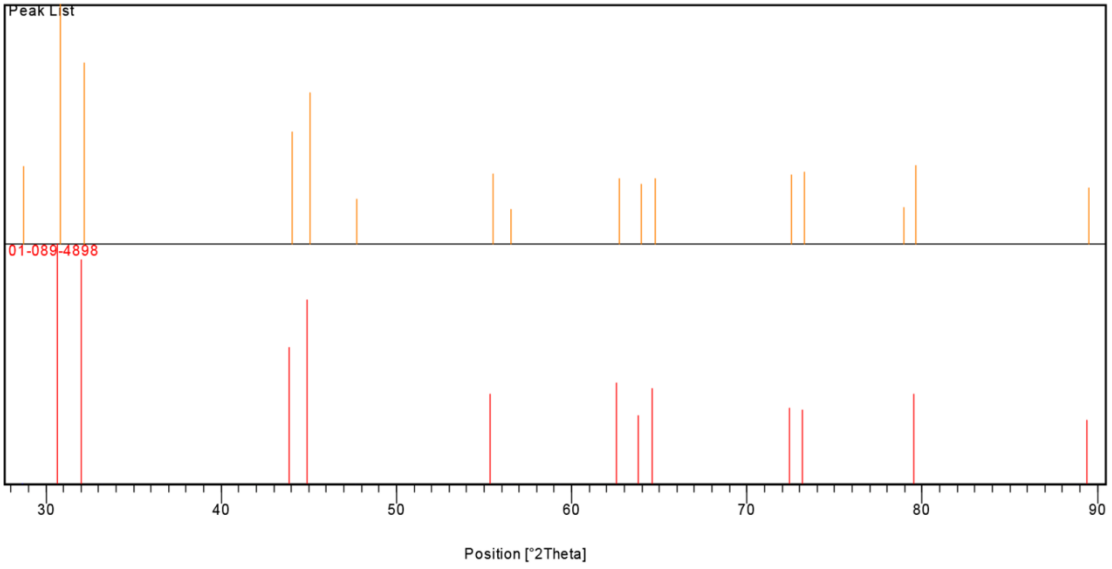

Identified Patterns List:

Visible	Ref. Code	Score	Compound Name	Displacement [°2Th.]	Scale Factor	Chemical Formula
*	01-089-4898	39	Tin	0.000	0.014	Sn

XRD analysis report of UFC/Sn35vol.% composite

X-ray diffractogram of UFC/Sn35vol.%:

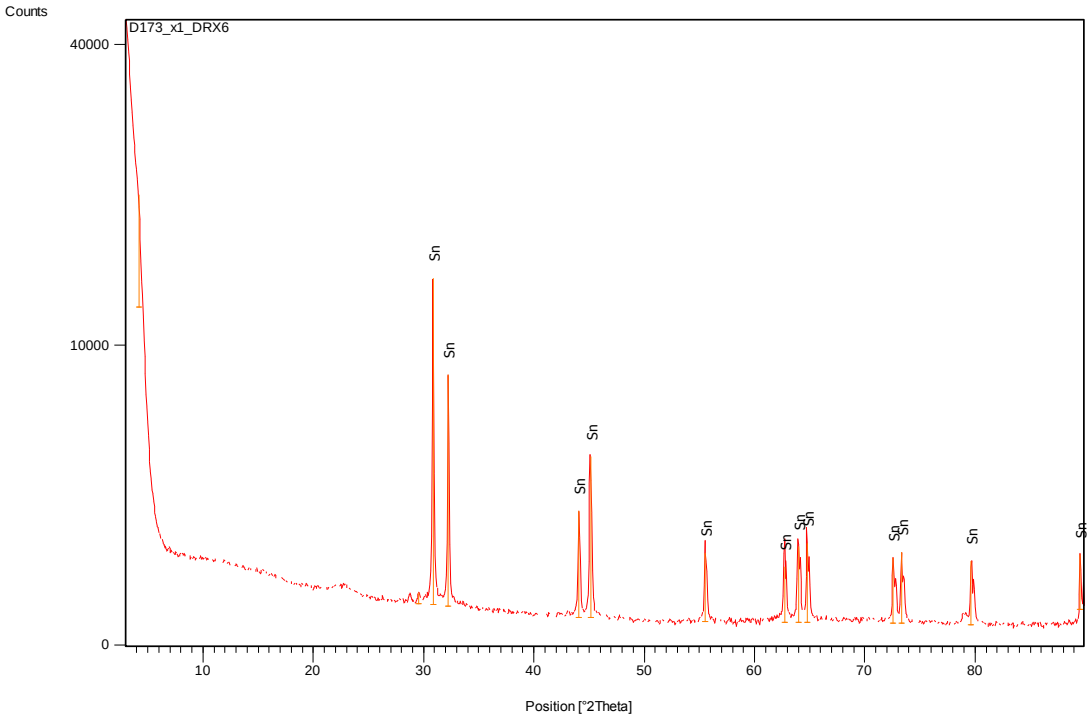

Peak List:

Pos. [°2Th.]	Height [cts]	FWHM [°2Th.]	d-spacing [Å]	Rel. Int. [%]	Tip width [°2Th.]	Matched by
29.5269	117.96	0.1978	3.02531	0.80	0.2373	
30.8552	14780.09	0.1978	2.89804	100.00	0.2373	03-065-2631
32.2414	7952.78	0.1978	2.77653	53.81	0.2373	03-065-2631
44.1034	1909.15	0.1978	2.05340	12.92	0.2373	03-065-2631
45.1284	3858.74	0.1978	2.00912	26.11	0.2373	03-065-2631
55.5633	885.78	0.2637	1.65401	5.99	0.3165	03-065-2631
62.7642	631.99	0.2637	1.48046	4.28	0.3165	03-065-2631
64.0069	1019.61	0.2637	1.45468	6.90	0.3165	03-065-

						2631
64.8039	1090.30	0.2637	1.43870	7.38	0.3165	03-065-2631
72.5803	796.05	0.2637	1.30254	5.39	0.3165	03-065-2631
73.3290	906.09	0.3956	1.29107	6.13	0.4747	03-065-2631
79.6417	733.38	0.2637	1.20386	4.96	0.3165	03-065-2631
89.5315	782.25	0.1608	1.09385	5.29	0.1930	03-065-2631

Plot of Identified Phases:

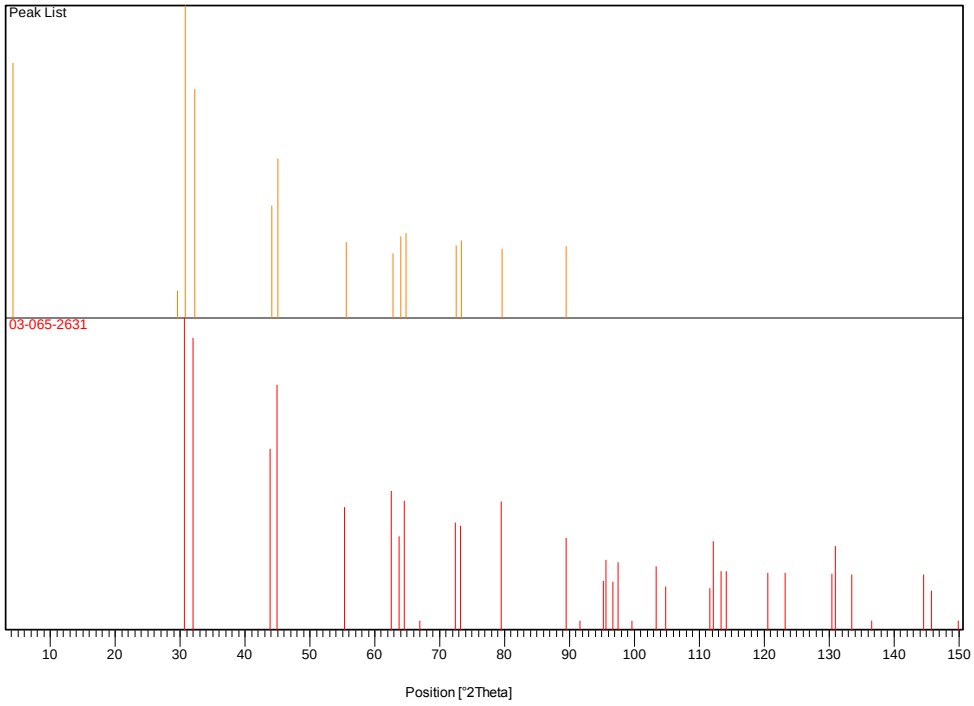

Identified Patterns List:

Visible	Ref. Code	Score	Compound Name	Displacement [°2Th.]	Scale Factor	Chemical Formula
*	03-065-2631	48	Tin	0.000	0.023	Sn

Annex C

Important materials for active layers in organic solar cells

The active layer consists of a donor and an acceptor. Some of the important donors and acceptors are given below:

Donors

The donor in the solar cell is the light absorbing material, a polymer or small molecule, in which an electron is excited and transferred to the acceptor. The most common light absorbing materials are presented here.

Poly(3-hexylthiophene) or briefly P3HT (Figure C1) is to date the most studied polymer for polymer solar cells. The efficiency of a P3HT/PCBM solar cell is typically 4-5 %, which is close to the optimal performance for this system.

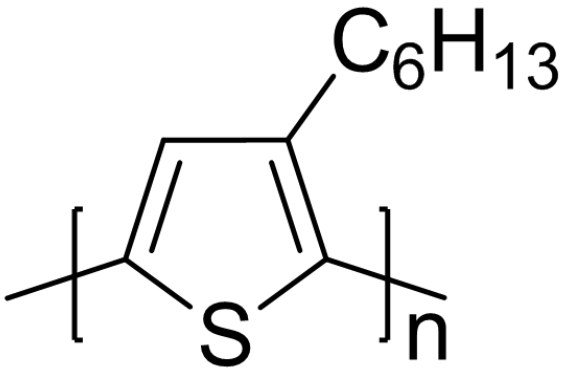

Figure C1: P3HT

Low band gap polymers absorb light with wavelengths longer than 650 nm corresponding to a band gap lower than 2 eV. This means that they have a better overlap with the solar spectrum and can potentially absorb more photons than P3HT and thereby increase the current and efficiency of the solar cell. In Figure C2 some low band gap polymers are shown. The low band gap polymers normally consist of an electron rich motif (a donor unit) and an electron poor motif (an acceptor unit). This donor-acceptor approach creates a partial charge separation at the backbone of the polymer, which results in a lowering of its band gap. The device performance has been increased to 7-10% by the use of low band gap polymers in the active layer.

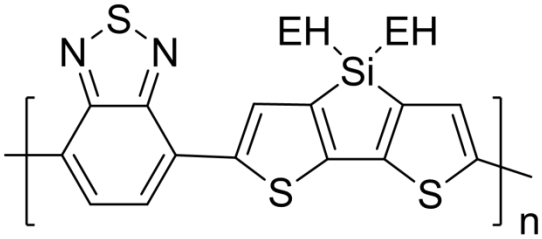

PSBTBT

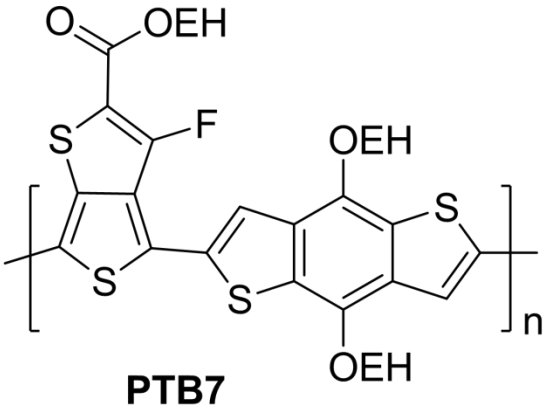

PTB7

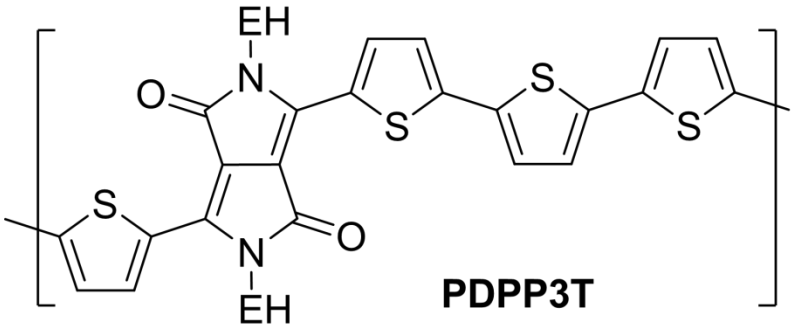

PDPP3T

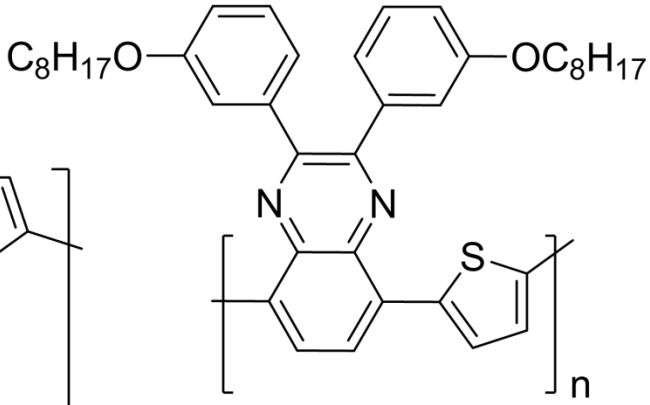

TQ1

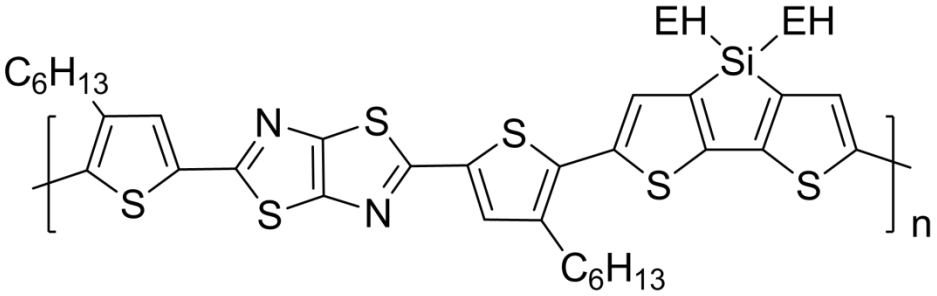

PDTSTTz

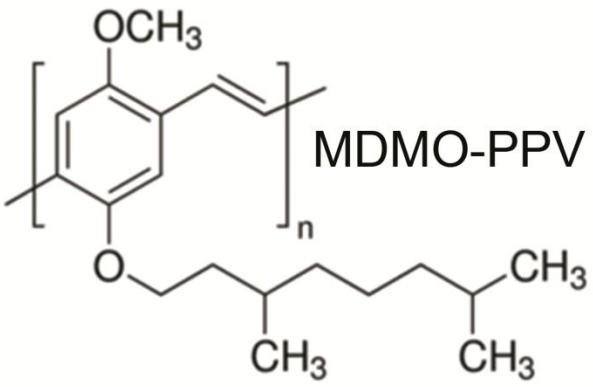

Figure C2: Examples of low band gap polymers based on donor and acceptor units.

Acceptors

An acceptor is the material which accepts the electrons from the donor and thus ensures charge separation. The most important acceptors for organic solar cells are detailed below. The most applied fullerene is the soluble PC61BM (phenyl-C61-butyric acid methyl ester) which is soluble in most organic solvents. In the early period of organic solar cells, the C60 fullerene was evaporated onto the polymer layer and the active layer of the solar cell was a bi-layer. With the PC61BM it was possible to blend the polymer and the acceptor in solution before spin coating and the active layer has now become a bulk heterojunction. In Figure C3, the C60 and the PC61BM are shown; PCBM is derived from C60 [265].

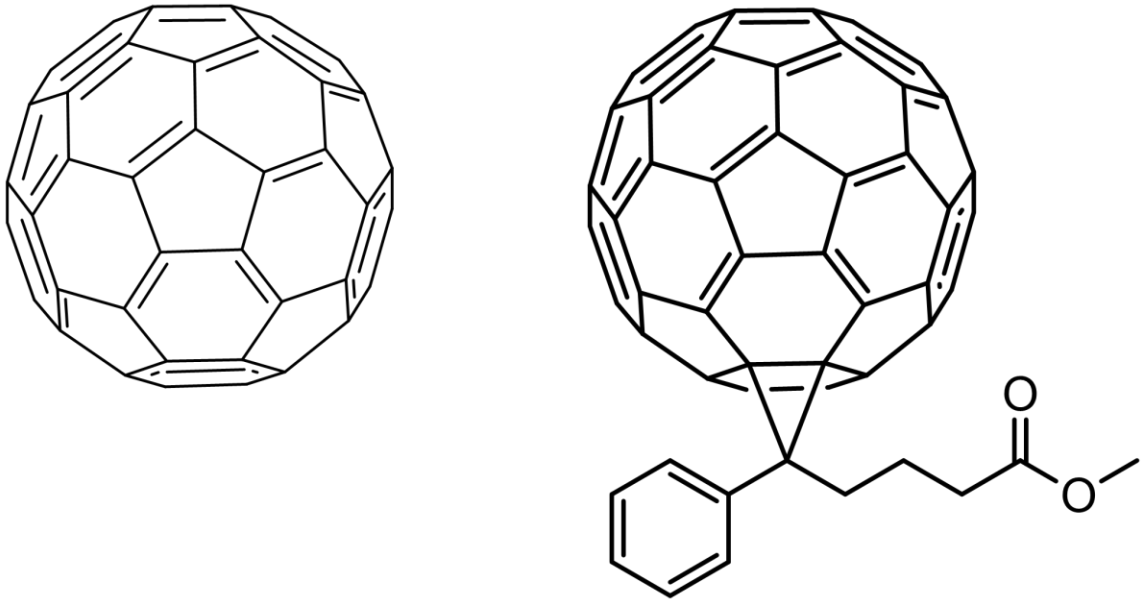

Figure C3: Illustrations of C60 and PC61BM.

In addition to PC61BM there are many other types of fullerene, most importantly is PC71BM which has the same functional group but is based on C70 (Figure C4).

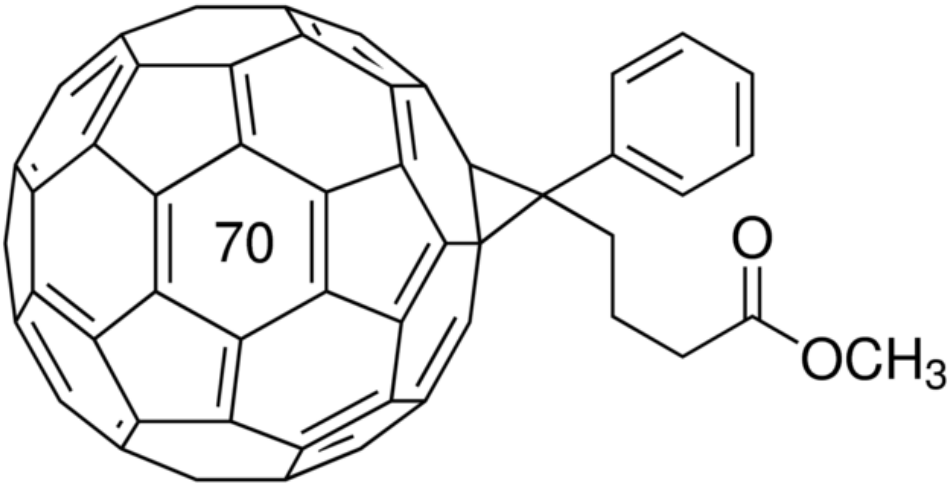

Figure C4: PC71BM

Another familiar acceptor is poly(3,4 ethylenedioxythiophene):polystyrene sulfonate or simply PEDOT:PSS) as shown below:

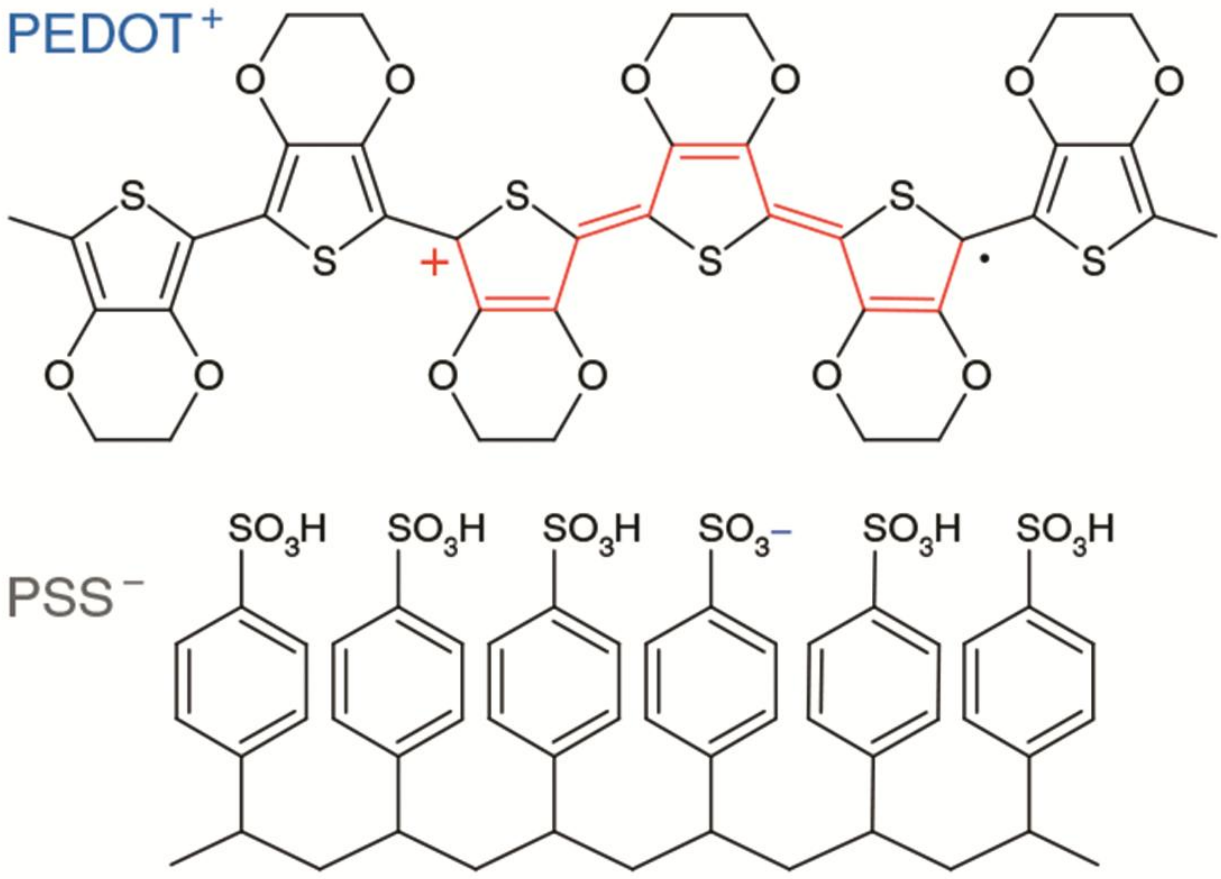

Figure C5: Chemical structure of poly(3,4-ethylenedioxythiophene):polystyrene sulfonate (PEDOT:PSS).

Dyes in dye-sensitized solar cells

DSC operation is much closer to photosynthetic processes than operation of standard solid-state photovoltaic devices such as silicon-based solar cells and/or organic photovoltaic cells. As with photosynthesis, the effectiveness of the light conversion in DSSC depends on the relative speed of reactions, i.e. kinetics. The electron injection into the TiO_2 conduction band is much faster than electronic relaxation processes back to the ground state or chemical side reactions involving the excited state of the dye (one of the key components for high power conversion efficiencies). Moreover, the reduction of the oxidized dye (Ru^{3+}) by I^- is significantly faster than the direct recombination reaction between the injected electron and Ru^{3+}. In recent years, considerable developments have been made in the engineering of novel dye structures in order to enhance the performance of the system. Figure C6 shows familiar ruthenium based dyes.

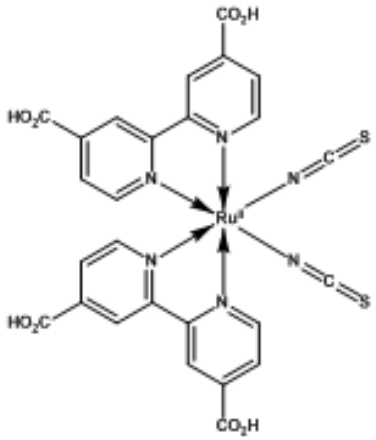

N-3

$C_{26}H_{16}N_6O_8RuS_2$

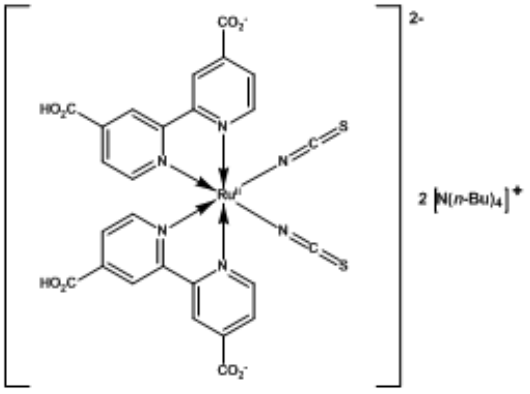

N-719

$C_{58}H_{86}N_8O_8RuS_2$

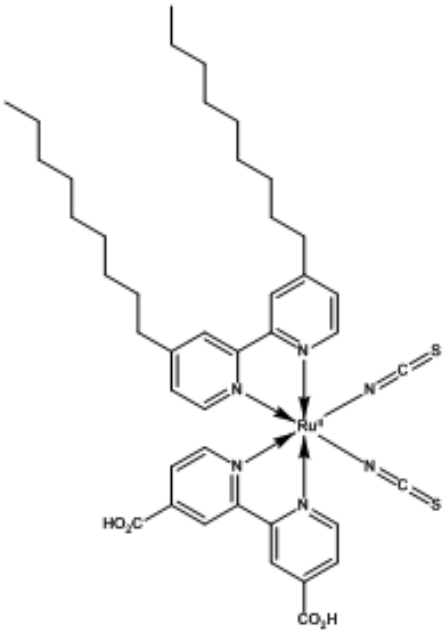

Z-907

$C_{42}H_{52}N_6O_4RuS_2$

Figure C6: Ruthenium-based N-3, N-719 and Z-907 dyes.

Annex D

Protocol for predicting reliable lifetimes of polymer solar cells

Generation of simulated kinetic data

In order to test the functionality of developed lifetime prediction method on a polymer solar cell, kinetic data are required under different thermal histories. Eqs. (6.5), (6.14), and (6.19) suggest that no matter how the extents of short circuit current density, moisture/oxygen uptake, and photoreactions vary with time/temperature, their degrees of reaction advancement i.e. x, y, and z remain always normalized within [0, 1]. It makes the availability of kinetic data of short circuit current density, moisture/oxygen uptake, and photoreactions of polymer solar cell convenient by simulating Eqs. (6.7), (6.15), and (6.20) with the help of Originlab software under isothermal conditions.

In the first case, the temperature acceleration of solar cell current density is simulated by using Eq. (6.7). It is supposed that the semiconductor of solar cell is subjected to various temperatures at; $T \in [45,\ 60]$ with a temperature difference of 5 °C under constant illumination provided by halogen lamp (avoiding UV radiations). Under these conditions, the process is assumed to follow zero order reaction, and its reaction rate is simulated by considering activation parameters E_x = 40 kJ.mol^{-1} and $A_x = 2.1\times10^2$ min^{-1}. At each temperature, the x-t plots are drawn by numerically integrating the dt/dx versus x curves, employing an efficient numerical integration algorithm namely, Gaussian Quadrature [161]. The obtained results are demonstrated in Figure D1a.

In the second case, thermally activated moisture uptake of solar cell is simulated by using Eq. (6.15). The solar cell is supposed to place in the dark humid environment under the same isothermal runs as described previously i.e. $T \in [45,\ 60]$ with a temperature difference of 5 °C. In this case, the absorption of moisture by solar cell is assumed to follow Ginstling-Brounshtein diffusion model (D4), and its reaction rate is simulated by considering activation parameters E_y = 65 kJ.mol^{-1} and $A_y = 5\times10^3$ min^{-1}. At each temperature, the y-t plots are drawn by numerically integrating the dt/dy versus y curves, and the results obtained are shown in Figure D1b.

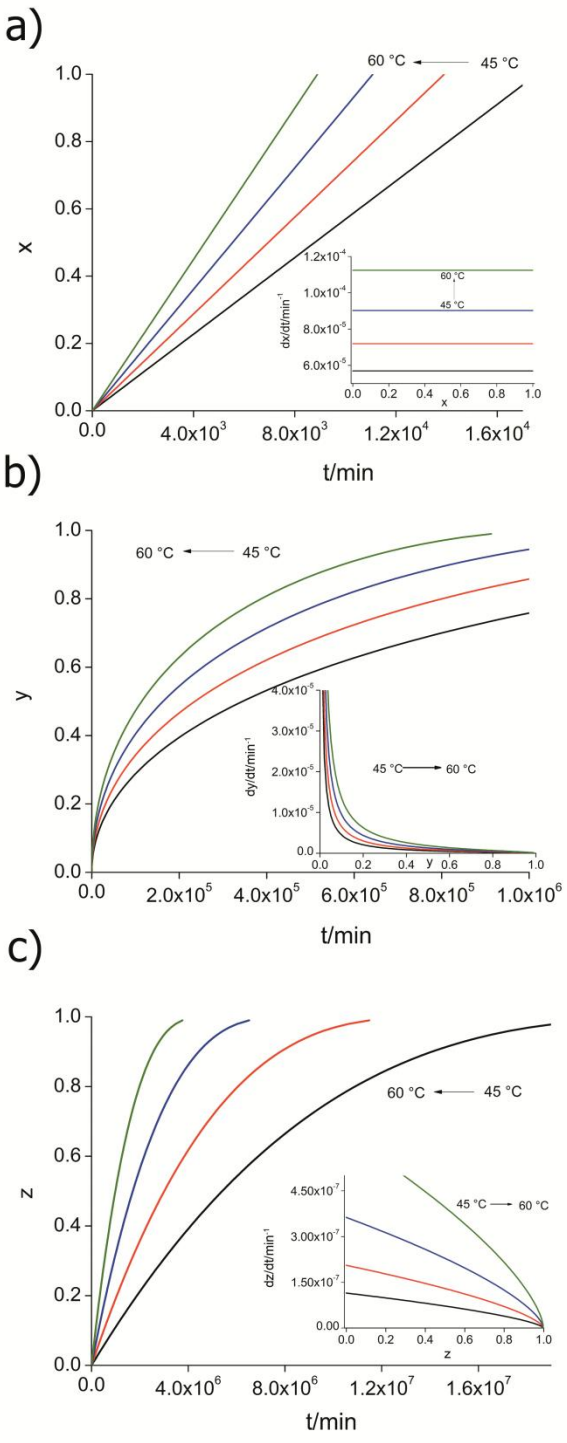

Figure D1: Generation of simulated kinetic data. (a) Temperature acceleration of solar cell current density. (b) Thermally activated moisture uptake of solar cell. (c) Thermally accelerated photoreaction in solar cell. Insets show the respective reaction rates.

In the third and the last case, thermally accelerated photoreactions occurring in solar cell are simulated by using Eq. (6.20). The cell is supposed to interact with UV radiations at constant wavelength (where semiconductor shows maximum absorbance) under the same isothermal histories as described previously i.e. $T \in [45,\ 60]$ with temperature difference of 5 °C. In this case, the process is assumed to follow contracting sphere reaction model (R_3), and its reaction rate is simulated by considering activation parameters E_z = 100 kJ.mol^{-1} and $A_z = 3\times10^9$ min^{-1}. At each temperature, the z-t plots are drawn by numerically integrating the dt/dz versus z curves, and the obtained results are shown in Figure D1c.

In addition to simulated data, a set of reference data is generated at 25 °C (room temperature conditions) by following the same considerations as discussed above and employing Eqs. (6.7), (6.15), and (6.20). The individual half lives of variation in short circuit current density, moisture uptake process, and photoreactions in these reference data i.e. $(t_{1/2})_x$, $(t_{1/2})_y$, and $(t_{1/2})_z$ are exploited to define the effective half life of polymer solar cell by using Eq. (6.26) at 25 °C, as depicted in Figure D2. A value of 2.4×10^4 min has been found as the reference half life of polymer solar cell under the ordinary temperature conditions. For the developed lifetime prediction method to be reliable and robust, it must evaluate a half life of approximately 2.4×10^4 min under room temperature conditions (outside the conditions used to generate the kinetic data).

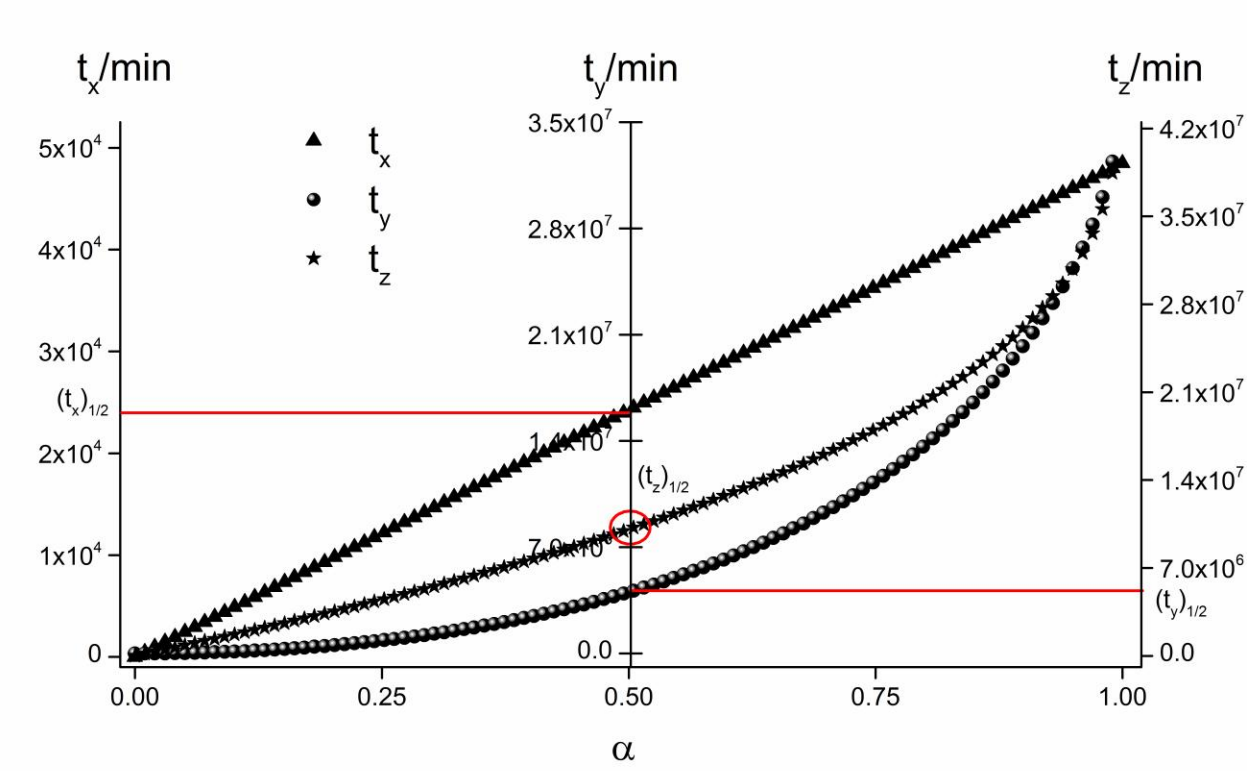

Figure D2: Reference half life determination at 25 °C of solar cell under consideration.

Application of kinetic approach to simulated data

In order to verify the efficacy of suggested method for predicting the lifetimes of solar cells, activation parameters and reaction models (kinetic triplet) of the kinetically simulated processes need evaluation.

At first, a systematic determination of the activation energies of the under consideration processes is carried out. The systematic determination of activation energy is credible because:

- Activation energy determined by taking into account different thermal histories reveals simple or complex nature of process. A process may fairly be approximated as single step if the variation in its activation energy with the degree of reaction advancement is insubstantial, otherwise, the reaction is perceived as following a complex reaction pathway.
- Different reaction models can potentially fit a single kinetic dataset by accomplishing mutual compensation between pre-exponential factors and activation energies; true kinetic triplet in that case remains obscure.

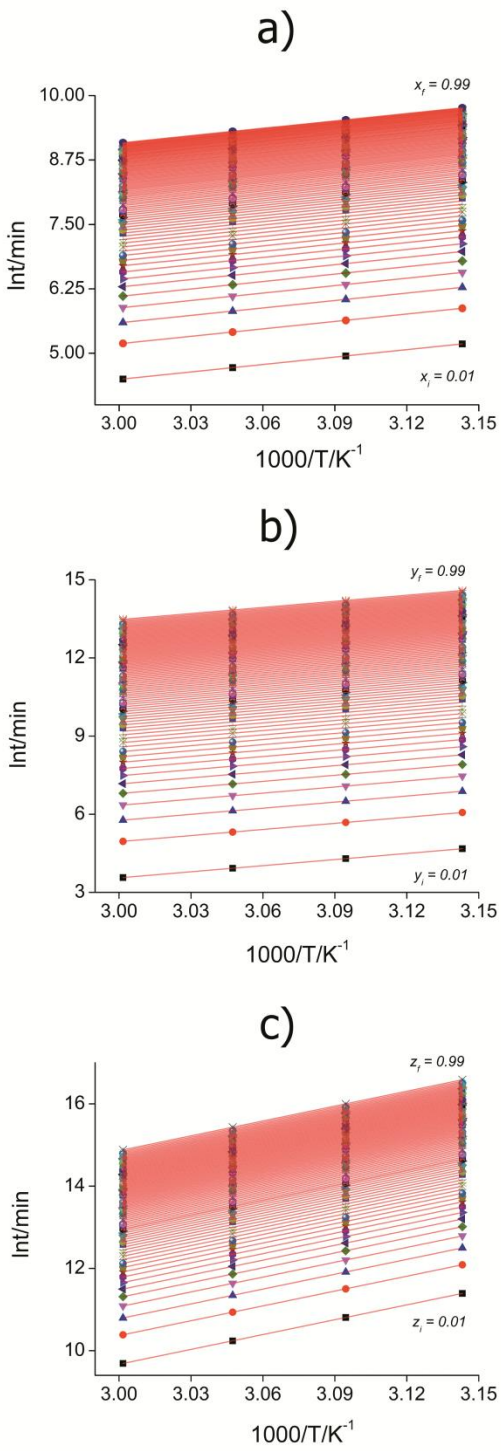

Figure D3: Determination of activation energies. (a) Temperature acceleration of solar cell current density. (b) Thermally activated moisture uptake of solar cell. (c) Thermally accelerated photoreaction in solar cell by Eqs. (6.10), (6.16), and (6.21).

The activation energies of simulated processes are evaluated by employing the data shown in Figure D1, using Eqs. (6.10), (6.16) and (6.21). In each case, the activation energy values have been determined by plotting lnt versus 1000/T at constant values of x, y and z which belong to the interval (0, 1) with $\Delta x = \Delta y = \Delta z = 0.01$, and the obtained results are shown in Figure D3a-c. It is evident in Figure D3 that the solid straight lines fit well the data with correlation factors nearly unity. The activation energy values of the thermally accelerated current density, moisture uptake processes, and photoreactions i.e. E_x, E_y, and E_z respectively, obtained from Figure D3 are shown in Figure D4 as functions of degree of reaction advancement.

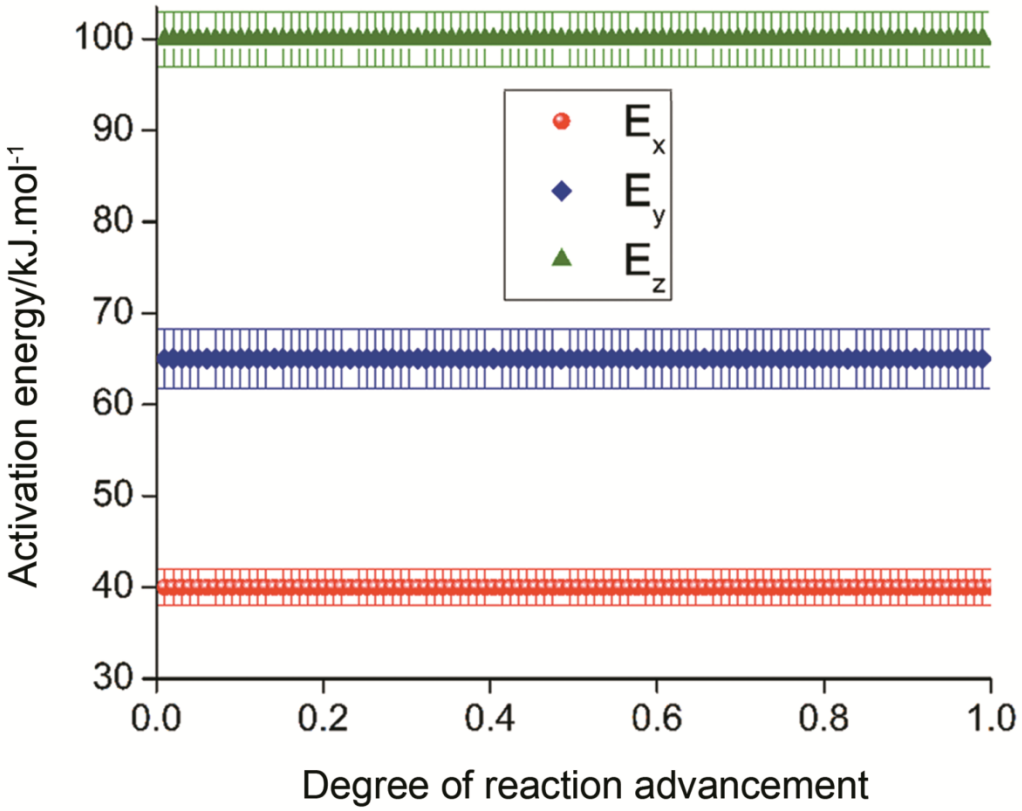

Figure D4: Activation energy values E_x, E_y, and E_z, of different respective processes occurring in solar cell versus degree of reaction advancement.

The invariant activation energy values of these processes verify their single step nature. The activation energies E_x, E_y, and E_z calculated from Figure D4 are 40±2 kJ.mol^{-1}, 65±3 kJ.mol^{-1}, and 100±3 kJ.mol^{-1} respectively, which agree with the activation energies used to generate the simulated data.

In the next step, reaction models for thermally accelerated short circuit current density, moisture uptake processes, and photoreactions in the solar cell i.e. f(x), f(y), and f(z) respectively, are determined by employing the data shown in Figure D1. Figure D1a points out that the thermally accelerated short circuit current density in the solar cell follows zero order reaction model since its reaction rate does not vary with x at each temperature. In order to determine f(y) and f(z), the mechanistic functions h(y) and h(z) are evaluated by Eqs. (6.17) and (6.22), and the obtained results are shown in Figure D5a. By comparing the shapes of h(y) and h(z) curves obtained with those available in Figure 2b, it is inferred that the thermally accelerated moisture uptake process follows a diffusion model, while thermally activated photoreaction follows reaction order model. The value of degree of reaction advancement i.e. $y_{max.}$ = 0.581 corresponding to the maximum of h(y) function as given in Table 1, verifies that the process obeys Ginstling-Brounshtein diffusion (D4) model. In thermally accelerated photoreaction case, the h(z) curve shown in Figure D5a is fitted by the theoretical expression of $h(z)_{RO}$ = -n/1-z as expressed in Table 1, and the obtained results are represented in Figure D5a.

In Figure D5a, the fit generates a value of n = 0.671 ≈ 2/3 with correlation factor approximately one, which is ascribed to contracting sphere reaction model (R_3). The obtained results show that all the evaluated reaction models, f(x), f(y), and f(z) show agreement with those used to generate the simulated kinetic data. Reaction models f(y) and f(z) are described in Figure D5b along with their integrated reaction models g(y) and g(z), in the inset.

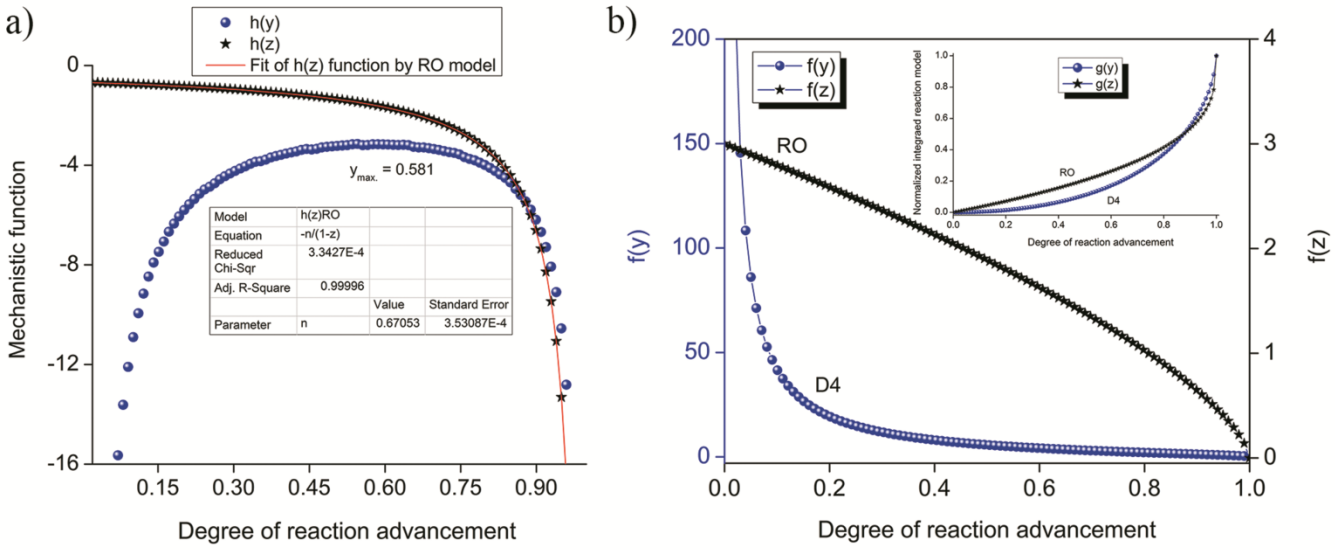

Figure D5: (a) Evaluation of reaction models f(y) and f(z) by employing h(y) and h(z) functions from Eqs. (6.17) and (6.22) at T = 45 °C. (b) Reaction models f(y) and f(z) versus degree of reaction advancement; inset: integrated reaction models g(y) and g(z) versus degree of reaction advancement.

Once the activation energies and reaction models are known, the pre-exponential factors A_x, A_y, and A_z of the respective processes can be calculated by Eqs. (6.13), (6.18), and (6.23). In Eq. (6.13), the function $\ln\{\exp(E_x/RT)dx/dt\}$ remains constant providing $\ln A_x$ value, while in Eqs. (6.18) and (6.23) $\ln A_y$ and $\ln A_z$ are determined by the intercepts of the respective straight lines as shown in Figure D6. The correlation factors in all the cases approach to unity. The obtained pre-exponential factors are; $\ln A_x$ = 5.35 min^{-1}, $\ln A_y$ = 8.52 min^{-1}, and $\ln A_z$ = 21.82 min^{-1} respectively, which corroborate the pre-exponential factors of the respective processes used to produce the simulated data.

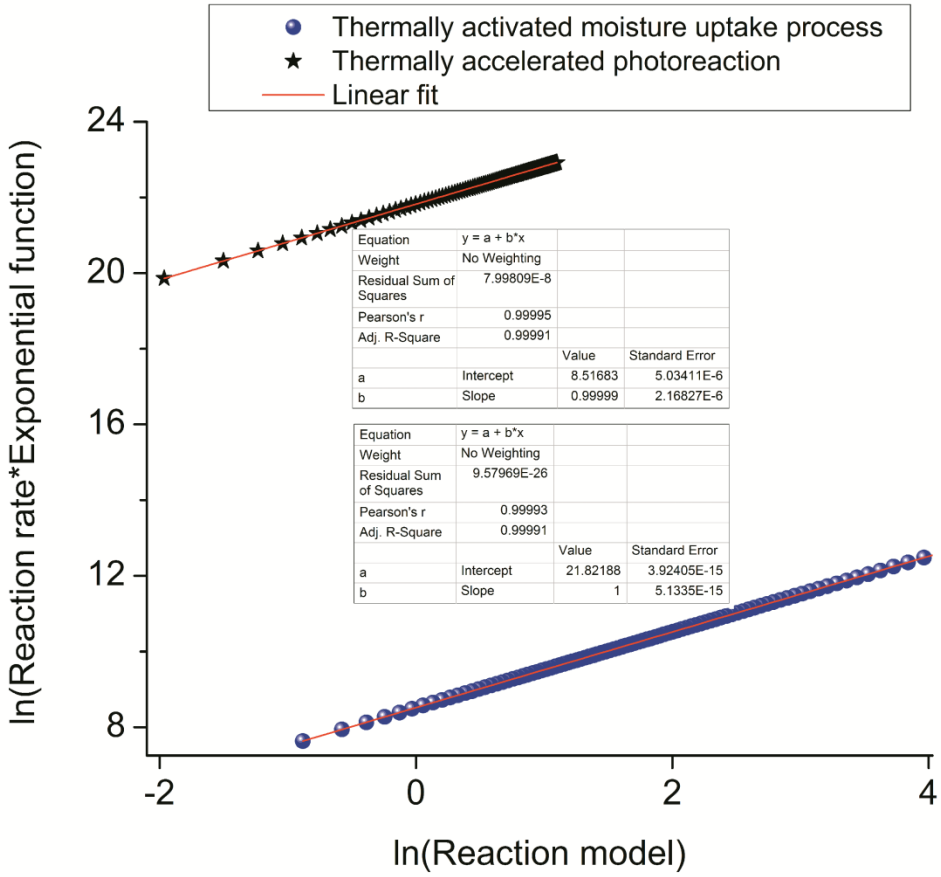

Figure D6: Determination of the pre-exponential factors of thermally accelerated moisture uptake process (A_y) and photoreaction (A_z) taking place in the assumed solar cell by employing respectively, Eq. (6.18) and Eq. (6.23) at T = 45 °C.

The obtained results can be employed to predict the lifetime of plastic solar cell under the conditions under consideration, which generates a diagram similar to Figure D2. Alternatively, the individual half lives of thermally accelerated short circuit current density, moisture uptake process, and photoreaction $(t_x)_{1/2}$, $(t_y)_{1/2}$, $(t_z)_{1/2}$ respectively obeyed by the solar cell, are calculated by Eqs. (6.10), (6.16), and (6.21) with $x = y = z = 0.5$, at different isothermal runs, noting that $g(x) = x$ in Eq. (6.10). The results obtained by these calculations are graphically shown in Figure D7.

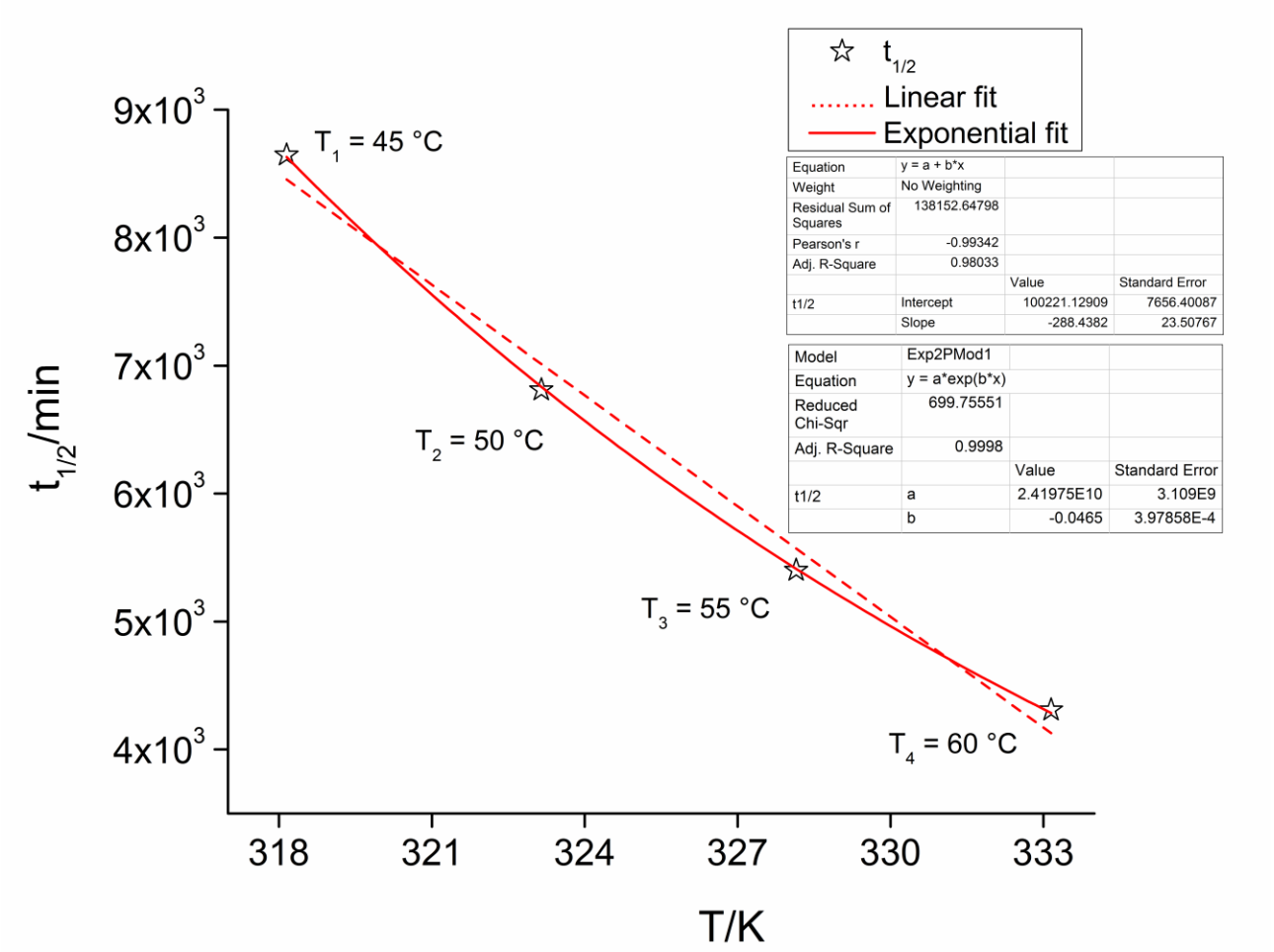

Figure D7: Modeling variation in effective half life of polymer solar cell with the operating.

Figure D7 shows that the half life of the considered polymer solar cell solar decreases exponentially with temperature. Figure D7 shows that the half life of polymer solar cell under simulated weathering conditions reduces considerably by increasing temperature which reveals the higher cell sensitivity to weathering conditions. Detailed insights associated with the

influence of simulated weathering conditions on the effective half life of polymer solar cell can be obtained by fitting the observed behavior of variation in half life with temperature. The obtained curve of variation in half life with temperature is fitted by a linear (dotted line) and an exponential (solid line) decay function, though exponential function (described by empirical equation S1) gives reliable results as evident in Figure D7.

$$t_{1/2} = a\exp(-bT) \tag{D1}$$

Where, 'a' and 'b' are empirical constants. Physically, parameter 'a' could be signified as the half life of polymer solar cell in the absence of any thermal stresses (absolute zero). While 'b' might probably be attributed to the logarithmic variation in effective half life of polymer solar cell per unit temperature. Eq. (D1) can then be expressed as following:

$$t_{1/2} = (t_{1/2})_{T\,=\,0K}\exp(-bT) \tag{D2}$$

Eq. (6.26) with the help of Eqs. (6.10), (6.16), and (6.21) seems useful in predicting the half lives of polymer solar cells. As an example, the relationship (D2) between effective half life of polymer solar cell and operating temperature derived from Eq. (6.26) can be extrapolated to 298.15 K (25 °C) to test the applicability of the suggested method on the reference kinetic data. This extrapolation to 25 °C by Eq. (D1) gives an effective half life value of 2.31×10^4 min which is in good agreement with the reference value of 2.4×10^4 min. The error is around 4 % which is more likely caused by numerical differentiation/integration of data. It should however be taken into account that despite the discussion on Eqs. (D1)/(D2), the $t_{1/2}$-T relationships depend on the nature of polymer solar cells and types of degradation processes taking place in them.

Abstract

Polymer composites filled with metal particles establish an interesting class of materials with wide-reaching applications from macro to nano scale. Our research group demonstrated in the previous researches that such polymer/metal composites possess fascinating electrical/dielectric properties. The present thesis continues developing these earlier researches by reporting a thorough study on structural, morphological and thermal properties of polymer/metal composites. For this purpose, insulating and conducting polymer composites comprising epoxy and urea-formaldehyde cellulose (UFC) resins filled with metal (aluminum, zinc and tin) particles are prepared and structurally characterized by SEM-EDX, XRD and FTIR analyses. Structural and morphological analyses reveal that the composites are homogenous and the polymer-metal interfaces are physical in nature. Thermogravimetric analysis (TGA) profiles of polymer/metal composites suggest that the thermal degradation of epoxy/metal composites follows quasi single-step process; however thermal degradation of UFC/metal composites goes to completion in several complex steps. Thus, an innovative reaction model determination methodology is put forward to address the encountered kinetic problem of determining the reaction model under variable activation energy conditions. Kinetic analysis of the thermal degradation of epoxy/metal composites predicts autocatalytic reaction mechanism for epoxy/metal composites; while, UFC/metal composites pursue highly complicated multi-step nucleation/growth mechanisms. The suggested methodology is exploited also to develop novel approaches for predicting accurate lifetimes of polymer solar cells and kinetically modeling the crystallization processes in amorphous materials.

Keywords: Polymer composites, metals, TGA/DTG, thermal degradation, kinetics, mechanism, organic photovoltaics, crystallization.

Résumé

Les composites polymères chargés par des particules du métal constituent une classe intéressante de matériaux avec des applications étendues de l'échelle macro à l'échelle nanométrique. Les recherches de notre équipe ont montré que les matériaux composites polymère/métal ont des propriétés électriques/diélectriques fascinantes. La présente thèse est une continuation du développement de ces recherches antérieures en rapportant une étude approfondie des propriétés structurales, morphologiques et thermiques des composites polymère/métal. A cet effet, des composites polymères isolants et conducteurs comprenant des résines époxy et urée-formaldéhyde cellulose (UFC) chargées par des particules métalliques (aluminium, zinc et étain) ont été préparés et structurellement caractérisés par des analyses SEM-EDX, XRD et FTIR. Les analyses structurales et morphologiques révèlent que les composites sont homogènes et que les interfaces polymère-métal sont de nature physique. Les profils d'analyses thermogravimétriques (ATG) des composites polymère/métal suggèrent que la dégradation thermique des composites époxy/métal suit un processus quasi-mono-étape, tandis que la dégradation thermique des composites UFC/métal est achevée en plusieurs étapes complexes. Pour cela, une méthodologie innovante de détermination du modèle de réaction a été proposée pour résoudre cet important problème cinétique de détermination du modèle de réaction dans des conditions d'énergie d'activation variable. L'analyse cinétique de la dégradation thermique des composites époxy/métal prédit un mécanisme de réaction auto-catalytique pour les composites époxy/métal. Tandis que, les composites UFC/métal obéissent à des mécanismes de nucléation/croissance très complexes en plusieurs étapes. La méthodologie suggérée a été exploitée aussi pour développer de nouvelles approches pour prédire les durées de vie précises des cellules solaires polymères et modéliser cinétiquement les processus de cristallisation dans les matériaux amorphes.

Mots-clés: Composite polymère, métaux, ATG/DTG, dégradation thermique, cinétique, mécanisme, photovoltaïque organique, cristallisation.